A RESILIENCE METRIC FOR MODERN POWER DISTRIBUTION SYSTEMS

by
Tyler Bennett Phillips

A dissertation
submitted in partial fulfillment
of the requirements for the degree of
Doctor of Philosophy in Computing
Boise State University

December 2020

BOISE STATE UNIVERSITY GRADUATE COLLEGE

DEFENSE COMMITTEE AND FINAL READING APPROVALS

of the dissertation submitted by

Tyler Bennett Phillips

Dissertation Title: A Resilience Metric for Modern Power Distribution Systems

Date of Final Oral Examination: 11 December 2020

The following individuals read and discussed the dissertation submitted by student Tyler Bennett Phillips, and they evaluated the students presentation and response to questions during the final oral examination. They found that the student passed the final oral examination.

Hoda Mehrpouyan, Ph.D.	Chair, Supervisory Committee
John Gardner, Ph.D.	Co-Chair, Supervisory Committee
Amit Jain, Ph.D.	Member, Supervisory Committee
Stephen Reese, P.E.	External Member, Supervisory Committee

The final reading approval of the dissertation was granted by Hoda Mehrpouyan Ph.D., Chair of the Supervisory Committee. The dissertation was approved by the Graduate College.

DEDICATION

to my family

ACKNOWLEDGMENT

It is with great pleasure that I express my deepest gratitude and appreciation to my advisors, Dr. Hoda Mehrpouyan and Dr. John Gardner, for their continuous support and endless commitment during this incredible endeavor of studies and research. All the achievements I have reached would not have been possible without their support, motivation, immense knowledge, and guidance throughout the entire process. I truly cannot thank them enough for their everlasting help and generous advice along the way.

Additionally, I need to show my sincerest appreciation to Dr. Craig Reiger and Timothy McJunkin at Idaho National Laboratory (INL). They have both been incredible mentors, I have learned so much from their guidance during my graduate fellowship at INL. The experience has been very beneficial to me, having been exposed to several areas of study. I have certainly learned numerous valuable skills that will help me throughout my career. Thank you Dr. Reiger for the incredible opportunity of being a graduate fellow at INL.

I am also very grateful to rest of my defense committee, Dr. Amit Jain and Stephen Reese. Their assistance and the time they have spent to improve the research covered in this dissertation is appreciated so much.

I also need to send a special thanks to all the co-authors of the work covered in this dissertation that I have not yet thanked. Thanks to those who contributed to the

Resilience Week publication covered in Chapter 4. Because of the great collaboration between INL and Pacific Northwest National Laboratory and the tremendous work done by Vishvas Chalishazar of PNNL, Tim McJunkin of INL, Manisha Maharjan of INL, S M Shafiul Alam of INL, Thomas Mosier of INL, and Abhishek Somani of PNNL we were awarded the best paper of Resilience Week 2020, thanks everyone.

Lastly, I need to thank the funding support for the work covered in this dissertation. The work in Chapter 2 was supported by the National Science Foundation Computer and Information Science and Engineering (CISE), award number 1846493 of the Security and Trustworthy Cyberspace (SaTC) program: Formal TOols foR SafEty aNd Security of Industrial Control Systems (FORENSICS). The work in Chapter 3 and 5 was supported by the US Department of Energy's Office of Energy Efficiency and Renewable Energy (EERE) under the Solar Energy Technology Office Award Number DE-0008775. The work in Chapter 4 was supported in part by Battelle Energy Alliance (BEA) LLC, under contract number DE-AC07-05ID14517 and BEA under contract number DE-AC05-76RL01830 with the US Department of Energy. Work supported through the US Department of Energy Water Power Technology Office HydroWIRES Initiative.

CITATIONS

Material from this dissertation has been published in the following form:

1. T. Phillips, H. Mehrpouyan, J. Gardner, S. Reese, "A Covert System Identification Attack on Constant Setpoint Control Systems," 2019 Seventh International Symposium on Computing and Networking Workshops (CANDARW), 2019 © 2019 IEEE

2. T. Phillips, T. McJunkin, C. Rieger, J. Gardner, and H. Mehrpouyan, "An Operational Resilience Metric for Modern Power Distribution Systems," 2020 IEEE International Conference on Software Quality, Reliability, and Security (QRS-C), Macau, China, 2020 © 2020 IEEE

3. T. Phillips, V. Chalishazar, T. McJunkin, M. Maharjan, SMS Alum, T. Mosier, and A. Somani, "A Metric Framework for Evaluating the Resilience Contribution of Hydropower to the Grid," 2020 Resilience Week (RWS), Salt Lake City, UT, USA, 2020 © 2020 IEEE

4. T. Phillips, T. McJunkin, C. Rieger, J. Gardner, and H. Mehrpouyan, "A Framework for Evaluating the Resilience Contribution of Solar PV and Battery Storage on the Grid," 2020 Resilience Week (RWS), Salt Lake City, UT, USA, 2020 © 2020 IEEE

ABSTRACT

Modern society has become increasingly reliant on the functioning of critical infrastructure. It is considered so vital that its incapacitation or destruction would have debilitating effects on the global economy, national security, and public health and safety. The electrical power system is uniquely positioned, as it is essential for all other sectors of critical infrastructure to operate as intended. However, it is constantly at risk due to factors such as natural disasters, climate change, aging infrastructure, and cyber threats. Thus, ensuring the efficient and continuous supply of electricity is of utmost importance and the topic of this dissertation.

The work in this dissertation covers two main topics; first the identification of a potential cyber threat to control system, and second, the foundation for a resilience framework to ensure a continuous supply of electricity in the grid.

Technology advancements have resulted in the integration of digital instrumentation and computational control through communication networks. This has resulted in systems which are more responsive, precise, reliable, and efficient. However, they are integrated into operational technologies without the necessary security defense. Designing an effective, layered security defense is not possible unless security threats are identified through a structural analysis of the control system. For that reason, an attacker's point of view is given for the reconnaissance effort necessary to gather details of the system dynamic that are required for the development of sophisticated

attacks. A reconnaissance approach is presented that uses the system's input and output data to infer the dynamic model of the system. In this effort, a novel cyber-attack that targets the controller proportional-integral-derivative gain values in a constant setpoint control system is proposed. These findings will help researchers design more secure control systems.

The electrical power grid has been designed to withstand single component failures based on a set of reliability metrics that have proven acceptable during normal operating conditions. However, in recent years there has been an increasing frequency of extreme weather events. Many have resulted in widespread long-term power outages, proving reliability metrics do not provide the adequate energy security that is needed.

As a result, researchers have focused their efforts on resilience metrics to ensure efficient operation of power systems during extreme events. A resilient system has the ability to resist, adapt, and recover from disruptions. Therefore, resilience is a promising concept for the current challenges facing power distribution systems.

An operational resilience metric for modern power distribution systems is presented. The metric is based on the aggregation of system assets adaptive capacity in real and reactive power. The metric indicates the control limits of the assets of the system. This also relates to the magnitude and duration of a disturbance the system can withstand. The mathematical details of the metric are covered and consider the real-time operational outputs of the assets, its ramp rates, latency, and energy limits. The metric is then focused on the resilience contribution of the three types of hydropower generation and their contribution to the various time scales or "Rs" of resilience. Further analysis demonstrates using very short-term (seconds) and short-

term (day-long) solar PV generation forecast with uncertainty. It was demonstrated that the addition of battery storage to a solar generation asset can be used to maintain adaptive capacity during times where solar generation is at the negative uncertainty scenario.

TABLE OF CONTENTS

LIST OF FIGURES

LIST OF TABLES

LIST OF ABBREVIATIONS

AGC Automatic Generation Control

CI Critical Infrastructure

CPS Cyber-Physical System

DER Distributed Energy Resources

DIRE Disturbance and Impact Resilience Evaluation

HILF High-Impact Low-Frequency

HWR Hydropower With Reservoir

I/O Input/Output

ICS Industrial Control System

IDS Intrusion Detection System

IEEE Institute of Electrical and Electronics Engineers

IT Information Technology

MDS Modern Distribution Systems

NRMSE Normalized Root Mean Square Error

OT Operational Technologies

PID Proportional-Integral-Derivative

PSH Pumped Storage Hydropower

PV PhotoVoltaic

ROR Run-Of-River

LIST OF SYMBOLS

D	Transfer function denominator polynomial
E	Energy
F	Force on inverted pendulum cart
H	Transfer function
I	Mass moment of inertial of inverted pendulum
K_d	Derivative gain
K_i	Integral gain
K_p	Proportional gain
M	Mass of inverted pendulum cart
N	Normal force on cart and pendulum
N	Transfer function numerator polynomial
P	Real power
P^+	Ramping up in real power
P^-	Ramping down in real power

P_{Δ} Flexibility in real power

$P_{\in}$ Real power domain

P_{AC} Real power adaptive capacity

Q Reactive power

Q^{+} Ramping up in reactive power

Q^{-} Ramping down in reactive power

Q_{Δ} Flexibility in reactive power

$Q_{\in}$ Reactive power domain

Q_{AC} Reactive power adaptive capacity

S Apparent power

$\ddot{\theta}$ Angular acceleration of inverted pendulum

$\ddot{x}$ Acceleration of inverted pendulum cart

$\dot{\theta}$ Angular velocity of inverted pendulum

$\dot{x}$ Velocity of inverted pendulum cart

$\hat{y}$ Estimated measurement

$\hat{y}_k$ Expected sensor measurement

λ Latency

σ Standard deviation

τ	Threshold value
θ	Angle of inverted pendulum, power factor angle
b	Friction on inverted pendulum cart
e	Error between setpoint and sensor value
g	Gravity
l	Length of inverted pendulum
m	Mass of inverted pendulum
n_k	System delay
q^{-1}	Backward shift operator
r_k	Residual values time series
t	Time
u	Control command
u	Uncertainty
x	Position of inverted pendulum cart
y	Sensor measurement
y_k	Current sensor measurement
y_{k-1}	Previous sensor measurement

CHAPTER 1:

INTRODUCTION

Modern society has become increasingly reliant on the functioning of Critical Infrastructure (CI). It is considered so vital that its incapacitation or destruction would have debilitating effects on the global economy, national security, and public health and safety. The electrical power system is uniquely positioned, as it is essential for all other CI sectors to operate as intended [112]. However, it is constantly at risk due to factors such as natural disasters, climate change, aging infrastructure, and cyber threats. Thus, ensuring the efficient and continuous supply of electricity is of upmost importance and the topic of this dissertation.

1.1 Modernization of the Electrical Power Grid

The electric grid is the largest and most complex machine ever built. Traditionally, it has been an intricate web of transmission and distribution systems with centralized generation largely based in fossil fuel and hydroelectric power generation which have high inertia. However, the electric grid has been going through a dramatic shift in the way power is generated and transmitted over the last several decades. The grid modernization includes rapid penetration of renewable energy generation and the application of sensors, computers, and communication devices which is often referred to as the "smart" grid.

Monitoring and controlling the electric system is a difficult task. In the past, it has been possible to reliably manage the grid by measuring the central power plants and the high voltage transmission lines. However, with the addition of distributed generation sources the management of the distribution system is getting attention as these sources can directly affect the performance of the grid [116, 124]. Unlike the traditional generation, distributed sources such as solar, are characterized as decentralized assets which do not consist of rotating masses and therefore do not contribute to inertia. In the U.S. the growth in renewable generation can largely be attributed to federal [15] and state [54] policies that incentivize both research and deployment. The push for renewables is in an effort to curb global carbon emissions, in light of climate change, and to increase energy independence for national security.

Although the increasing presence of renewable generation on the power system is being spurred by climate change and security concerns, the dramatic reduction in investment have made it cost competitive with more traditional resources. From 2011 to 2017 solar generation in the U.S. went form generating 3 to 47 gigawatts of electricity. From 2010 to 2017 the reduction in cost to install solar generation was 69% for residential, 73% for commercial, and 79% for utility scale. Furthermore, the Solar Energy Technologies Office set a 2030 goal for a further 50% reduction of cost. Achieving this goal would make solar one of the cheapest sources of electricity generation and push further expansion of solar PhotoVoltaic (PV) installation [67]. Figure 1.1 shows the growth in renewable generation in comparison to traditional sources on the left and the large contribution of solar and wind on the right [2]

The grid is not only seeing an increase in the integration of renewables, it is also experiencing rapid deployment of digital technologies. This is allowing two-way

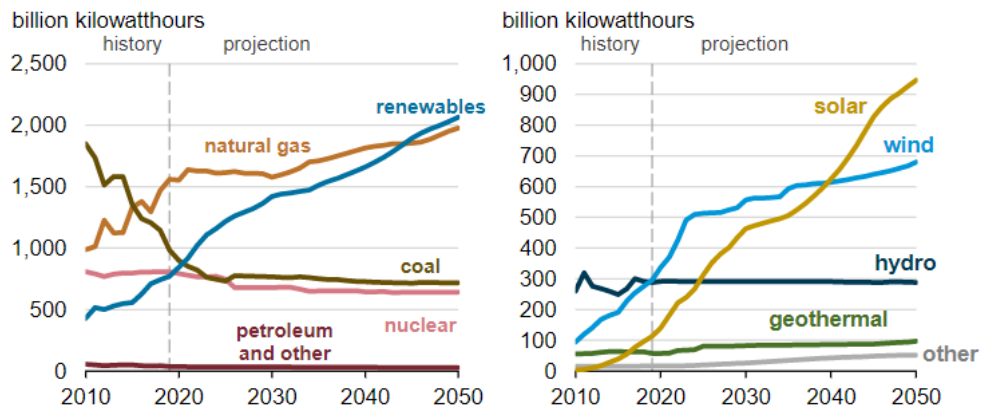

Figure 1.1 U.S. energy generation by type shown in the left plot and mix in renewable generation on the right. Image taken from [2]

communication between the utility and customers, as well as additional sensing along the power grid allowing for computational control of system resources. The smart grid consist of computational control, computers, communication devices, and other equipment working together to respond to changes in electrical demand in near real-time. The smart grid allows the opportunity to move the energy industry into a new era of reliability, availability, and efficiency [78]. However, the increase in computing and communication on the electric grid which gives so much promise, does not come without a cost. It has given cyber attackers an increasing number of vulnerabilities to attack the electrical power systems. The cyber and physical threats are covered in the next section.

1.2 Emerging Threats to the Electrical Power Grid

The electric power grid has always been under threat from weather related outages. However, the addition of computational control and communication to modernize the power grid has made it a target for cyber attackers.

Extreme weather events and natural disasters are the major cause of power outages

in the United States. Of the different components of the power grid, the distribution system is the most susceptible to adverse weather. Transmission lines are built to withstand high wind speeds, but distribution systems are much more vulnerable [122, 111, 7]. They are designed to be structurally safe in normal operating condition, but not sever weather. Electrical component failures during extreme weather in the U.S. between 2003 and 2012 have caused an estimated 679 widespread power outages affecting at least 50,000 customers [111]. Notable events include Hurricane Katrina [94], Hurricane Sandy [31], and the wildfires burring across California [37]. A reason of concern is that the frequency and intensity of these extreme weather events is increasing [111]. A 2012 study estimates the cost of these weather-related outages between $25 and $75 billion annually [8]. Moreover, these power outages during extreme weather put the public at risk. Data indicates that the 2003 blackout resulted in approximately 90 deaths [5].

The number of cyberattacks are on the rise and the energy industry is no exception. The cyber vulnerability of power systems has become more dangerous than ever. The smart grid is adding more computational and communication devices which is making them more vulnerable to a cyberattack [47]. Since the devices are connected to one another, hacking one device can be enough to gain access to more important parts of the system. Many of the smart devices are notorious for putting functionality and ease of use first and security second.

The U.S. Department of Energy reported 150 successful attacks between 2010 and 2014 that targeted systems holding information regarding electricity grids. Motivation behind cybercrime generally involves monetary gain, however, electric grids may involve politics and cyber warfare. Cyber warfare on power systems between

states are attractive because the scale and consequences can be extremely large as law enforcement, hospitals, and other critical systems depend on power.

Cyberattacks on the electric grid are on the rise. The first documented case occurred in 2015 and affected several electricity providers in Ukraine. More than 230,000 people were left without power for several hours during the winter [50]. The attackers were able to gain unauthorized access to the system by obtaining credentials of workers. Ukraine was again the target in 2016 when hackers left customers in parts of Kyiv without electricity for an hour after disabling a substation. In 2019 attackers used firewall vulnerabilities to cause periodic "blind spots" for grid operators in the western U.S. for about 10 hours [107]. They did not disrupt the flow of electricity but it does highlight the vulnerabilities of the U.S. power sector [106].

Power outages can be caused by physical damage during storms or cyberattacks. Today, there is a great need for operators to make resilience informed decisions to better serve customers. The concept of resilience is covered in the next section.

1.3 Resilience of Electrical Power Systems

Regulation of electrical power systems is largely based on the Energy Policy Act of 2005 [77]. Congress gave the Federal Energy Regulatory Commission authority to oversee the reliability of the bulk-power system for the purpose of ensuring reliable power operation. There are two main metrics used to measure reliability; the system average interruption duration index and the system average interruption frequency index. However, some jurisdictions consider storm related outages as extreme events, and thus, do not include them as inputs into the reliability metric [18].

In the wake of many recent natural disasters, such as hurricanes, hardening the distribution system is a potential method to reduce outages. However, this is imprac-

tical as it is far too costly and many researchers are now interested in the concept of resilience [13]. Resilience has been increasingly recognized as a new design and operation goal for power systems as it is becoming clear that it is not possible to resist all events at all times. New strategies beyond traditional reliability are needed to keep the lights on under extreme events.

Resilience and reliability are similar but differ in time and scale. For example, reliability concentrates on small-scale random faults and components caused by internal factors. It encompasses the N-1 contingency planning, or a single component failure. At the basic level, it ensures that no single point of failure would cause the entire system to stop working. On the other hand, the concept of resilience acknowledges High-Impact Low-Frequency (HILF) or extreme conditions where there are many more than a single component failure.

The concept of resilience of complex systems was originally introduced by Holling [33] in the ecology area. Holling defined the resilience of a system as the rate and speed of returning to normal conditions after an extreme event. Pioneering work in resilience of engineering systems is presented by Hollnagel, Woods, and Leveson in [34]. Many definitions have been coined by well respected organizations in engineering literature [38, 69, 99, 63, 61], policy directives [112], and the academic community [97]. A general commonality among sources are the ability to anticipate a possible disaster, adopt effective measures to decrease loss of load and system component failure before and during the disaster, and restore power quickly through controlled reconfiguration. Quantification of resilience in power systems is an emerging field. It is an important open area of research, of great interest to utilities and stakeholders.

There have been several proposed resilience metrics, such as the resilience triangle

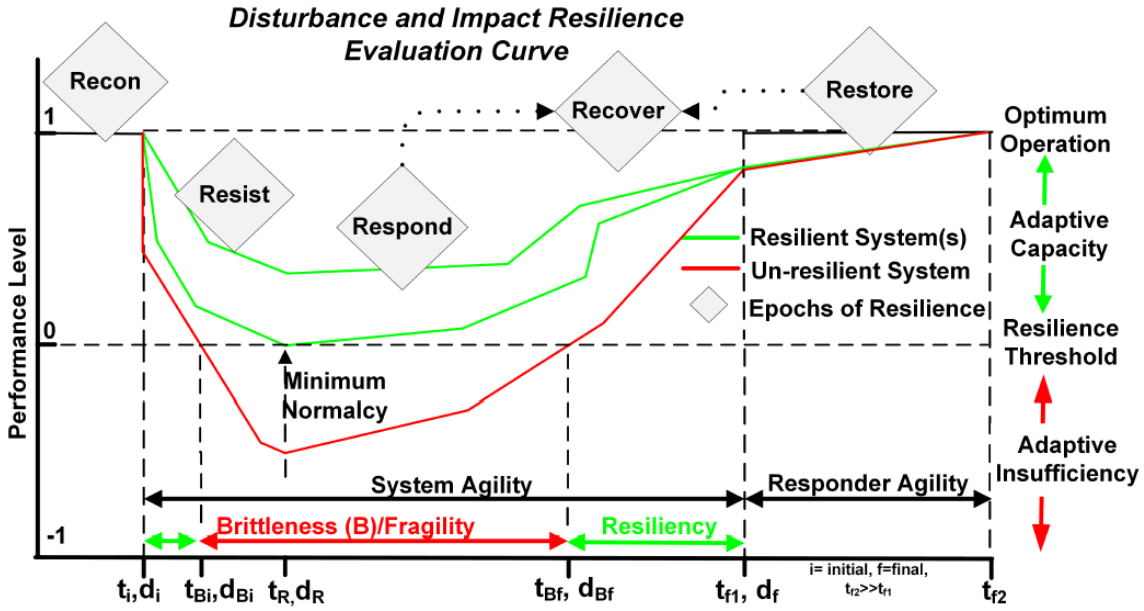

Figure 1.2 The disturbance and impact resilience evaluation curve, show-ing the 5R's of resilience. Image adapted from [96].

and trapezoid. The resilience trapezoid is an extension of the resilience triangle proposed in [109] by Tierney and Bruneau. Unlike the triangle which only considers the disturbance of a system, the trapezoid assesses the resilience through three phases; the disturbance, degradation, and the restorative state. Another approach given in [96] is shown by the notional Disturbance and Impact Resilience Evaluation (DIRE) curve in Fig. 1.2 which gives a resilience threshold, or the maximum acceptable level of degradation to the system.

It can be seen in the DIRE curve that resilience isn't a short-term or a long-term property. It considers the continuum of time frames from prior to the impact of a disturbance through the return to normalcy. The epochs or time frames can be described as the "Rs" of resilience. The *recon*naissance phase is a continuous process during operation to assess the state and health of the system. The situational

awareness allows for operation in a way that the system can be biased in a position to withstand a potential disturbance or threat. The *resist* phase is of short time and consists of assets which oppose the disturbance without the need for sensors and control action. For example, the resistance to frequency drop is provided by the accumulative spinning mass referred to as inertia of large synchronous generators. Assets that act based on feedback from sensors but work to react to disturbances in near real-time are able to *respond* and further arrest the drop in performance. The respond phase could be in the time second of milliseconds depending on sensors and control system response or could be minutes or even hours if a human response requiring analysis is required. In the *recover* phase, assets that were not needed or held in reserve would now be deployed and network reconfiguration can be used to move the system back towards optimal or a normal mode of operation. The *restore* phase generally consists of sending out line crews to repair damaged equipment and begins after the system has already recovered to the highest point possible given the resources that have remained available.

Woods describes an aspect of assessing a systems' resilience is whether the system is known to be near an operation boundary condition [125]. In the context of power systems the adaptive capacity in real and reactive power of the assets can be used to define this boundary. The adaptive capacity of real and reactive power is of interest because it is used to maintain stability in both frequency and voltage. To maintain frequency, the balance of real power generation needs to meet demand, and the balancing of reactive power is needed to maintain voltage. Furthermore, the temporal consideration of the assets can be utilized and a mapping of the assets' adaptive capacity can be made to the "Rs" of resilience.

1.4 Objectives and Contributions of This Work

The main goal of this research is to lay the foundation for an operational resilience metric framework for modern power distribution systems. The contributions are as follows:

1. Demonstrate the vulnerability in constant setpoint control systems to a cyber attack which targets the Proportional-Integral-Derivative (PID) algorithm.
    - Attack forces excitation of system variables
    - Increased accuracy of system identification.
    - Covert to physics-based anomaly detection.
    - Attackers can better design future attacks against the system.
2. Formalize the mathematical basis of an operational resilience metric.
    - Resilience metric is based on the adaptive capacity in real and reactive power of assets.
    - Adaptive capacity considers the real-time operational state, asset ramp rate, latency, and energy constraints.
    - Aggregation of asset adaptive capacity for resilience measure of distribution systems
3. Formalization of an operational framework with evaluation of hydropower assets.
    - Demonstrate hydropowers contribution to the “Rs” of resilience.

  - Run-of-river
  - Reservoir storage
  - Pumped hydro storage

4. Formalize the resilience contribution of solar PV and battery storage.

   - Mathematical formalization for uncertainty quantification using solar forecast data.
   - Demonstrate solar and battery storage systems can contribute to resilience during poor solar conditions.

1.5 Dissertation Outline

This dissertation begins by pointing out a potential weakness in control systems to cyber attackers in Chapter 2. This is demonstrated with a covert attack on an Industrial Control System (ICS) by targeting the PID control algorithm. This attack will force excitation of system variables, leading to a more accurate representation of the dynamic model of the system through system identification. This work highlights a cyber threat that could potentially be used by an attacker to learn about the power system and develop and carry out sophisticated cyber attacks.

Next, the focus is on the development of an operational resilience metric for power distribution systems. Chapter 3 presents the mathematical formalization of a resilience metric which is based on the adaptive capacity of real and reactive power that can be aggregated over assets on the power grid. Chapter 4 provides a detailed framework for resilience and the contribution of different types of hydroelectric generation. Chapter 5 focuses on the resilience contribution of solar generation and battery

storage assets and introduces an uncertainty quantification to the metric. Chapter 6 summarizes the work covered in this dissertation, gives concluding remarks, and presents the future work.

CHAPTER 2:

A COVERT SYSTEM IDENTIFICATION ATTACK ON CONSTANT SETPOINT CONTROL SYSTEMS[1]

2.1 Introduction

Technology advancements and investments in smart manufacturing have resulted in the integration of digital instrumentation and computational control through communication networks. Smart manufacturing not only results in processes which are more responsive, precise, reliable, and efficient, they also provide better operational and management capabilities through factory and supply chain visibility [21]. Although, this transformation has many advantages, it has resulted in systems that are traditionally configured to operate in an air gap environment (i.e. a server cluster without access to the internet) to be exposed to new threats that originate in the cyber domain [71, 76, 105, 121, 93]. The perceived threat of a large impact cyber-attack on control systems proved to be a reality in 2010 with the launch of the Stuxnet worm [48], prompting plant owners, engineers, technicians, and researchers

[1] © 2019 IEEE. Reprinted, with permission from, T. Phillips, H. Mehrpouyan, J. Gardner, S. Reese, "A Covert System Identification Attack on Constant Setpoint Control Systems," 2019 Seventh International Symposium on Computing and Networking Workshops (CANDARW), 2019

to feel the need to design and develop algorithms, tools, and techniques to protect the security of control systems. There are core features that separate the security of control systems from that of the traditional Information Technology (IT) domain. The fact that Operational Technologies (OT) and process control systems comprise proprietary hardware, software, and communication protocols, presents a new set of opportunities that require detection and protection techniques beyond what IT security can offer. Security technologies in the IT domain aim at protection of data and software by not allowing access from unauthorized users. The integration of IT security in control systems has lead to a false sense of security, as no amount of perimeter hardening can guarantee restriction of access by an attacker [79, 110, 49]. To address this issue, researchers have put forth efforts in physics-based detection methods to identify irregularities in the physics of the system [28].

In order to design and develop appropriate detection and protection techniques, researchers first turned their focus on constructing attack models [3, 102, 101, 108, 62, 64]. However, there is a lack of research on how the attackers are able to gain specific system knowledge that is required to carry out a successful attack. In most research studies, it is assumed that the reconnaissance efforts have been already carried out and the dynamics of the systems are known to the attackers. While attacks on Cyber-Physical System (CPS) and ICS can have devastating impacts on human lives and the environment, it is not easy for attackers to inflict their desired effects on a targeted system. Krotofil and Larsen [46] outline five questions that an attacker should be able to answer to successfully complete the stages of an ICS kill chain[2]: (I) *Access*: How to utilize traditional IT network hacking, (II) *Discovery*: How to discover the system

[2]https://www.sans.org/reading-room/whitepapers/ICS/industrial-control-system-cyber-kill-chain-36297

configuration and dynamics, (III) *Control*: What system parameters can be modified and in what degree these changes can be implemented so they are not detected, (IV) *Damage*: How can the attack scenario cause the greatest damage, (V) *Cleanup*: How to stay undetected after the attack is completed.

This chapter provides a perspective from an attacker's point of view on the reconnaissance effort necessary to gather details of the system dynamics - which are required for the development of sophisticated attacks. Our findings will help researchers to design a more secure control system. We present a reconnaissance approach which is based on a data-driven technique using the system's Input/Output (I/O) data to infer the dynamic model of the system. This process is known as system identification. We propose a novel cyber-attack that targets the controller PID gain values in a constant setpoint control system. Accurately identifying the dynamic model of constant setpoint control systems is challenging, because there is little excitation of the system variables, i.e. the signal-to-noise ratio of the dynamic characteristics of the system are too low. Thus, the intent of our PID attack is to initiate excitation in the data so the dynamic characteristics of the system are present in the data, leading to more accurate system models. Additionally, we demonstrate the covertness of our attack in regards to physics-based detection algorithms.

The rest of this chapter is organized as follows: Section 2.2 introduces related works and gives necessary background information. In Section 2.3, we present our proposed system identification attack and analyze the accuracy and covertness of the attack. Finally, conclusions and possible directions of future work are covered in Section 2.4.

2.2 Background and Related Work

Numerous research studies have investigated security issues of control systems; however, research communities (i.e. control engineers and cybersecurity experts) often work independent of one another in the areas of *"cyber"* and *"physical"* and do not consider the overlap of the two domains. A good example of this is when in the control area mathematical models are constructed from the observed data to discover the dynamic models of the system. This process is known as *system identification* [51], which could be utilized by an attacker to learn about the system dynamics, and as a result, carry out more targeted attacks. However, not all system identification approaches used by the control community, such as an impulse-response, could be used by attackers for the discovery of the system dynamics, because it might raise an alarm by physics-based detection algorithms. In order to provide more details on the proposed approach, we first study control systems and the specific architecture that is the focus of this chapter.

A control system is composed of four general components; the plant or physical system, sensors that measure the physical state of the plant, the controller that calculates control commands to send the actuators, and the actuators that make the physical changes to the plant. A continuous feedback-loop design, depicted in Figure 2.1, is the general landscape used for continuous control of a system. Here, controlled variables such as pressure, temperature, or flow rate are measured using sensors, $y(t)$, and new control commands, $u(t)$, are sent to actuators based on the calculated error, $e(t)$, from their desired setpoint. In this work, we consider constant setpoint systems, i.e. the desired setpoint does not change in time. New control commands are calculated using the error between the setpoint and sensor measure-

ments using the PID algorithm. The PID is the most commonly applied algorithm in practice today [118]. It calculates the control command sent to plant actuators using three terms; proportion, integral, and derivative, hence the name. Mathematically this is given as

$$u(t) = K_p e(t) + K_i \int_0^t e(t)dt + K_d \frac{de(t)}{dt} \tag{2.1}$$

here, K_p, K_i, and K_d are the gain values of the proportional, integral, and derivative terms, respectively. In practice on a controller such as a programmable logic controller, a discrete form of the PID is used, given as

$$u_k = K_p e_k + K_i \sum_{n=1}^{k} e_n + K_d \left[e_k - e_{k-1}\right] \tag{2.2}$$

Discrete PID control is usually implemented using the so-called velocity form

$$u_k = u_{k-1} + K_p[e_k - e_{k-1}] + K_i e_k + K_d[e_k - 2e_{k-1} + e_{k-2}] \tag{2.3}$$

which is obtained by subtracting u_{k-1} from u_k. The obvious advantage of the velocity form is that there is no need to keep track of the sum of the errors.

In these types of controllers, it is possible to target and alter the PID gain values on the controller. This attack can influence the I/O data and result in a more accurate dynamic model of the physical system.

2.2.1 System Models and System Identification

System models are a representation of real-world phenomena where the essential aspects of a system are described by mathematical equations [80]. Historically, system modeling has been based on physical laws to derive the system model. For example,

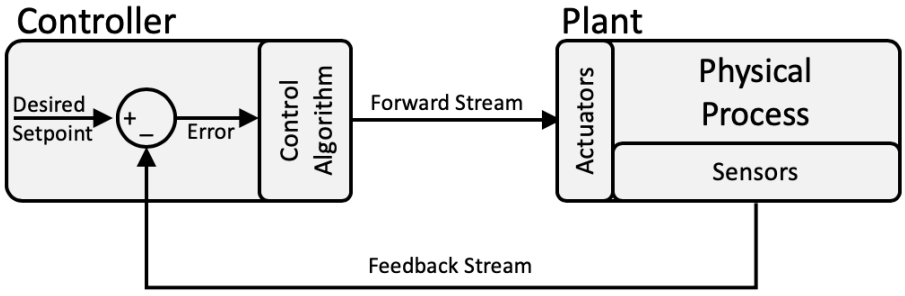

Figure 2.1 Block diagram of a feedback-loop industrial control system. The controller calculates control commands using the setpoint and feedback data from the sensor measurements to control actuators.

mechanical systems follow Newton's and Hooke's laws, electrical systems follow Ohm's and Kirchoff's laws, and thermodynamics follow the ideal gas law and entropy.

As complexity of systems has increased, the models that describe their dynamics have become extremely complex as well. Researchers could rely on abstraction or simplification of the model, however, this could result in loss of information about physical phenomena that might be crucial for system discovery and analysis. In these cases, control engineers generally rely on system identification methods which construct the mathematical models using the system's I/O data. One of these mathematical models is the transfer function, which is the ratio of the output of a system to the input in the Laplace domain. The mathematical formula for the transfer function H is given as

$$H(s) = \frac{N(s)}{D(s)} \tag{2.4}$$

Here, N and D are polynomials with unknown parameters in the frequency domain, (s).

To estimate the polynomial coefficients of the transfer function we apply the MATLAB [57] discrete-time transfer function estimation algorithm, *tfest*. This algorithm

applies an estimated output-error polynomial model represented as

$$y(t) = \frac{B(q)}{F(q)}u(t - n_k) + e(t) \tag{2.5}$$

where $y(t)$ is the output, $u(t)$ is the input, n_k is the system delay, and $e(t)$ is the error. $B(q)$ and $F(q)$ are polynomials with respect to the backward shift operator, q^{-1}, and defined as follows

$$B(q) = b_1 + b_2 q^{-1} + \cdots + b_{nb} q^{-nb+1} \tag{2.6}$$

and

$$F(q) = 1 + f_1 q^{-1} + \cdots + f_{nf} q^{-nf} \tag{2.7}$$

In this algorithm, the polynomial coefficients are initialized using ARX, followed by nonlinear least squares search-based updates to minimize a weighted prediction error norm.

The objective for control engineers and attackers is to estimate the unknown parameters of the system model as accurately as possible. Based on this accuracy, control engineers can optimize system performance, whereas attackers can better design attacks that are more likely to remain covert and reach their goals.

2.2.2 Attack Scenarios for Control Systems

In order to compromise the control system, an attacker could affect its forward and feedback streams by attacking any of its components (i.e. controller, sensor, and actuator) or its communication system. Long et al. [52] and Farooqui et al. [26] provide examples of such attack models. In [52], the communication network of the control

system is arbitrarily flooded, causing jitter and packet loss in the communication links. Whereas [26] uses false signals that are randomly generated and transmitted to the controller and actuator to impact the overall system. In these tactics, the system may become unstable leading to unpredictable behavior which is easier to identify using physics-based detection.

To this point, Teixeira et al. [108] investigated the attack models demonstrated in [3, 102, 19] and concluded that the design of a successful covert attack requires a high level of knowledge about the dynamics of the system. For example, the design and development of the man-in-the-middle attacks carried out in [102, 101] was based on the assumption that the dynamics of the control systems are known to the attack model. Based on that, the proper values were computed and injected into the feedback stream to remain covert. Hence, these attacks require an inside knowledge of the dynamics of the system and is limited to, and dependent on, inside attackers.

To overcome this limitation, de Sá et al. [19, 20] designed and developed cyber-attack techniques known as *cyber-physical intelligence attacks* to acquire the system knowledge necessary to model covert and controlled attacks. In their earlier work, de Sá et al. [19] carried out a passive system identification attack and eavesdropped on the forward and feedback data streams to estimate the system model's *transfer function*. However, since the effectiveness of the passive attack depends on the occurrence of events or excitation of the system variables, the authors introduced an active system identification attack [20]. In the second attempt, they tailor signals to insert into the communication channel and observe the resulting response. While, the active system identification resulted in a faster discovery of system dynamics, there is a higher probability of getting detected by an anomaly detection algorithm.

In this chapter, we further investigate an active system identification attack by altering the control command PID gain calculation. We will demonstrate that while the attack is still effective, it is much more difficult to detect our proposed approach. In order to prove the covertness of the proposed attack, we need to be able to pass the Intrusion Detection System (IDS) used by these type of control systems. In the next section, we will discuss the different types of attacks that occur in control systems and the IDS approaches that are utilized to detect these attacks.

2.2.3 Physics-Based Anomaly Detection

The types of attacks that occur in a control system are depicted in Figure 2.2 and summarized as follows:

1. When an actuator or forward stream is compromised, the actuation, v_k, to the plant is different than the intended action by the controller, $v_k \neq u_k$. This false actuation will in turn affect the measured variables of the plant.

2. When a sensor or feedback stream is compromised, the controller logic will accept incorrect input that is different than the real state of the plant, $y_k \neq z_k$.

3. When the controller is compromised, it will generate a control command that does not satisfy the intended logic of the controller, $u_k \neq K(y_k)$, where K is the control logic and a function of the sensor measurements, y_k.

In order to detect the above attacks, hardware- and/or software-based intrusion detection systems are designed and developed to monitor network and system activities to detect malicious acts [41]. An attack's ability to elude detection by the IDS determines its covertness. Covertness can be analyzed in the traditional IT domain as well as the physical domain; in this work we are interested in the latter.

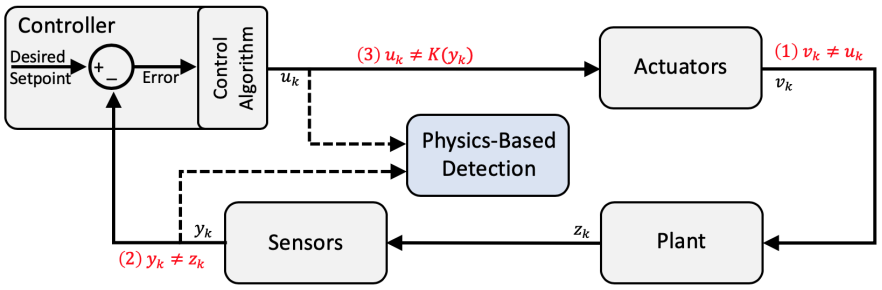

Figure 2.2 General block diagram of an ICS continuous feedback-loop indicating where cyber-attacks can target and compromise the system: (1) actuators, (2) sensors, or (3) controller. Here, altered data from the attack is highlighted in red which the physics-based detection intends to detect.

Physics-based detection focuses on the problem of using real-time measurements to detect attacks. Two popular methods are anomaly-based and safety limit detection. Anomaly-based detection relies on the fact that physical processes must follow immutable laws of physics. In general, detection is done through the use of mathematical models of the system to predict the expected measurement, $\hat{y}_k$, using the current control commands, u_k, and previous sensor measurement, y_{k-1}.

The anomaly detection test itself uses a time series of residual values, r_k. The residual is the difference between the measured and predicted values, given as

$$r_k = |y_k - \hat{y}_k| \tag{2.8}$$

The residuals are then used in either a stateless or stateful anomaly test. A stateless test raises an alarm every time a residual value reaches a threshold value, $r_k \geq \tau$, shown by Figure 2.3. In a stateful test the historical changes of the residual are kept as an additional statistic denoted as S_k, to generate an alert if $S_k \geq \tau$. There are many

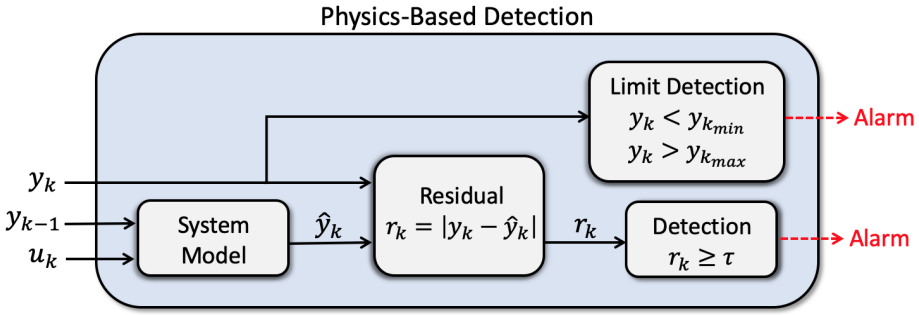

Figure 2.3 Physics-based detection where the residual between the measured value, y_k, and model prediction, $\hat{y}_k$, is used for an alarm if exceeding a given threshold, τ.

ways to keep track of the residual for a stateful test, such as taking an average over a time-window, an exponential weighted moving average, or using change detection statistics such as the non-parametric cumulative sum statistic.

On the other hand, safety limit detection is based on the normal operating range of the system variables. In this case an alarm is raised if the sensor measurement, y_k, exceeds lower or upper limits, given as

$$y_k < y_{k_{\min}} \tag{2.9}$$

and

$$y_k > y_{k_{\max}} \tag{2.10}$$

From the standpoint of a cyber-attacker the measure of covertness in regards to physics-based detection is important. Remaining covert is often necessary in order to be successful in reaching their attack goals.

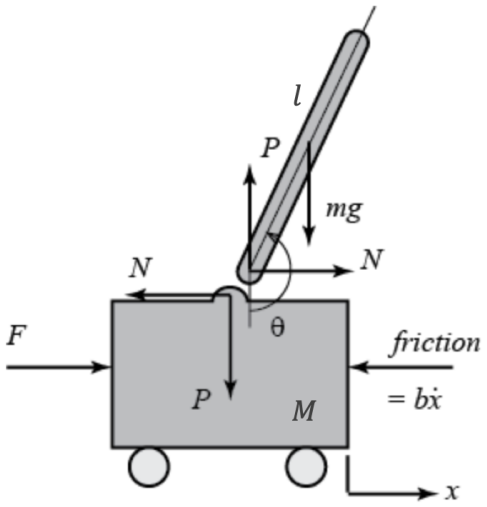

Figure 2.4 Schematic showing the forces acting on an inverted pendulum attached to a cart. Image adapted from Messner and Tilbury [66].

2.3 Proposed System Identification Attack

In this section, we present the proposed covert active system identification attack approach along with the running example of an inverted pendulum. We begin by deriving the *transfer function* of the inverted pendulum, which mathematically describes the behavior of the system. The transfer function is then used to perform simulations that model the behavior of the system under normal and attack scenarios. We then analyze the effectiveness and covertness of attacks that alter the derivative gain value.

2.3.1 Inverted Pendulum as a Target System

In this example, the control system objective is to keep the pendulum at the vertical position, i.e. a constant setpoint. To accomplish this objective, a PID controller is used to apply an input force to the cart on which the inverted pendulum is mounted. The input and system forces are shown in Figure 2.4. Using the system forces,

the transfer function can be derived. We present a partial derivation, for the full derivation the reader is referred to Messner and Tilbury [66]. First, the horizontal forces acting on the cart lead to the following

$$M\ddot{x} + b\dot{x} + N = F \tag{2.11}$$

and summing the forces on the pendulum results in

$$N = m\ddot{x} + ml\ddot{\theta}\cos\theta - ml\dot{\theta}^2\sin\theta \tag{2.12}$$

From here, substitution gives the first governing equation

$$(M+m)\ddot{x} + b\dot{x} + ml\ddot{\theta}\cos\theta - ml\dot{\theta}^2\sin\theta = F \tag{2.13}$$

We get the second governing equation by summing the forces perpendicular to the pendulum at the axis, giving

$$(I + ml^2)\ddot{\theta} + mgl\sin\theta = -ml\ddot{x}\cos\theta \tag{2.14}$$

where I is the moment of inertia of the pendulum. To linearize the governing equations we assume that the pendulum only has small deviations from the vertical position and use the small angle approximation. This lead to a set of linearized governing equations

$$(I + ml^2)\ddot{\phi} - mgl\phi = ml\ddot{x} \tag{2.15}$$

and

$$(M+m)\ddot{x} + b\dot{x} - ml\ddot{\phi} = F \tag{2.16}$$

To obtain the transfer function of the linearized governing equations, we first take the Laplace transform and assume zero initial conditions. The resulting Laplace transforms are given as

$$(I+ml^2)\Phi(s)s^2 - mgl\Phi(s) = mlX(s)s^2 \tag{2.17}$$

and

$$(M+m)X(s)s^2 + bX(s)s - ml\Phi(s)s^2 = U(s) \tag{2.18}$$

In this study, we are concerned with the output of the angle, $\Phi(s)$, and its relation to the force input, $U(s)$. We eliminate $X(s)$ from (2.17) and (2.18) by solving for $X(s)$ and then using substitution. The transfer function of the pendulum angle becomes

$$P_{\text{pend}}(s) = \frac{\frac{ml}{q}s^2}{s^3 + \frac{b(I+ml^2)}{q}s^2 - \frac{(M+m)mgl}{q}s - \frac{bmgl}{q}} \tag{2.19}$$

where

$$q = [(M+m)(I+ml^2) - (ml)^2] \tag{2.20}$$

The linearized transfer function of the inverted pendulum is used for the simulations carried out in this work.

2.3.2 Active System Identification Attack

The goal of a system identification attack is to increase the accuracy of the transfer function estimation - which represents the dynamics of the system. The accuracy

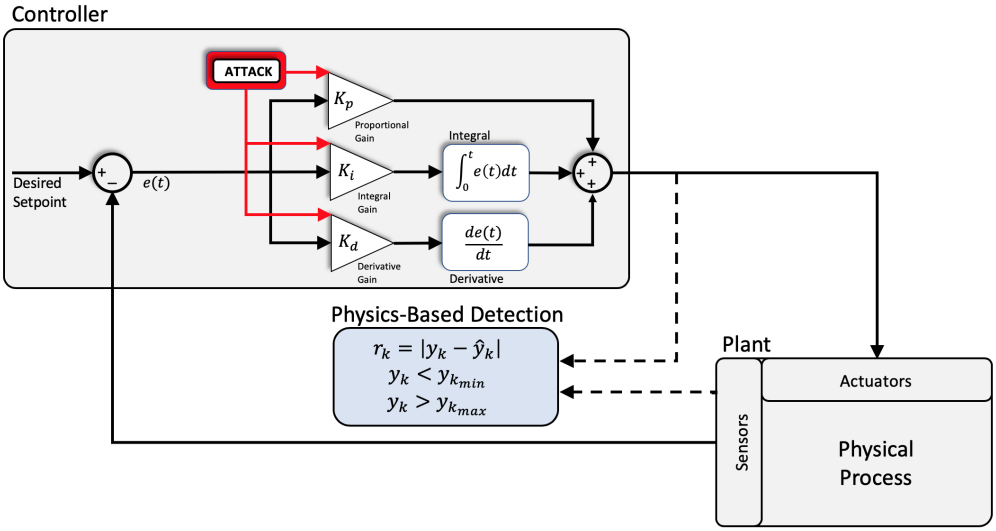

Figure 2.5 Block diagram of a continuous feedback-loop control system showing where our system identification attack targets the Proportional-integral-derivative (PID) gain calculation.

of system identification algorithms increases for data types that have high signal-to-noise ratios for the dynamic characteristics of the system, i.e. variable excitation. Thus, in order to force the excitation in the system, we employ a novel attack which briefly targets the PID gain values, K_p, K_i, and K_d, as depicted by Figure 2.5.

The performance of the attack is evaluated through a set of simulations performed in Simulink [58]. Simulink is a graphical programming environment for modeling, simulating, and analyzing multi-domain dynamic systems. We utilize its environment to compute the control command, u_k, using the angle measurement, y_k, in a simulated environment, shown in Figure 2.6.

In this experiment, we ran 100 trial simulations under normal and different attack scenarios. The normal operation is based on "tuned" PID gain values of 162, 124, and 5, respectively. The different attack scenarios in this work reduces the derivative

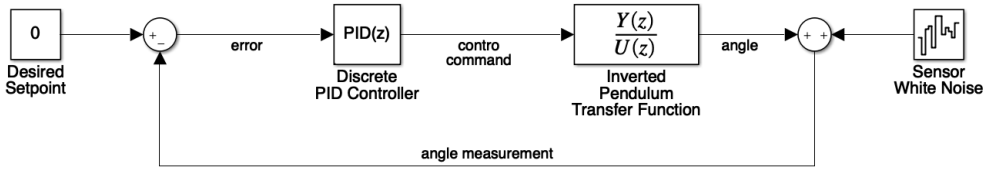

Figure 2.6 Simulink block diagram of an inverted pendulum transfer func-tion controlled using a discrete PID controller.

gain in intervals of 20%, i.e. the derivative gain value is 5, 4, 3.2, 2.56, etc. In order to emulate a real-world control system, we apply a discrete PID controller running at 200 Hertz, add white noise to the sensor measurements, and run the simulation for 4 seconds of real-time. The resulting angle measurements under different derivative values is shown in Figure 2.7. Hence, it is clear that the derivative gain attack can force excitation of the system variable, forcing the pendulum to oscillate about its setpoint.

To evaluate the accuracy of the estimated transfer functions we calculate the Normalized Root Mean Square Error (NRMSE) measure of the goodness of the fit. The NRMSE is a fitness value indicator of how well an estimated model matches validation data, given mathematically as

$$\text{NRMSE} = 100\left(1 - \frac{\parallel y - \hat{y} \parallel}{\parallel y - \text{mean}(y) \parallel}\right) \tag{2.21}$$

where y is the validation data and $\hat{y}$ is the estimation model. The validation data used in this analysis is generated using an impulse response simulation using the linearized transfer function given in (2.19). To make a direct comparison, the sensor noise is removed from these simulations. It can be seen in Figure 2.8 that the esti-

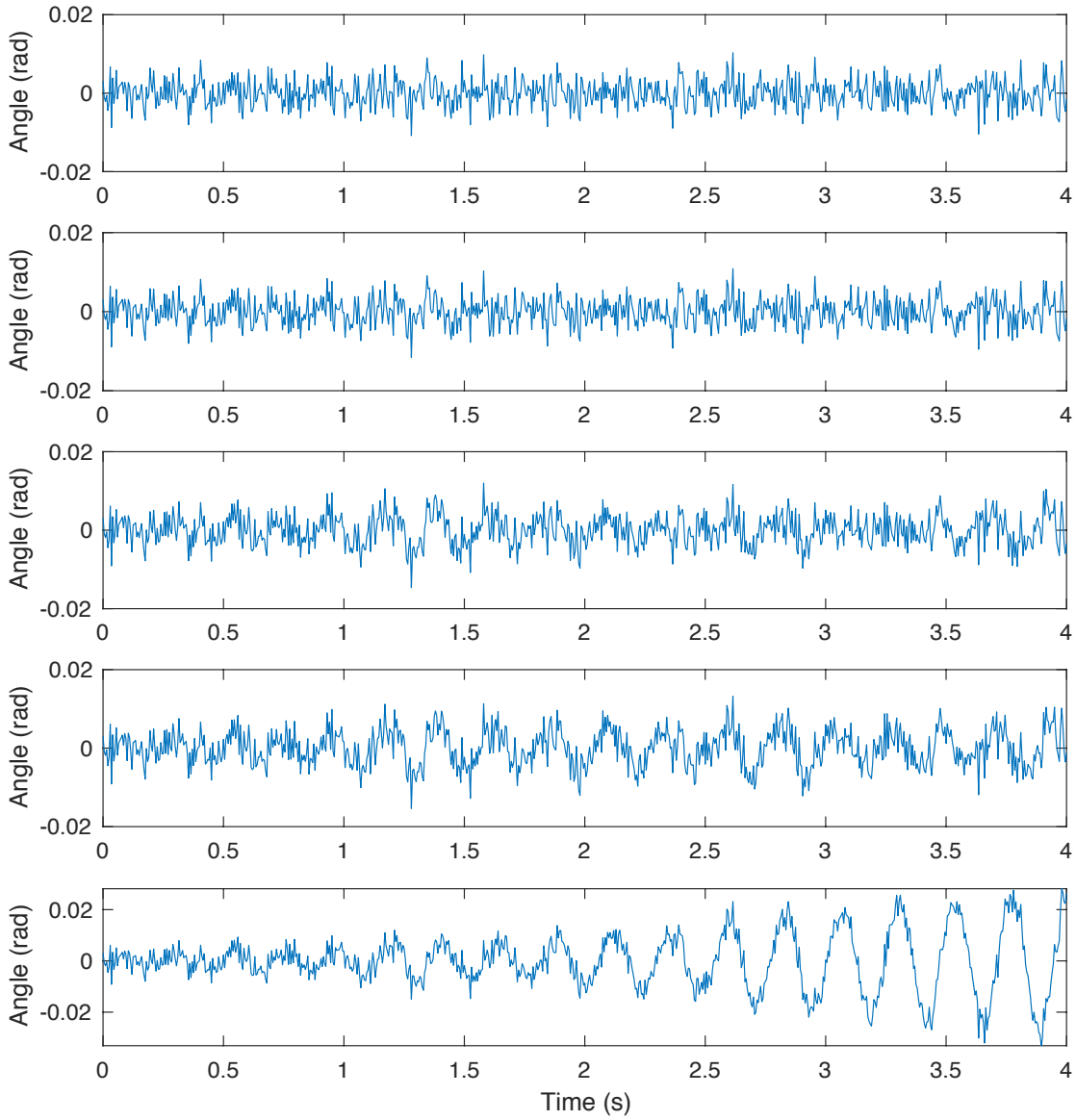

Figure 2.7 Results of the inverted pendulum angle under different derivative attack scenarios. From top to bottom the derivative gain is 5 (no attack), 3.2, 1.05, 0.67, and 0.27, respectively.

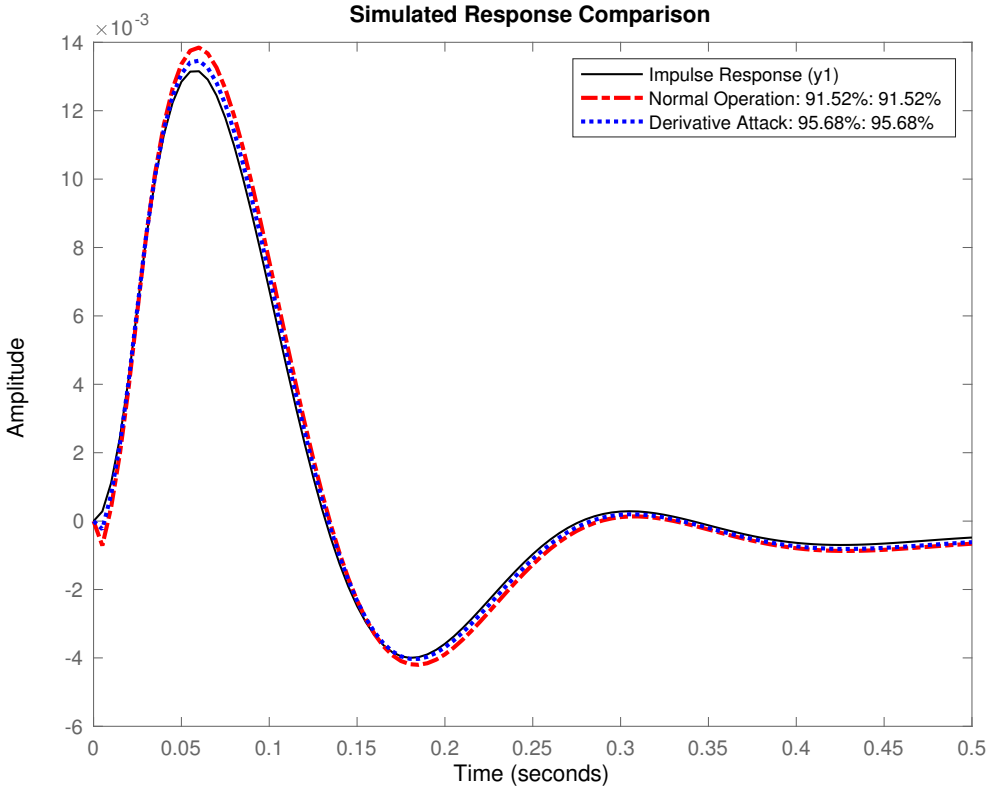

Figure 2.8 Normalized root mean square error of an estimated transfer function. Here the derivative of the attack estimation has been reduced from 5 (no attack) to 1.05.

mated transfer function has an increased NRMSE when we employ our attack and the derivative term is decreased. The NRMSE mean value under the different attack scenarios is presented in Figure 2.9. It is demonstrated that the transfer function estimation in general increases as the derivative term is reduced and excitation of the angle measurement is increased. However, we must also consider the covertness of these attacks, which is analyzed in the next section.

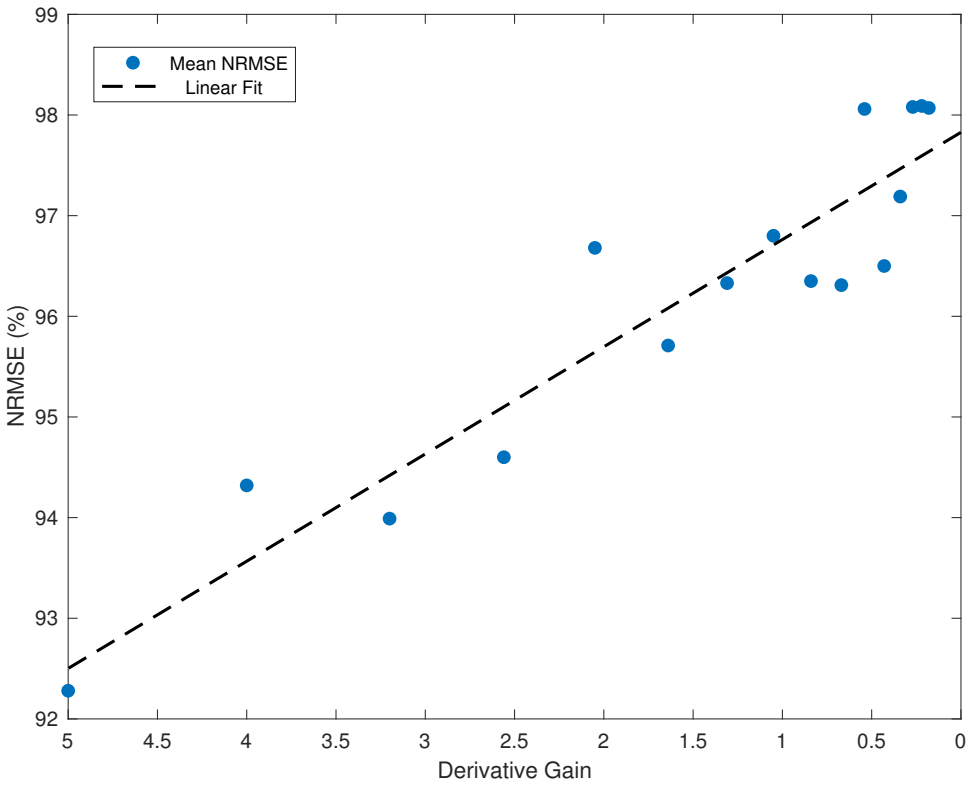

Figure 2.9 Normalized root mean square error results under different derivative attack scenarios. Each data point represent the mean of 100 simulations.

2.3.3 Covertness to Physics-based Detection

The measure of covertness in regards to physics-based detection is analyzed in both anomaly and limits detection. In an anomaly detection test the time-series residual values are calculated based on control commands that are sent to the actuator and the resulting angle measurement based on the previous measurement (Figure 2.3). In our attack, we do not inject false data into the control loop, i.e. the actuator and anomaly detection algorithm receive the same control command. Therefore, the residual values are calculated to be the sensor noise when system disturbances are not present. Thus, we argue that our attack is covert to anomaly based detection statistics.

On the other hand, the attack affects the angle measurements and limit based detection can potentially identify the attack. Therefore, the covertness depends on the amount of excitation we force during the attack and the allowable limits that are set. To determine the limits in this study, we assume the angle data follows a Gaussian or normal distribution and select a limit that would give a false positive alarm once per year. This is calculated using the approximate expected frequency equation where the frequency of occurrence is 1 in

$$\frac{1}{1 - \text{erf}\left(\frac{k\sigma}{\sqrt{2}}\right)} \tag{2.22}$$

Here, erf is the error function and k is the number of standard deviations, σ. Using the frequency of our controller we get $k \sim 6.4$. Since the angle mean is 0 and our

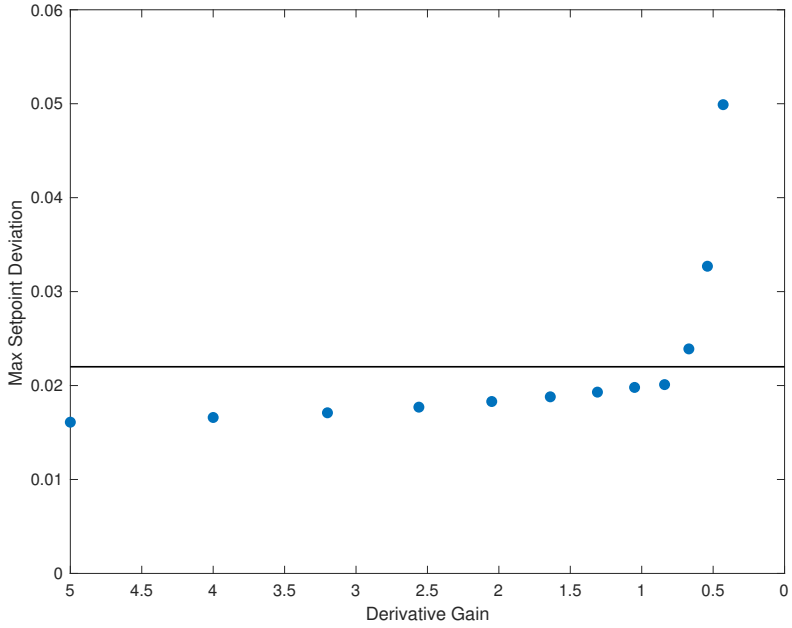

Figure 2.10 Absolute maximum deviation of the angle measurement from the setpoint under normal (Derivative = 5) and different derivative attack scenarios. Here the horizontal line represents the maximum value of once a year deviation under normal operation.

limits are symmetric, the detection limit for an alarm is calculated as

$$|y_k| > 0.022 \tag{2.23}$$

Therefore, we infer the covertness of the attack with a comparison of the absolute maximum deviation from the setpoint under each derivative attack scenario. It can be seen in Figure 2.10 that the absolute maximum deviation from the setpoint slowly increases until the derivative is reduced to below a value of ~ 0.6, where the system becomes unstable. We argue that the attack would likely remain covert until the unstable region is reached.

2.4 Conclusion

At present time, we propose an attack which targets the PID gain values of a controller. The intent of the attack is to force excitation in system parameters in order to increase the accuracy of data-driven system identification in constant setpoint control systems. The effectiveness of the attack is analyzed with the use of simulations, and we demonstrate that the estimated system model's accuracy increases as we reduce the derivative gain value. Additionally, the PID attack is covert in regards to physics-based anomaly detection by virtue of not injecting false data into the system. However, physics-based limits detection can potentially detect our attack if the altered PID gains force too much excitation into the system.

Currently, we manually change the derivative gain and check the results of the estimated model. Since the actual system model is unknown from an attackers standpoint, our future work includes the implementation of an algorithm that watches the parameter deviations from the setpoint and alters the PID gains in order to maximize excitation while staying covert to limits detection. Additionally, we plan to investigate the effectiveness of our PID attack in a real-world simulated environment such as the Tennessee Eastman Process. However, we encourage the development of new identification techniques in order to identify attacks of this nature.

The electrical power system has always been at a constant threat to physical damage from storms. However, cyber attacks such as the PID attack are now presenting researchers with new challenges for energy security. The next three chapters will describe an operational resilience metric for Modern Distribution Systems (MDS) to better ensure energy security in the future.

CHAPTER 3:

AN OPERATIONAL RESILIENCE METRIC FOR MODERN POWER DISTRIBUTION SYSTEMS[1]

3.1 Introduction

Today's modern society has become increasingly dependent on the safety and efficiency of modern control systems. At the foundation of our social and economic way of life, you will find the electrical power system. It constitutes the most vital component of the nation's interdependent critical infrastructure systems. To ensure a constant supply of electrical power, utilities and researchers have designed and operated the power system under the consideration of a set of reliability metrics. These metrics account for normal weather conditions and component failure but do not consider extreme events [39] as it is generally not cost effective [59].

In the early stages of power system construction, relatively little attention was given to the distribution networks when compared with generation and transmission. Generation and transmission outages are large impact events, whereas distribution

[1] © 2020 IEEE. Reprinted, with permission from, T. Phillips, T. McJunkin, C. Rieger, J. Gardner, and H. Mehrpouyan, "An Operational Resilience Metric for Modern Power Distribution Systems," 2020 IEEE International Conference on Software Quality, Reliability, and Security (QRS-C), Macau, China, 2020

outages have smaller localized effects. However, analysis of practical utility failure registers and fault statistics reveals that distribution networks contribute the most to customer interruptions and failure events [122]. The data shows that 90% of power outages occur in the distribution system alone [111].

Complete disaster-resistant protection of the distribution system is highly impractical, requiring far too much investment [13]. Therefore, researchers have begun to focus their efforts on resilience, not reliability, metrics. The concept of reliability and resilience are similar but have distinct differences in both scale and duration. Reliability research concentrates on small-scale random faults of power system components caused by internal factors [65]. For example, reliability encompass the N-1 contingency planning or a single component failure. At the basic level, it ensures that no single point of failure would cause the entire system to stop working. In contrast, resilience considers extreme conditions, or N-k failures, where k may extend well beyond a single failure point. Resilience anticipates that during extreme events a certain amount of degradation to the system is unavoidable. Thus, it can be said that resilience is characterized by a systems ability to resist, respond, and recover from a disturbance or attack in order to maintain core operations [87].

Electrical component failures during extreme weather events such as hurricanes, winter storms, flooding, wildfires, etc., push well beyond the limitations of the current distribution system which has been designed to meet reliability metrics. In the United States, between 2003 and 2012, extreme weather events caused an estimated 679 widespread power outages, affecting at least 50,000 customers [111]. Notable events include Hurricane Katrina [94], Hurricane Sandy [31], and the wildfires across California [37] which forced the utility company to de-energize power lines in an effort

to mitigate the risk of starting new fires, resulting in widespread blackouts. Making matters worse, our energy infrastructure is aging [123] and climate change is expected to continually increase the frequency and intensity of extreme weather[111]. A 2012 study [8] estimates the cost of weather-related outages to the tune of $25 to $70 billion annually. Moreover, these prolonged power outages can put the public at a significant risk, having the potential for loss of life. Data indicates that the 2003 blackout in New York resulted in approximately 90 deaths [5]. In light of these factors, it is of upmost importance for researchers to address the growing concern of electrical power supply during extreme weather events. New methodologies which enable utilities to effectively manage power systems must be developed.

In this work, we present a novel real-time operational resilience metric that utilizes the controllable assets in modern distribution systems. The metric is an operational aggregation of assets adaptive capacity in real and reactive power. It indicates the magnitude and duration of a disturbance a system is capable of withstanding, and maintain load demand and stability in voltage and frequency.

The rest of this chapter is organized as follows: Section 3.2 gives an introduction to resilience and a literature review. The modern distribution system (MDS) and background on power stability is discussed in Section 3.3. We introduce our resilience metric and give the mathematical details in Section 3.4. Finally, the conclusion and future work are covered in Section 3.6.

3.2 Resilience in Power Systems

Pioneering work in resilience of engineering systems is presented by Hollnagel, Woods, and Leveson in [34]. Many definitions have been coined by well respected organizations in engineering literature [38, 69, 99, 63, 61], policy directives [112], and the

academic community [97]. A general commonality among sources are the ability to anticipate a possible disaster, adopt effective measures to decrease loss of load and system component failure before and during the disaster, and restore power quickly through controlled reconfiguration. Quantification of resilience in power systems is an emerging field. It is an important open area of research, of great interest to utilities and stakeholders.

To date, power systems are regulated based upon reliability metrics. This dates back to the Energy Policy Act of 2005 [77], where Congress gave the Federal Energy Regulatory Commission authority to oversee the reliability of the bulk-power systems. The purpose was to ensure the reliable operation where an instability, uncontrolled separation, or cascading failures would not occur as a result of a sudden disturbance. There are two main metrics used to measure the reliability; the system average interruption duration index and the system average interruption frequency index. However, some jurisdictions consider storm related outages as extreme events, and thus, do not include them as inputs into the reliability metrics [18].

There have been several proposed resilience metrics, such as the resilience triangle and trapezoid. The resilience trapezoid is an extension of the resilience triangle proposed in [109] by Tierney and Bruneau. Unlike the triangle which only considers the disturbance of a system, the trapezoid assesses the resilience through three phases; the disturbance, degradation, and the restorative state. The resilience trapezoid has been applied to a power system framework as proposed by Panteli et. al [86], which extends the works in [98, 82, 32, 81].

Another proposed resilience approach is introduced by Rieger [96]. In this work he takes a controls systems perspective but doesn't apply the metric directly to power

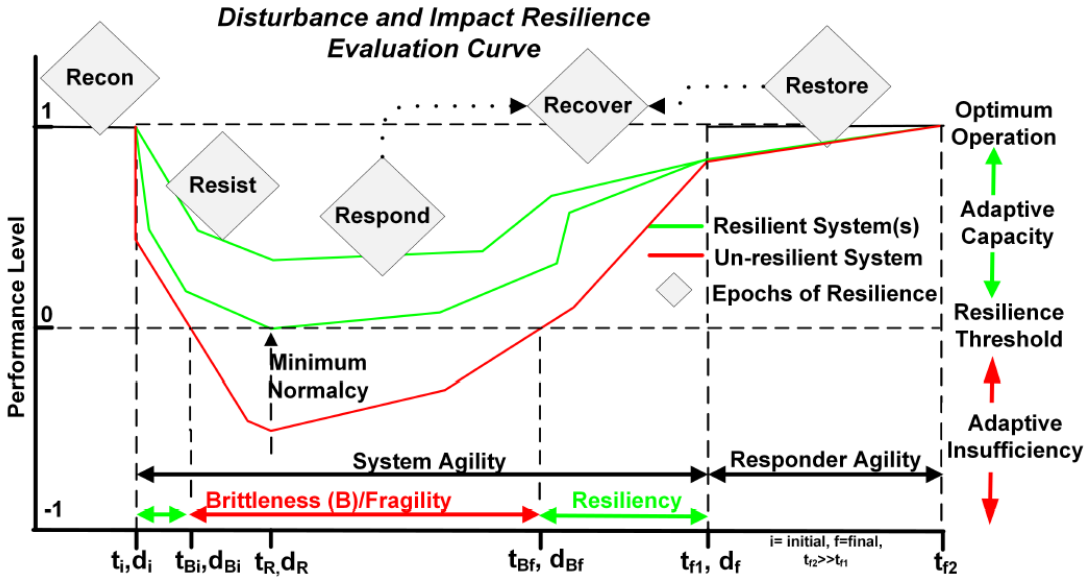

Figure 3.1 The disturbance and impact resilience evaluation curve, show-ing the 5R's of resilience. Image adapted from [96].

systems. System resilience is shown by the notional DIRE curve in Fig. 3.1. The novel concept introduced is the idea of a resilience threshold, or the maximum ac-ceptable level of degradation to the system. This degradation level may be defined by a percentage of loss load in the system, ability to retain critical loads, etc. The performance level from optimal operation to the resilience threshold is defined by the systems adaptive capacity. The adaptive capacity can be defined as the ability of the system to adapt or transform from an impact event. An adaptive insufficiency can be considered the inability of the system to adapt or transform from an impact, indicating an unacceptable performance loss due to the given disturbance.

In [125], Woods describes an aspect of assessing a systems resilience is whether the system is known to be near an operation boundary condition. This provides information about how well the system can stretch in response to a future disturbance. In the context of power systems, McJunkin and Rieger expand this concept and

introduce a resilience metric to evaluate the design of MDS [60]. Their approach is based on the adaptive capacity of a system, defined by an asset or aggregation of assets. In this work, they demonstrate the temporal adaptive capacity, or amount of flexibility or stretch, in the real and reactive power of the controllable assets while also considering energy limitations. The resulting metric can by represented by a three dimensional surface, referred to as a manifold, that represents the maximum adaptive capacity in real and reactive power over time. The metric can be thought of as a mapping to the DIRE curve, indicating the maximum disturbance in amplitude and duration due to cyber or physical disturbances that can be withstood.

The most recent contributions of the resilience metric proposed in [60] have been developed as a design tool for MDS. The metric uses a neutral bias assumption to describe the adaptive capacity of the assets which limits the ability to accurately model many assets. In addition, the metric does not lend itself well for use as a real-time operational metric. Therefore, the goal of this paper is to develop the metric to have a more accurate representation of the asset adaptive capacity. In addition, we will bring the metric to a state where it is suitable to be used as a real-time operational tool. Therefore, it can be utilized by control operators to make resilience based decisions before, during, and after disturbances. The details of the extension of the metric are covered in Section 3.4. First, a background on MDS is covered in the following section.

3.3 Power Distribution System

In this section, a brief introduction to the modernization of the power grid is given. Then the concepts of power stability in voltage and frequency necessary for the development of the metric proposed in this paper are covered in sufficient detail.

3.3.1 Grid Modernization

The current modernization of the electrical power system has presented a dramatic shift in the way power is generated and transmitted. It is moving from the traditional centralized generation to a more distributed power generation architecture. The MDS integrates information and operational technologies which can monitor, communicate, and control assets in real-time. It is predicted that these systems will include a high penetration of controllable distributed assets in generation and storage, as well as controllable loads. Control of these assets have many purposes, including support of the voltage and frequency across the distribution network, economic benefits, and reliable utilization of interconnections such as power lines, transformers, and switches.

This evolving landscape has added a new layer of complexity to distribution systems. It presents many new technical challenges and opportunities for researchers. For example, what metric best describes the systems resilience and how should these metrics be utilized to make control decisions during normal operation or before, during, and after extreme events? The modernization of the grid has a tremendous potential for increasing resilience but much work is still needed in how to accomplish it. In this context, researchers have suggested numerous resilience based improvements in areas including microgrids [14, 12], circuit reconfiguration [22, 126, 74, 44, 120, 127, 35, 75], improved dispatch and scheduling of resources [17, 36, 43], and flexible local resources, such as generation, load, and energy storage [70].

3.3.2 Power and Stability

Stability of the distribution system is defined in terms of voltage and frequency. Frequency stability requires balancing of the generation of real power, P, and the load demand. On the other hand, voltage stability requires the balancing of reactive power,

Q, across the network due to different types of loading on the system. Therefore, a resilience metric must address both the real and reactive power to be extensible in distribution systems. The real and reactive power components define a systems apparent power, S in the complex S-plane where

$$S(\theta) = \sqrt{P^2 + Q^2} \tag{3.1}$$

where the real power in relation to the apparent power is

$$P(\theta) = S\cos(\theta) \tag{3.2}$$

and the reactive power is

$$Q(\theta) = S\sin(\theta) \tag{3.3}$$

here θ is the angle measured from horizontal. In power systems this angle is often referred to as the power factor angle, given as

$$\theta = \arctan\left(\frac{Q}{P}\right) \tag{3.4}$$

In this paper, the angle θ is the measurement from 0 to 2π. Here, the left hand plane, $\pi/2 < \theta < 3\pi/4$, is where an asset acts as a sink absorbing power from the system.

The normalized maximum apparent power at power factor angle θ is depicted in the S-plane in Fig. 3.2. Here, only quadrant I is shown, where real and reactive power are positive. The highlighted region is the domain or reachable output in real and reactive power. In the following section we use these principles to define the domain of assets power output used in our operational adaptive capacity metric.

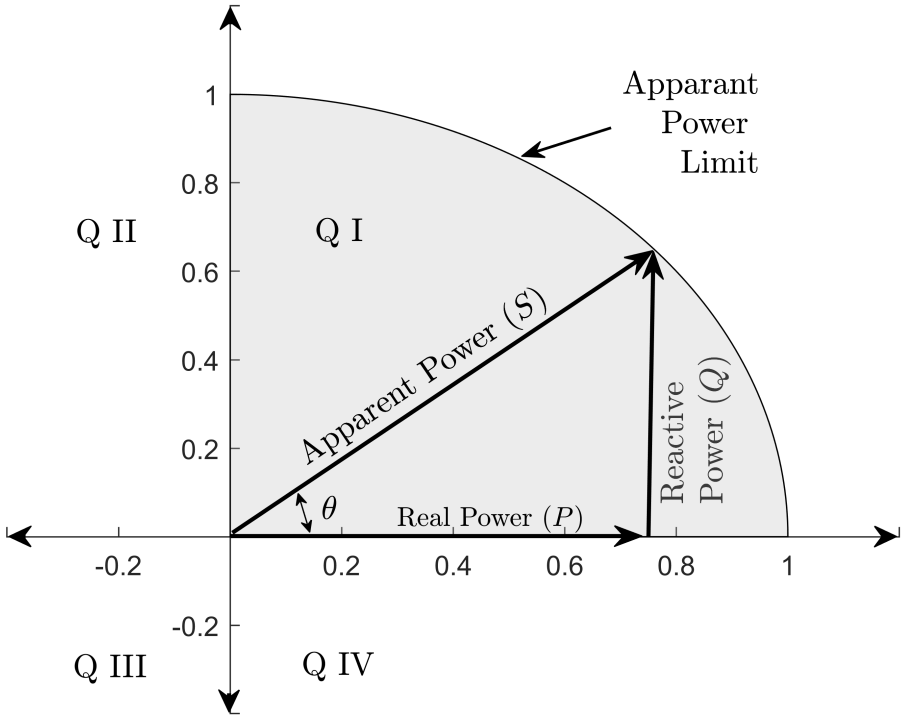

Figure 3.2 Normalized apparent power, S, in quadrant I of the complex S-plane. The highlighted region represents the domain or reachable output in real and reactive power.

3.4 Adaptive Capacity Methodology

This section describes the mathematical background to calculate the operational adaptive capacity resilience metric herein proposed. The metric is based on the adaptive capacity of the assets, which is a measure of their control ability to move from the current operating point in both real and reactive power over time. Assets must be described by a set of operational characteristics which include the nameplate rated capacity, energy capacity, latency, and rate of change limitations. Using these characteristics, the general process to calculate the adaptive capacity is as follows: determine the control domain of the real and reactive power, determine the flexibility from the current operating point, then account for latency and ramp rates, then impose energy constraints.

3.4.1 Real and Reactive Power Domain

The real and reactive power domain, or capability of the asset, is denoted $P_{\in}$ and $Q_{\in}$, respectively. The assets nameplate capacity defines the real power maximum, $P_{\max}$, and minimum, $P_{\min}$, as well as the reactive power maximum, $Q_{\max}$, and minimum, $Q_{\min}$. Thus, the first limit placed on the domain of the real power is

$$P_{\min} \leq P \leq P_{\max} \tag{3.5}$$

and the reactive power is

$$Q_{\min} \leq Q \leq Q_{\max} \tag{3.6}$$

here, the maximum is assumed to be in the positive plane and the minimum in the negative plane, given mathematically for the real power

$$P_{\min} \leq 0 \leq P_{\max} \tag{3.7}$$

and for the reactive power

$$Q_{\min} \leq 0 \leq Q_{\max} \tag{3.8}$$

These values are then used to determine the bounding constraints of the asset in the complex S-plane, given as

$$S(\theta) \leq \sqrt{P^2 + Q^2} \tag{3.9}$$

here, the real and reactive power is a function of the power factor angle and dependant on the maximum power in each quadrant of the S-plane. The calculation for the apparent power constraint for quadrant I to quadrant IV is then given respectively as

$$\underset{0 \leq \theta \leq \frac{\pi}{2}}{S(\theta)} \leq \left(P_{\max}^2 \cos(\theta) + Q_{\max}^2 \sin(\theta)\right)^{\frac{1}{2}} \tag{3.10}$$

$$\underset{\frac{\pi}{2} \leq \theta \leq \pi}{S(\theta)} \leq \left(P_{\min}^2 \cos(\theta) + Q_{\max}^2 \sin(\theta)\right)^{\frac{1}{2}} \tag{3.11}$$

$$\underset{\pi \leq \theta \leq \frac{3\pi}{2}}{S(\theta)} \leq \left(P_{\min}^2 \cos(\theta) + Q_{\min}^2 \sin(\theta)\right)^{\frac{1}{2}} \tag{3.12}$$

$$\underset{\frac{3\pi}{2} \leq \theta \leq 2\pi}{S(\theta)} \leq \left(P_{\max}^2 \cos(\theta) + Q_{\min}^2 \sin(\theta)\right)^{\frac{1}{2}} \tag{3.13}$$

Using the rated power and limits in the S-plane, the asset capability in the real and reactive power can be calculated. In the positive plane the minimum of the two constraints will define the boundary of the domain. In the negative plane, the

absolute minimum of the two constraints defines the domain boundary. Therefore, the real power domain for quadrants I and IV, where the real power is positive, is given by

$$\underset{\frac{3\pi}{2}\leq\theta\leq\frac{\pi}{2}}{P(\theta)} \leq \min\left[S\cos(\theta),\ P_{\max}\right] \tag{3.14}$$

and the domain for quadrants II and III, where the real power is negative is

$$\underset{\frac{\pi}{2}\leq\theta\leq\frac{3\pi}{2}}{P(\theta)} \geq -\min\left[|S\cos(\theta)|,\ |P_{\min}|\right] \tag{3.15}$$

Similarly, the domain of reactive power in quadrants I and II is given by

$$\underset{0\leq\theta\leq\pi}{Q(\theta)} \leq \min\left[S\sin(\theta),\ Q_{\max}\right] \tag{3.16}$$

and in quadrants III and IV are

$$\underset{\pi\leq\theta\leq2\pi}{Q(\theta)} \geq -\min\left[|S\sin(\theta)|,\ |Q_{\min}|\right] \tag{3.17}$$

Using the real and reactive power domain in the positive and negative quadrants, the union of the two gives the overall domain. For the real power this is given as

$$P_{\in}(\theta) = \left\{P\middle|\frac{3\pi}{2}\leq\theta\leq\frac{\pi}{2}\right\}\cup\left\{P\middle|\frac{\pi}{2}\leq\theta\leq\frac{3\pi}{2}\right\} \tag{3.18}$$

and similar for the reactive power

$$Q_{\in}(\theta) = \left\{Q\middle|0\leq\theta\leq\pi\right\}\cup\left\{Q\middle|\pi\leq\theta\leq2\pi\right\} \tag{3.19}$$

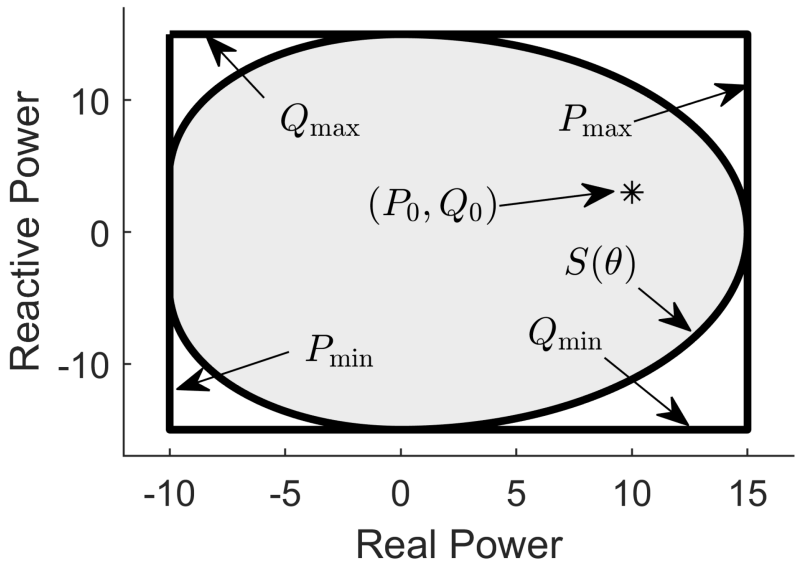

Figure 3.3 The shaded region represents an assets real and reactive power domain based on its rated nameplate power capacity. The negative real power represents an asset absorbing power from the grid, such as battery storage when charging.

The domain of the asset real and reactive power capability is depicted by the shaded region in Fig. 3.3. It should be noted that some assets, such as solar, wind, and hydro, should not be considered to have constant rated limits and the domain may need to be updated. For example, solar generation is dependant on real-time solar irradiation and therefore should be updated as solar conditions change. Next, we will discuss how the power flexibility is calculated using the operational power output.

3.4.2 Real and Reactive Flexibility

The amount of flexibility the asset has in the real and reactive power from the operating point is denoted as, P_Δ and Q_Δ, respectively. This flexibility is calculated using the real and reactive power domain of the asset and the current operation point of

the asset, P_0 and Q_0. Thus, it is a transformation of the power domain around the operating point, given as

$$P_\Delta(\theta) = P_\in - P_0 \tag{3.20}$$

and the flexibility of the reactive power is the same transformation using the reactive power domain and the current operating point

$$Q_\Delta(\theta) = Q_\in - Q_0 \tag{3.21}$$

Here, and in further adaptive capacity derivation, θ is the angle measured from the operating point. The resulting flexibility is depicted in the top plot of Fig. 3.4. However, the temporal characteristics of the asset, shown in the bottom plot of Fig. 3.4, need to be accounted for and are developed in the following section.

3.4.3 Latency and Ramp Rate

The latency of an asset is the time delay before changes to the power output can be made. It may consist of multiple factors including starting latency or a control latency. Starting latency is a property of the asset, for example, a diesel generator can't supply power right when turned on. Control latency is the time required between data being received, adjustments made to the output power, computationally or by an operator, to the time the control command is received by the asset. For the purpose of this paper, we consider all latencies to be aggregated into a single latency variable, λ.

The ramp rate defines how quick an asset can ramp up or down, after the latency, from the current operating position over time, t. The real power output when ramping

up is given as

$$P(t)^{+} = \begin{cases} 0, & \text{if } t \leq \lambda \\ \frac{dP^{+}}{dt}(t-\lambda) & \text{if } t > \lambda \end{cases} \tag{3.22}$$

and when ramping down is

$$P(t)^{-} = \begin{cases} 0, & \text{if } t \leq \lambda \\ \frac{dP^{-}}{dt}(t-\lambda) & \text{if } t > \lambda \end{cases} \tag{3.23}$$

Similarly, the reactive power is given as

$$Q(t)^{+} = \begin{cases} 0, & \text{if } t \leq \lambda \\ \frac{dQ^{+}}{dt}(t-\lambda) & \text{if } t > \lambda \end{cases} \tag{3.24}$$

when ramping up, and

$$Q(t)^{-} = \begin{cases} 0, & \text{if } t \leq \lambda \\ \frac{dQ^{-}}{dt}(t-\lambda) & \text{if } t > \lambda \end{cases} \tag{3.25}$$

when ramping down. The latency and ramp rate constraints are depicted by the temporal flexibility in real power shown in the bottom plot in Fig. 3.4. Here, the shaded region represents the real power domain and the bounds are defined by the latency and ramp rates from the operation point, the maximum flexibility, and energy constraints. The following section describes the energy constraint of the asset.

3.4.4 Energy Constraints

It is possible that assets are constrained with energy limitations in the amount of real power when acting as a source providing power, or as a sink absorbing power. In the case of battery storage, it is constrained on both ends where it has an initial energy of E_0, and can only be charged (sink) to 100%, or $E_{\max}$, and it can only output power (source) until it is fully drained at 0%, or $E_{\min}$. The energy of the system changes as

$$E(t) = E_0 + \int_{t=0}^{t} P(t) * dt \tag{3.26}$$

where $P(t)$ is the operating real power over time. When an asset runs out of energy or the ability to absorb energy, the real power must go to zero. The necessary mathematical details have been covered to give the adaptive capacity equations covered in the next section.

3.4.5 Adaptive Capacity and Aggregation of Assets

The adaptive capacity of the asset is the bounded region between the flexibility and the temporal constraints in the positive and negative planes with respect to the operating point. The real power in the positive plane is given as

$$\underset{\frac{3\pi}{2} \leq \theta \leq \frac{\pi}{2}}{P_{\text{AC}}(\theta, t)} = \min \left[P(t)^{+},\ P_{\Delta}(\theta) \right] \tag{3.27}$$

and the negative plane

$$\underset{\frac{\pi}{2} \leq \theta \leq \frac{3\pi}{2}}{P_{\text{AC}}(\theta, t)} = -\min \left[|P(t)^{-}|,\ |P_{\Delta}(\theta)| \right] \tag{3.28}$$

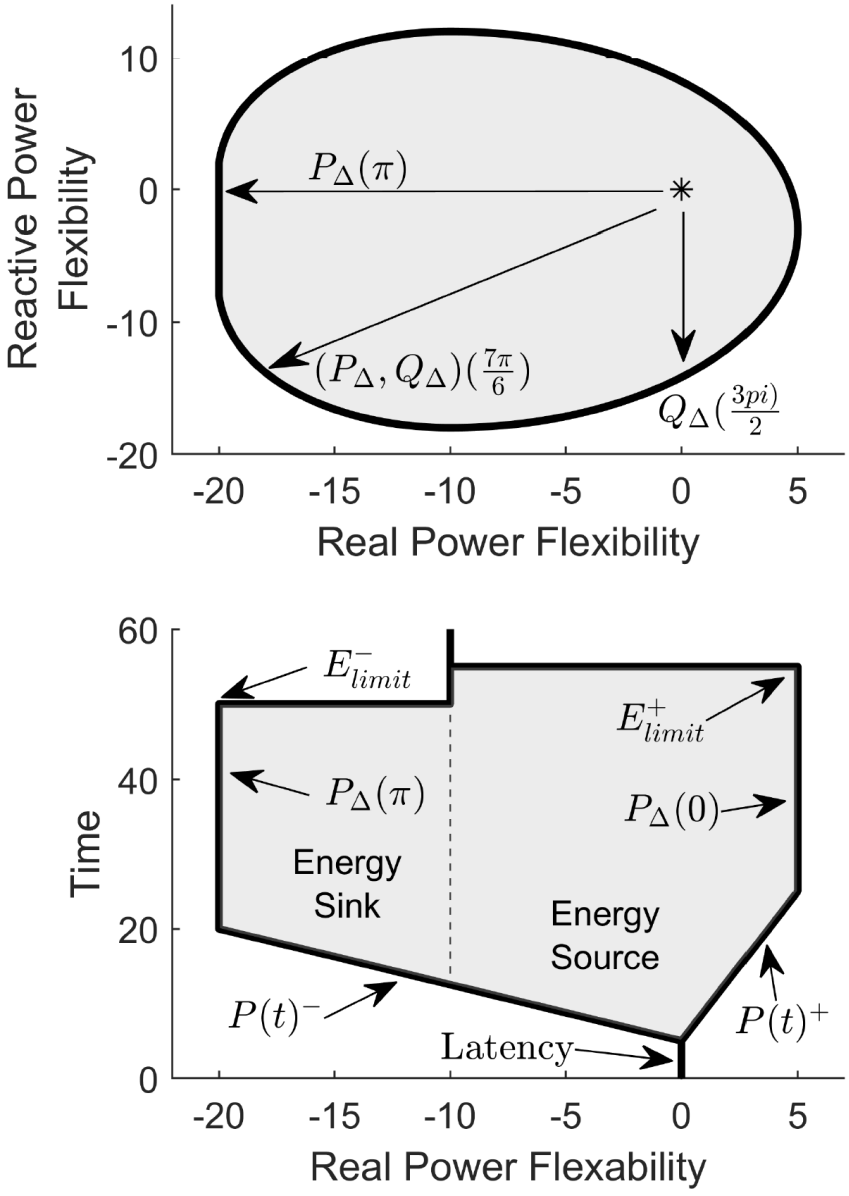

Figure 3.4 Top plot shows an assets real and reactive power flexibility from its current operating point. The bottom plot shows the temporal flexibility from the operating point which considers latency, ramp rates, and energy limits.

The reactive power it is given as

$$\underset{0\leq\theta\leq\pi}{Q_{\mathrm{AC}}(\theta,t)} = \min\left[Q(t)^{+},\ Q_{\Delta}(\theta)\right] \tag{3.29}$$

in the positive plane, and

$$\underset{\pi\leq\theta\leq 2\pi}{Q_{\mathrm{AC}}(\theta,t)} = -\min\left[|Q(t)^{-}|,\ |Q_{\Delta}(\theta)|\right] \tag{3.30}$$

for the negative plane. The resulting adaptive capacity using the ongoing example in this section is depicted by the manifold in Fig. 3.5. The manifold surface represents the maximum change the asset can make in real and reactive power, from the current operating point, over time. Recall that the x/y axis represent the adaptive capacity from the operating power. Therefore, when the energy limit has been reached the output power goes to zero which is indicated by the dashed line separating where the asset transitions between a sink and a source.

It is expected that the MDS will comprise a collection of distributed assets. The adaptive capacity may be an aggregation of local assets, such as a microgrid. The aggregation of assets determines the adaptive capacity of the controllable assets in the microgrid including the network connection. The aggregation in terms of real power is

$$P_{\mathrm{AC}}(\theta,t) = \sum_{k=1}^{n} P_{\mathrm{AC}_k} \tag{3.31}$$

and the reactive power is given by

$$Q_{\mathrm{AC}}(\theta,t) = \sum_{k=1}^{n} Q_{\mathrm{AC}_k} \tag{3.32}$$

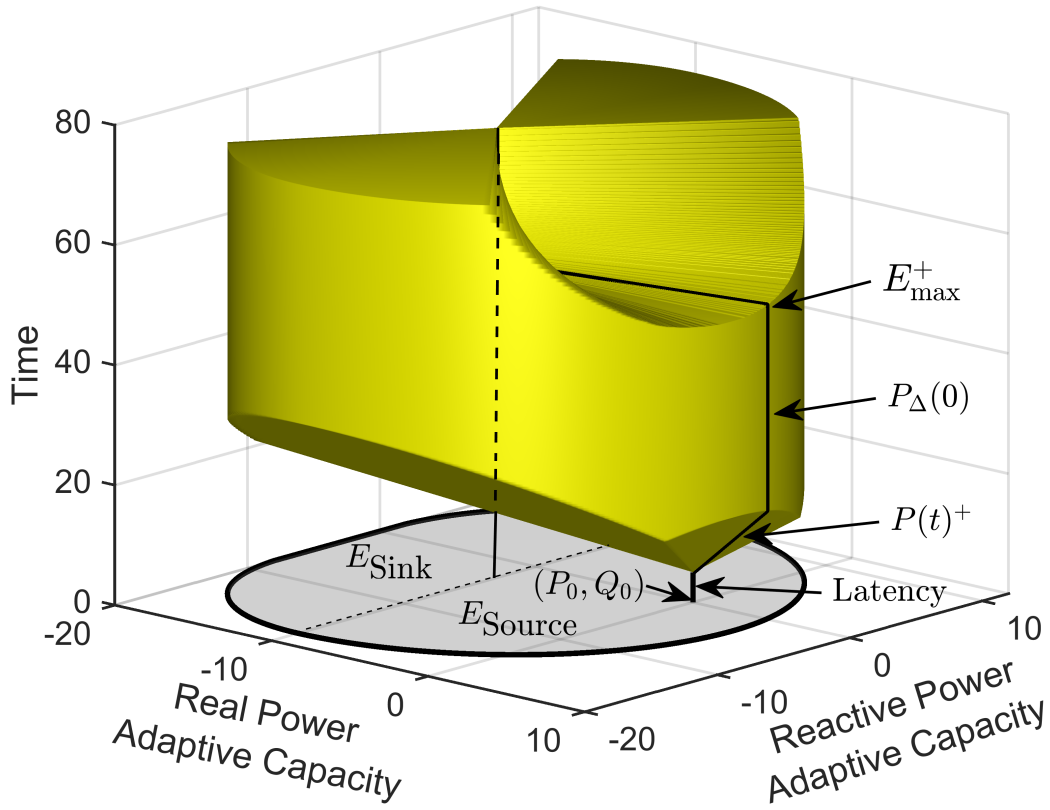

Figure 3.5 Asset's adaptive capacity manifold which represents the max-imum change in real and reactive power, from current operation, over time.

where n represents the total number of assets. The following section will demonstrate how this metric can be utilized as an operational metric.

3.4.6 Real-Time Operational Metric

Power distribution is a real-time system, therefore it's imperative that a resilience metric has the ability to reflect the real-time operation and conditions on the system. In this context, our algorithm updates the adaptive capacity using threshold triggers in power outputs, energy changes, and environmental conditions which we denote

C. Relevant environmental conditions depend on the assets in the system but may include factors such as solar irradiation, wind velocity, head pressure, etc... The operational metric is outlined by Algorithm 1.

Algorithm 1: Real-Time Adaptive Capacity Algorithm

Input : System assets, Real-time system data
Output: Assets adaptive capacity

begin
  Initialize: $P_{\in}, Q_{\in}$
  while system running
    $P_{\delta} = |P_{0_{n-1}} - P_{0_n}|$
    $Q_{\delta} = |Q_{0_{n-1}} - Q_{0_n}|$
    $E_{\delta} = |E_{0_{n-1}} - E_{0_n}|$
    $C_{\delta} = |C_{0_{n-1}} - C_{0_n}|$
    if any $\delta >$ threshold
      Update $P_{\in}, Q_{\in}$
      Update P_{Δ}, Q_{Δ}
      for time = 0 to t_{end}
        Update $P(t), Q(t)$
        Update $E(t)$
        for $\theta = 0$ to 2π
          Solve $P_{\mathrm{AC}}(\theta, t)$
          Solve $Q_{\mathrm{AC}}(\theta, t)$
        end
      end
    end
    for k=1 to n
      $\sum P_{\mathrm{AC}_k}(\theta, t)$
      $\sum Q_{\mathrm{AC}_k}(\theta, t)$
    end
  end
end

Table 3.1: Assets power parameters.

	Limits				Case I		Case II	
Asset	$P_{\max}$	$P_{\min}$	$Q_{\max}$	$Q_{\min}$	P_0	Q_0	P_0	Q_0
Network	1,050	-1,050	1,050	-1,050	930	450	0	0
Tie-line	500	-500	500	-500	0	0	450	217
Solar PV	315	0	315	-315	315	0	283	137
Battery	315	-315	315	-315	-315	0	197	96

3.5 Case Study

In this section, we demonstrate the adaptive capacity resilience metric proposed using the modified Institute of Electrical and Electronics Engineers (IEEE) 33-bus distribution system. We first introduce the modified IEEE 33-bus system and use a selected portion, or microgrid, to demonstrate in a case study the resilience of the system under two different scenarios. The first case represents the system under normal operation and the second represents a scenario where the network line experiences an outage.

3.5.1 IEEE 33-bus Model

The original IEEE model was designed as a radial network configuration. However, many studies have adapted the model to include tie-lines, thus, resembling a MDS meshed network, shown in Fig. 3.6. Here, the section used for this study has been highlighted and additional solar and battery storage assets have been added. The capacity limitations on the power line conductor for the network is given as $1,050$ kW and $1,050$ kVAR, and the tie-line limits are 500 kW and 500 kVAR for real and reactive power, respectively. Loading on buses 23-25 for the real power is 90, 420, and 420 kW, and the reactive power is 50, 200, and 200 kVAR, respectively.

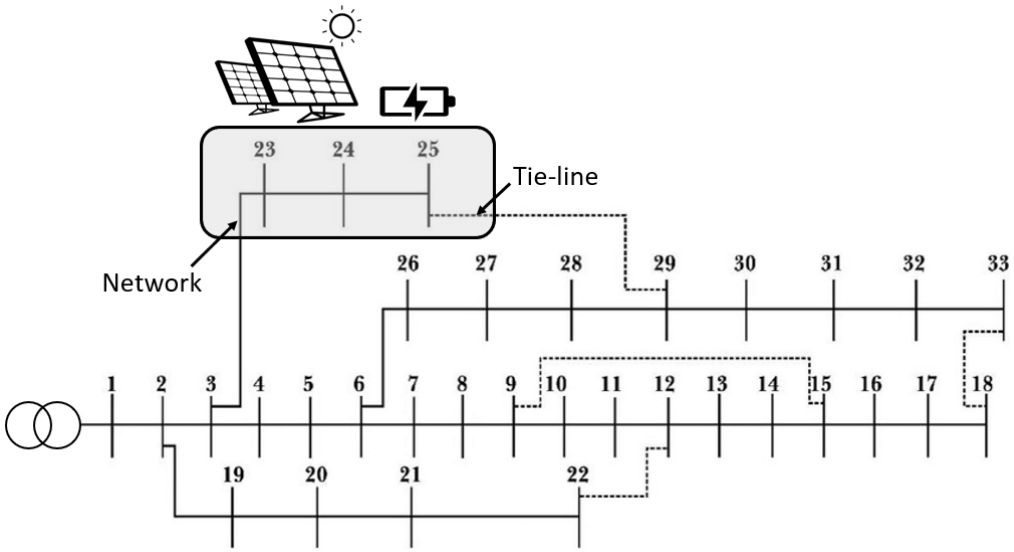

Figure 3.6 IEEE 33-bus distribution system model. Image adapted from [95].

To resemble a MDS solar generation and battery storage asset have been added to the model. Their limits are based on a high penetration of Distributed Energy Resources (DER). The maximum power is 30% of the maximum load which can be supplied by the network conductor, 315 kW. The battery storage is assumed to have a total capacity of 1,260 kWh, i.e. under its max output (315 kW) it would go from fully charged to empty in four hours. The asset operational characteristics are given in Table 3.1.

3.5.2 Simulation and Results

Two scenarios are considered to demonstrate the difference in adaptive capacity of the system assets acting as a microgrid. The first case is under what can be considered normal operation and the second case is when network connection has been lost, such as a storm outage or potentially a cyberattack, where the attacker forces a breaker open. For these cases, the loading conditions on the system are assumed to be constant

and the assets operational power output for both cases is given in Table 3.1.

Under normal operation the load is fully supplied by the network and the solar generation is therefore being used to charge the battery storage asset which is currently assumed to be at 75% of capacity. The adaptive capacity is calculated for each of the assets and their manifolds are shown in the top two rows of Fig. 3.7, and the aggregation of the assets is shown by the large manifold at the bottom. The temporal flexibility of the assets real and reactive power in the positive and negative direction is shown in the top of Fig. 3.9.

The second case which considered a loss of the network connection with reconfiguration where the tie-line is being used to supply power. However, based on its limiting characteristics, it cannot fully support the high loading conditions. In this situation, the solar asset is supplying power at its full capacity and the battery storage is able to supply the remaining load. In this case, we assume that the battery has 197 kWh of stored energy, and therefore can maintain its output of 197 kW for one hour. The aggregation of the assets adaptive capacity is shown in Fig. 3.8. The temporal flexibility in real and reactive power is shown in the bottom of Fig. 3.9.

3.5.3 Discussion

Results of the case study bring to light a few important concepts in reliability and resilience of power systems. It can be stated that even when the network was lost the system is reliable, as no load needed to be shed. However, when evaluating the systems using the proposed adaptive capacity metric there is a quantifiable impact to the resilience of the system. This is visible by examining the difference in manifolds and easy to distinguish by inspection of Fig. 3.9. The top plot shows that there is adaptive capacity in the real and reactive power in all directions, but is most

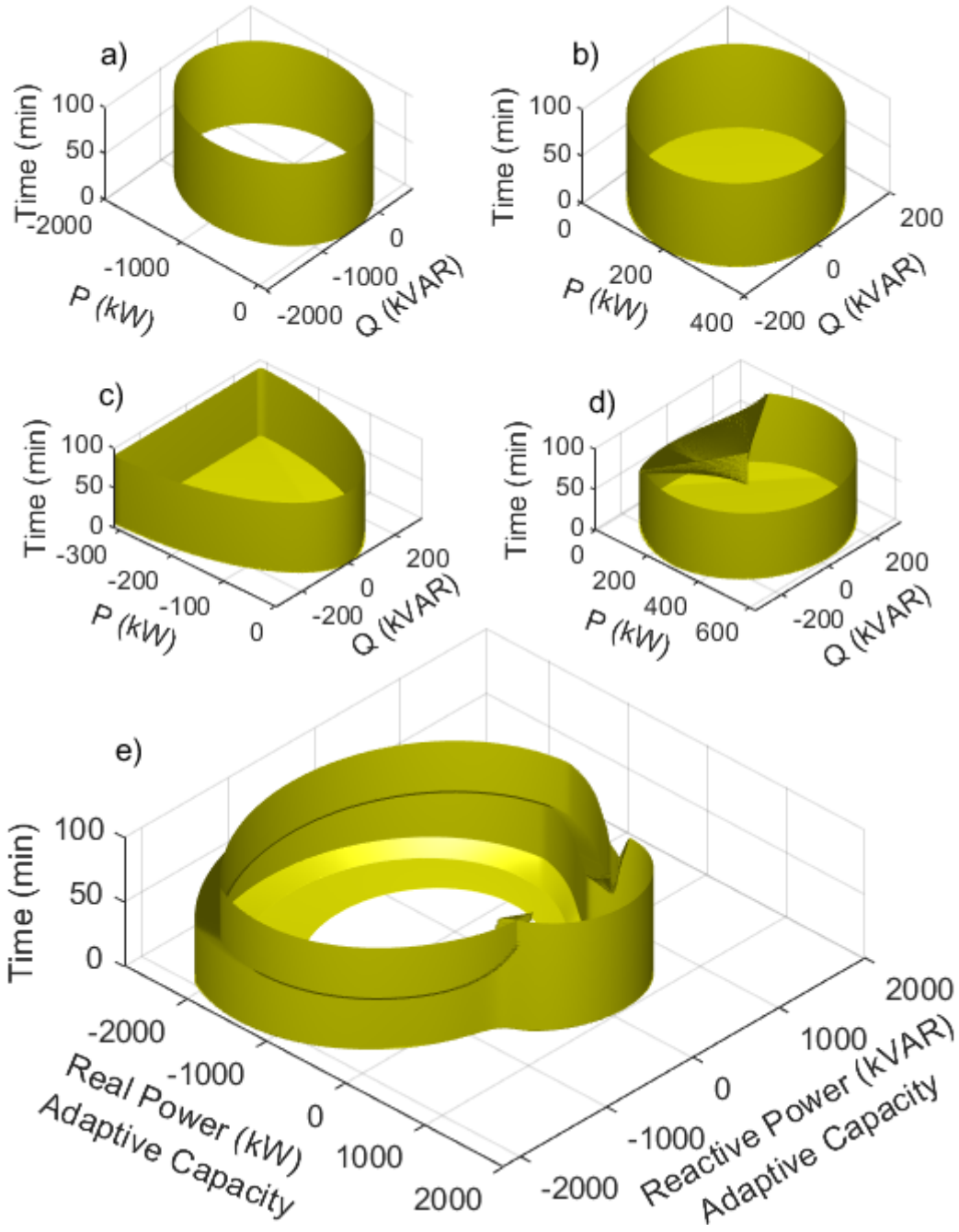

Figure 3.7 Resulting adaptive capacity of the assets under normal condi-tions: a) network connection, b) tie-line connection, c) solar generation, d) battery storage, and e) aggregation of the assets.

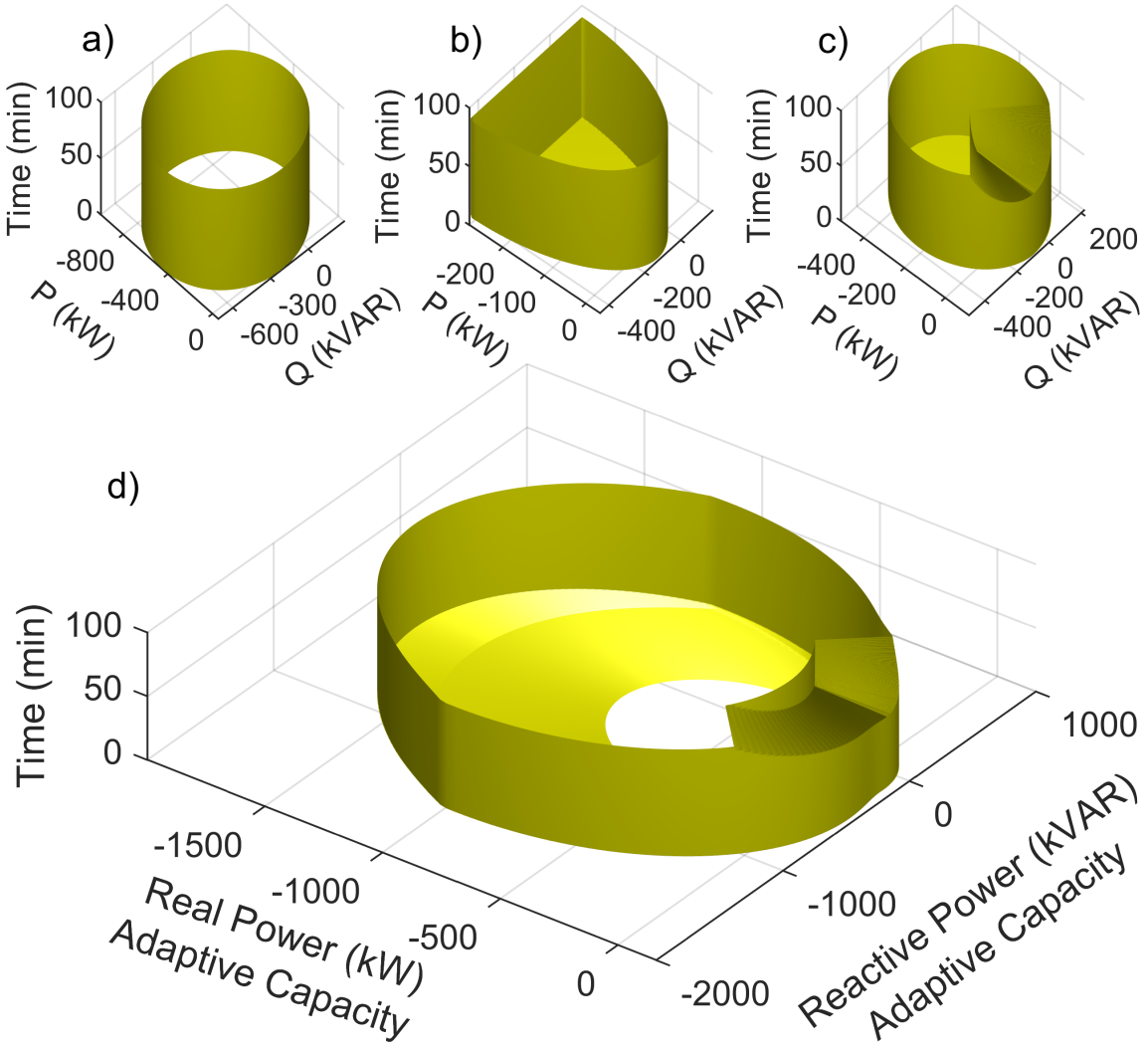

Figure 3.8 Resulting adaptive capacity of the assets when network connection lost: a) tie-line connection, b) solar generation, c) battery storage, and d) aggregation of the assets.

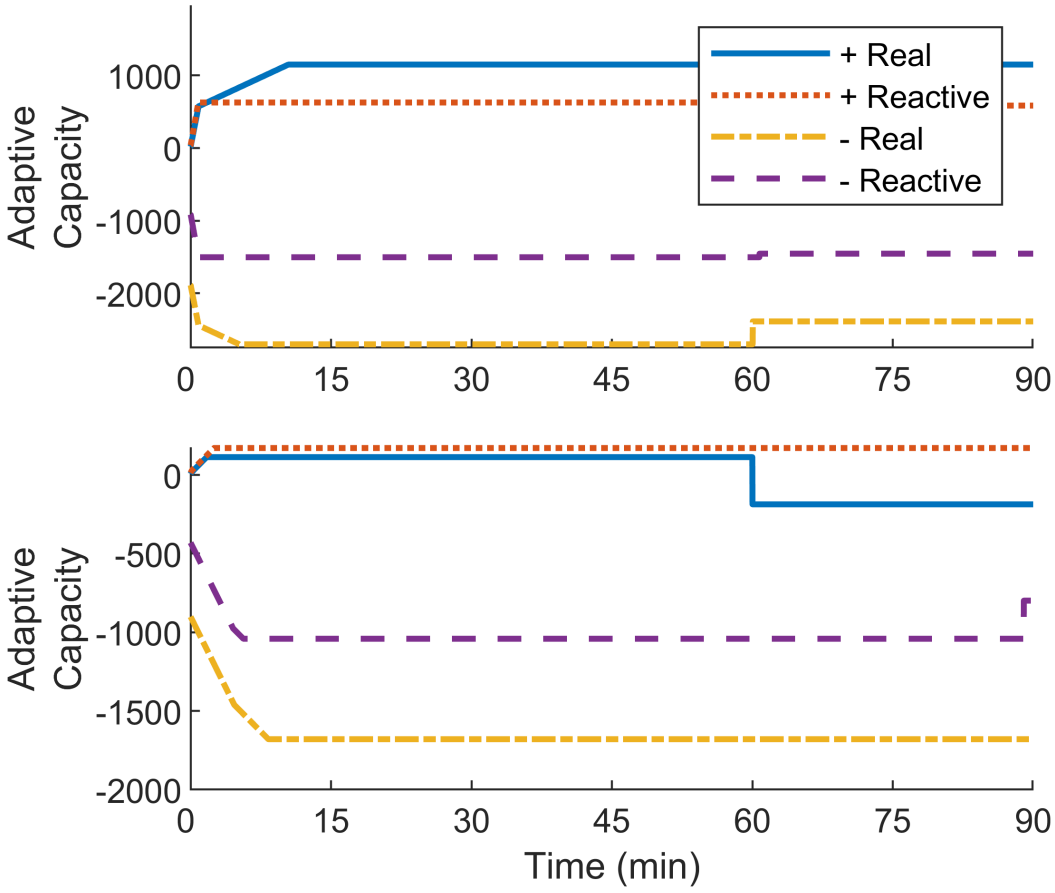

Figure 3.9 **Flexibility at power factor angles in the direction of real (kW) and reactive (kVAR) power. The top plot is under normal operation and the bottom is when network connection is lost.**

"constrained" by the real (1,149 kW) and reactive (627 kVAR) power in the positive direction. In the case of losing network connection this constrain becomes 113 kW and 171 kVAR. Therefore, the ability to adapt to a future disturbance has been dramatically reduced. In fact, the system will lose capability to supply the real power necessary in one hour when the battery storage runs out of energy. This will result in a loss of the ability to maintain the frequency of the system if loads are not shed.

3.6 Conclusion and Future Work

In this paper, we present a resilience metric based on adaptive capacity for modern distribution systems that have a high penetration of distributed resources. The proposed metric provides insight to the ability to control aggregated assets in terms of real and reactive power over time. The metric is used to analyze a microgrid under different scenarios, such as a loss of network connection. The metric is demonstrated indicating the distributed resources can maintain the loads when the connection is lost, however, the systems adaptive capacity is greatly reduced, having very little capability to support stability of voltage and frequency if further disruptions occur.

Future work with respect to improvements to the adaptive capacity metric include replacing the linear ramp rates with non-linear rates. Similarly, the real and reactive bounds in certain assets which are not constant, should be replaced by a function or table to provide better accuracy in the metric. For example, the ramp rate of a hydro generator is not constant but dependant on the head pressure. Additionally, the maximum power is also dependant on the pressure and should be reflected in the metric.

In the next chapter, the resilience contribution of hydropower generation is studied. The resilience of the three different classes of hydropower generation units are

presented and their time scales of resilience are mapped to the "Rs" of resilience. This analysis lays the foundation for a framework to evaluate hydropowers resilience contribution to the grid.

CHAPTER 4:
A METRIC FRAMEWORK FOR EVALUATING THE RESILIENCE CONTRIBUTION OF HYDROPOWER TO THE GRID[1]

4.1 Introduction

The electric power grid is undergoing dramatic shifts in sources of power and increasing infrastructure stresses. The desire to improve the ability of the grid to ride through or recover from large events with natural or man-made causes have increased interest in the area of resilience for the electricity grid. The need arises to understand the resilience contribution from bulk power and distributed energy resources. Providing a quantifiable measure of resilience of all types of components in power systems to add resilience to the electric grid is needed. Creating a framework for characterizing the resilience of hydropower satisfies one of those needs and is the subject of this paper.

To arrive at a framework to measure resilience, relevant prior work is in engineering systems [34], national institutions [69, 89], and the resilient controls community [97].

[1] © 2020 IEEE. Reprinted, with permission from, T. Phillips, V. Chalishazar, T. McJunkin, M. Maharjan, SMS Alum, T. Mosier, and A. Somani, "A Metric Framework for Evaluating the Resilience Contribution of Hydropower to the Grid," 2020 Resilience Week (RWS), Salt Lake City, UT, USA, 2020

This paper considers asset level and system level metrics in addition to metrics from [89]. Both asset and system metrics connect to the notional construction of the system performance compared to the performance objective in the DIRE curve [96] shown in Fig. 4.1. Important time frames in the evolution of the effects of a disturbance on the system are mapped to the time frame of the DIRE curve as the "R"s of resilience: Reconnaissance, Resistance, Response, Recovery, and Restoration. Woods introduces the term *adaptive capacity* to assess a system's resilience based on the proximity of the operation point to a boundary constraint [125]. When operation is near a boundary, adaptive capacity to *respond* to disturbances is limited. A system operator that prudently anticipates disturbances will seek to keep adequate adaptive capacity. The *resist* epoch gives the system more time to respond. For power systems the determining resist factors are the voltage margin and the inertia in the system. In the *response* epoch, the magnitude and duration of a disturbance the system can absorb and maintain minimum operational normalcy is determined by the adaptive capacity of the system. In [60], McJunkin and Rieger constructed a method to efficiently capture and aggregate the response adaptive capacity of power system assets, which was extended to an asymmetric operational metric in [90].

The main contribution of this work is the formalization of an operational framework that allows evaluation of the contributions to resilience by three types of hydropower assets. From the framework, we show hydropower's contributions to the "R"s of resilience. The rest of the chapter is organized as follows: Section 4.2 gives an overview of resilience and hydropower's contribution to the grid. Section 4.3 summarizes and adapts the mathematical background given in [90] for hydropower plants. Section 4.4 introduces the proposed framework and applies the metric to different

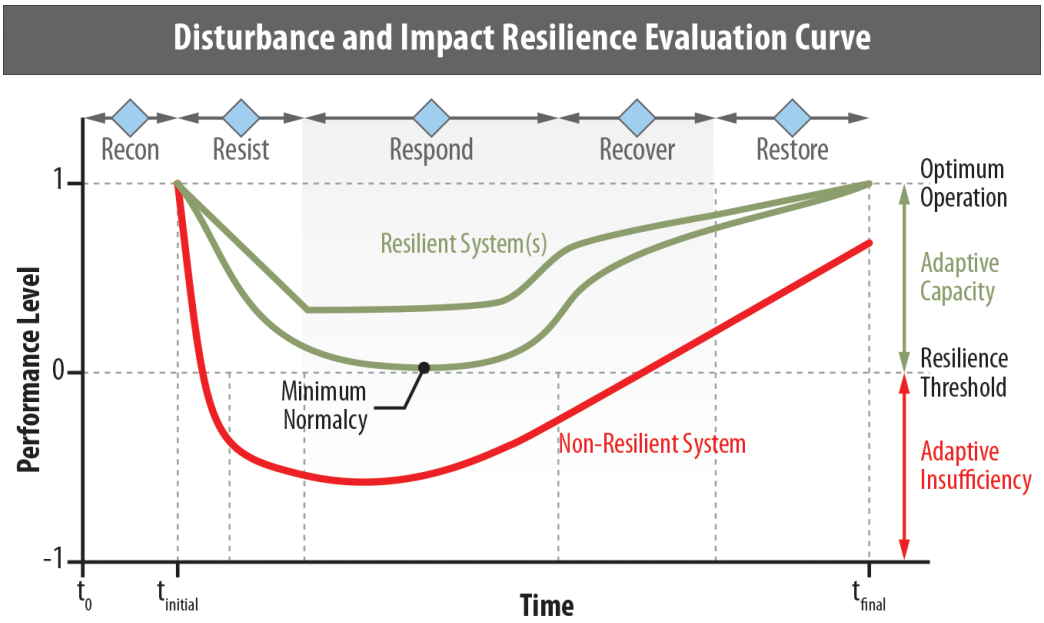

Figure 4.1 A simplified version of the Disturbance and Impact Resilience Curve [96, 97].

types of hydropower assets. Concluding remarks are given in Section 4.5 and future work is discussed in Section 4.6.

4.2 Adaptive Capacity Contribution of Hydropower

4.2.1 System Level

The conceptual DIRE curve, Fig. 4.1, describes the performance level of the system as a whole, during and after a major disturbance or HILP event. Most of the resilience studies use some form of the DIRE curve to develop and evaluate resilience metrics to know the system health and its ability to absorb, adapt and recover rapidly after an HILP event. Even though there are several resilience metrics already proposed it is still difficult to accurately quantify and represent resilience. Resilience is a complex multidimensional dynamic concept [83]. Numerous different metrics exist and some

of the most relevant and commonly used metrics are:

- Demand/energy not served [40],
- The "FLEP" resilience metric system (Φ, Λ, $\mathcal{E}$, Π), where Φ is how fast and Λ is how low the resilience level drops, $\mathcal{E}$ is for how extensive the post-event degraded state and Π is how promptly the network recovers to its pre-event resilient state. [84, 85],
- Time to recovery, cost of recovery, load recovery factor and lost revenue [9, 10],
- Vulnerability index, degradation index, restoration efficiency index and microgrid resilience index [4], and
- Maximum number of customers out of service [42]

All of these metrics do a relatively good job at describing power systems resilience to an external disturbance, however, they are not very useful in describing the contribution of any particular power generation asset (for example the Grand Coulee hydropower plant) or family of generation assets (for example hydropower as a whole) towards achieving that level of resilience. To address this problem for the power transmission system, prior work has used augmentation of a traditional bus-branch model into a node-breaker model so that the fragility and vulnerability of each substation asset (such as the transformers and circuit breakers) can be included in the evaluation of resilience levels [11].

Each family of assets contributes in its own way towards resilience and it is important to understand how to utilize these assets to their fullest potential. To that end, the asset level metrics for hydroelectric generation is discussed in the next sub-section to quantify its contribution towards resilience.

4.2.2 Asset Level

Hydropower generation has numerous qualities that contribute towards overall grid resilience. Hydro is also the preferred generation and is prioritized for tripping in case of over generation scenarios because of an extreme event. This is primarily because of the following reasons: 1) hydropower leads to least cost when compared to other generation trips, 2) pumped storage efficiency helps in restoring the hydro resource back by pumping spilled water and 3) it is easier to bring hydropower back online. Hydro is also the preferred generation for wind compensation [16] because it provides a major part of the total required governor response and also hydro can provide, if needed, more output than its nameplate capacity but at a lower efficiency. All of these qualities and capabilities make hydro's contribution to grid resilience significant and the proposed asset level metrics are a step in the direction to be able to accurately represent the said contribution.

A generic example of real power output generation of a hydropower plant going through a major grid scale disturbance event is shown in Fig. 4.2. Here, different asset level metrics are shown for different time periods before and after an event. These proposed metrics, their contributing capabilities and their constraints/dependencies are further discussed in Table 4.1.

These metrics capture hydro asset's flexibility and its multifaceted contribution towards overall grid resilience and system stability which enables rapid recovery of the system following an extreme event. In this paper, we focus on the *response* epoch for hydropower resilience and describe the adaptive capacity fundamentals in the next section.

Table 4.1 Asset level metrics, their capabilities and their dependencies

Metrics	Epoch	Dependencies/constraints
Inertia	Resist	Number of online units, Seasonal Constraints, Planned maintenance, etc.
Ramp-up rate	Respond	Number of online units, Environmental constraints, Flow rate Constraints, etc.
Sustained generation at maximum output	Recover & Restore	Resource availability, Environmental constraints, Energy limits, etc.
Ramp-down rate	Respond	Flow rate constraints, Environmental constraints, Grid requirements, etc.
Lost capacity	Restore & Recon	Initial capacity, Impact of extreme event, Amount of sustained generation at maximum output, etc.

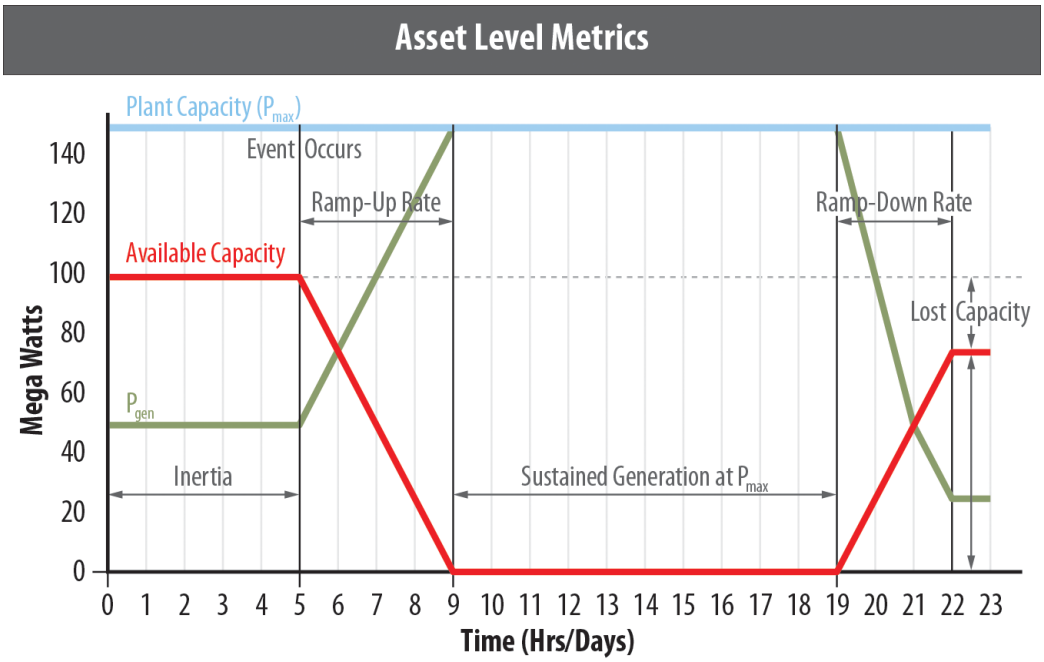

Figure 4.2 Asset level metrics from a hydropower plant perspective.

4.3 Hydropower Response Capacity

The calculation of the adaptive capacity of hydropower plants is based on the real and reactive power generation capability, the current operating output, latency, ramp rate, and energy constraints. The first constraint on the operational power output of the asset in real power, P, and reactive power, Q, is defined by the complex S-plane. At any given power factor angle, θ, the apparent power is bounded by

$$S(\theta) \leq \sqrt{P^2 + Q^2}, \quad 0 \leq \theta < 2\pi \tag{4.1}$$

In the context of hydropower generators and pumped storage hydropower (PSH), the apparent power is not the only constraint on the power output. The real power is

also constrained, given mathematically as

$$P(\theta) = \begin{cases} \min\left[S\cos(\theta),\ P_{\max}\right], & 0 \leq \theta < \frac{\pi}{2} \\ \min\left[S\cos(\theta),\ P_{\max}\right], & \frac{3\pi}{2} < \theta < 2\pi \\ -\min\left[|S\cos(\theta)|,\ |P_{\min}|\right], & \frac{\pi}{2} \leq \theta \leq \frac{3\pi}{2} \end{cases} \tag{4.2}$$

here, the generator only operates in the positive plane so $P_{\min} = 0$. Additionally, the maximum real power, $P_{\max}$, may not be the nameplate capacity due to a decrease in the reservoir head height. On the other hand, PSH can also operate in the negative plane (pump mode) and positive plane (generation mode).

The flexibility of the asset is defined as the amount of change it can make from the current operating point to the bounding limits. Thus, it is the translation from $P = 0$, $Q = 0$, to the operating point, P_0 and Q_0. The limits on the operating power $S, P_{\max}$ and $P_{\min}$ then take the form $S', P'_{\max}$, and $P'_{\min}$ after the translation, given mathematically as

$$P_{\Delta}(\theta) = \begin{cases} \min\left[S'\cos(\theta),\ P'_{\max}\right], & 0 \leq \theta \leq \frac{\pi}{2} \\ \min\left[S'\cos(\theta),\ P'_{\max}\right], & \frac{3\pi}{2} \leq \theta < 2\pi \\ -\min\left[|S'\cos(\theta)|,\ |P'_{\min}|\right], & \frac{\pi}{2} < \theta < \frac{3\pi}{2} \end{cases} \tag{4.3}$$

for the real power. The reactive power is given as

$$Q_{\Delta} = S'\sin(\theta) \tag{4.4}$$

The flexibility of a hydropower generator is shown in Fig. 4.3. This example

depicts a 10 MW generator that is currently being operated at 6 MW and 2 MVAR. The shaded region in the top plot represent the flexibility when the asset is limited by $P'_{\max}$ due to a reduced reservoir head height. The apparent power limits shown here are a simplification of the general constraints of a generator like the capability curve shown in [25, 113]. The flexibility does not consider the temporal constraints of the asset which define how quick it can change from its current operating output to the flexibility limits.

Temporal constraints of the asset are captured by the latency and ramp rate. Latency is the time lag before the asset can begin changing its output. It may consist of multiple factors, such as grid synchronization and decisions which can be done computationally or by an operator. In this work, we consider all latency to be contained in a single variable, λ.

The ramp rate defines the rate of change in real or reactive power after the latency. Again, hydropower assets have several considerations such as Automatic Generation Control (AGC) and environmental regulations. In this work, we consider these to be contained in a single variable for the ramp rate in real power, dP/dt, and reactive power, dQ/dt. Thus, the temporal real power constraint, relative to the current real power output, is given as

$$P(t) = \begin{cases} 0 & \text{if } t \leq \lambda \\ \frac{dP}{dt}(t - \lambda) & \text{if } t > \lambda \end{cases} \tag{4.5}$$

and the reactive power is

$$Q(t) = \begin{cases} 0 & \text{if } t \leq \lambda \\ \frac{dQ}{dt}(t-\lambda) & \text{if } t > \lambda \end{cases} \tag{4.6}$$

where t is the future time from current operation. In addition, the ramp rates may be direction dependent and non-linear, i.e. the asset may ramp down quicker than it can ramp up. We denote the the real power constraint as $P(t)^+$ when ramping up and as $P(t)^-$ when ramping down. The same is done for the reactive power. The temporal constraints in real power are shown in the bottom plot in Fig. 4.3.

The adaptive capacity is then calculated as the minimum between the temporal constraint and the flexibility of the asset. The adaptive capacity in real power is given as

$$P_{\text{AC}}(\theta, t) = \begin{cases} \min\left[P_\Delta,\ P(t)^+\right], & 0 \leq \theta < \frac{\pi}{2} \\ \min\left[P_\Delta,\ P(t)^+\right], & \frac{3\pi}{2} < \theta < 2\pi \\ -\min\left[|P_\Delta|,\ |P(t)^-|\right], & \frac{\pi}{2} \leq \theta \leq \frac{3\pi}{2} \end{cases} \tag{4.7}$$

and the adaptive capacity in reactive power is given as

$$Q_{\text{AC}}(\theta, t) = \begin{cases} \min\left[Q_\Delta,\ Q(t)^+\right], & 0 \leq \theta \leq \pi \\ -\min\left[|Q_\Delta|,\ |Q(t)^-|\right], & \pi < \theta < 2\pi \end{cases} \tag{4.8}$$

The adaptive capacity in real power where $\theta = 0$ and π over 12 minutes is depicted in the bottom plot of Fig. 4.3. It can be seen that the adaptive capacity is initially limited by the temporal constraints, but after ramping, the flexibility constraints are reached and constrain the adaptive capacity of the asset.

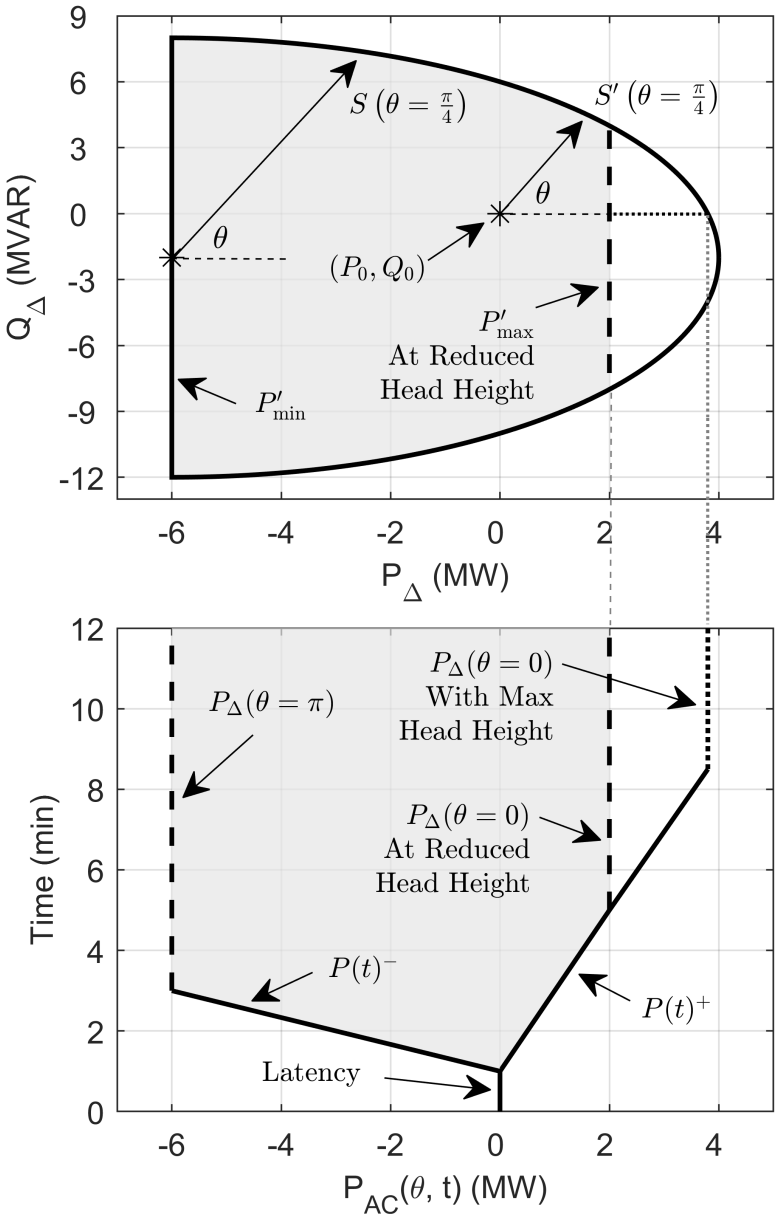

Figure 4.3 The top plot depicts the flexibility of a 10 MW hydropower generator operated at 6 MW and 2 MVAR using the transformation from S to S'. The highlighted region represents the flexibility when there is a reduced reservoir head height limiting the real power at $P'_{\max}$. The bottom plot illustrates the temporal and flexibility constraints on the adaptive capacity calculation in real power at $\theta = 0$ and π over 12 minutes.

Furthermore, the adaptive capacity of assets can be aggregated in real and reactive power where the angle measurement is consistent from the operation point. The aggregation of real power is given as

$$P_{\mathrm{AC}}(\theta, t) = \sum_{k=1}^{n} P_{\mathrm{AC}_k} \tag{4.9}$$

and the reactive power is given as

$$Q_{\mathrm{AC}}(\theta, t) = \sum_{k=1}^{n} Q_{\mathrm{AC}_k} \tag{4.10}$$

where n represents the total number of aggregated assets. P_{AC_k} and Q_{AC_k} represent the adaptive real and reactive power capacity of the k^{th} asset, respectively. For a detailed mathematical background, the reader is referred to [90]. In the following section, we carry out a series of case studies to demonstrate the difference in adaptive capacity between three types of hydropower assets: 1) Run-Of-River (ROR) hydropower, 2) Hydropower With Reservoir (HWR), and 3) Pumped Storage Hydropower (PSH).

4.4 Framework

This section provides a description of the framework for incorporating the factors that influence hydropower's available response for different types of hydropower resources in terms of operational flexibility and technical constraints. We illustrate the adaptive capacity resilience metric. The study includes a case for each of the three different types of hydropower assets. Input parameters were selected to convey the adaptive capacity concept and display their ability to support stability of the power grid.

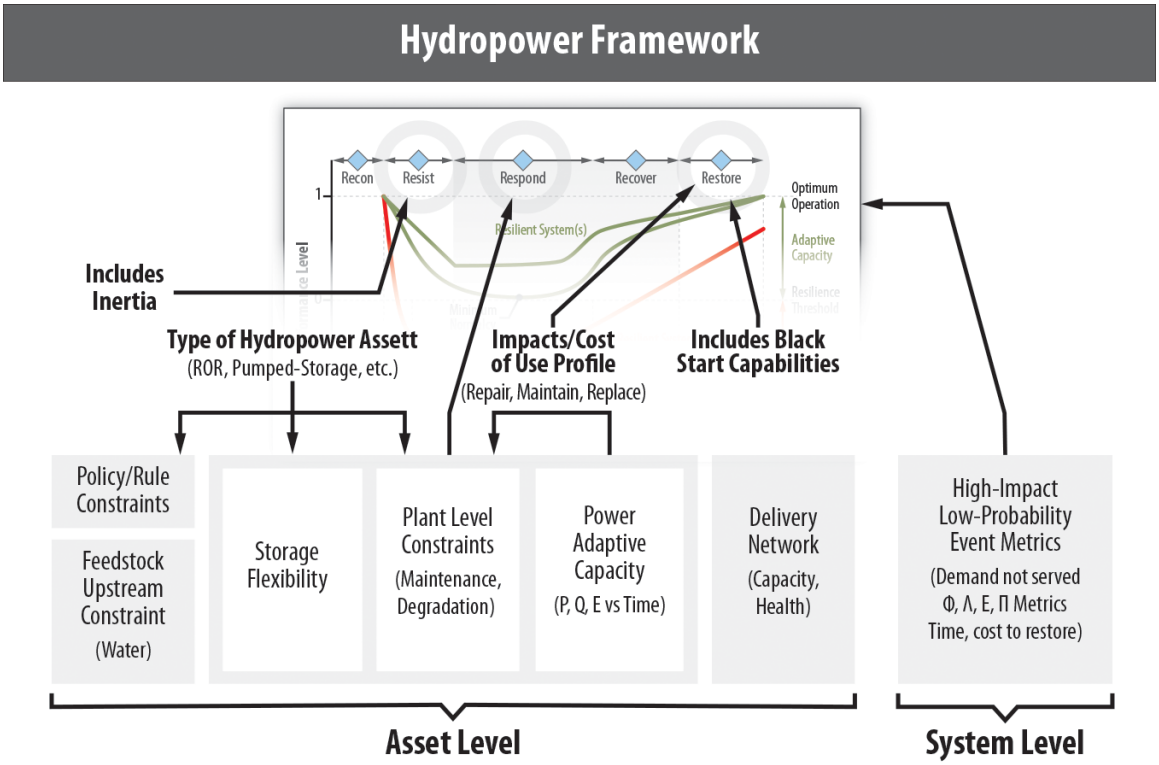

Figure 4.4 Hydropower framework connecting the constraints on the ca-pability to aid the resilience of the power systems.

Fig. 4.4 presents a hydropower framework that identifies contributions of hydropower assets in different epochs of the DIRE curve. There are numerous factors to consider while assessing a hydropower asset's contribution to grid resilience. These factors, like storage flexibility, plant level constraints, adaptive capacity and regulatory policies differ with the type of hydropower resource and alters the hydro's resilience response. In this chapter, we focus on the adaptive capacity as it plays a key role in managing infrastructure integrity and service reliability [30].

Major operational constraints like maximum and minimum amount of power that can be generated, operation and maintenance requirements, ramping rates conditions, and elevation levels [117] are considered in all three types of hydropower. Water quantity, water head height, and reservoir level are the raw data that determines the amount of power generated by the hydropower asset. The plant level constraints, such as the operational capabilities of the generators, optimal operating range of the turbines, and the turbine efficiency also affects the reaction of the hydropower. Likewise, regulatory and environmental constraints, such as minimum water discharge, reservoir level restrictions, flow rate requirements, downstream impacts and power purchase contracts and agreements, also limit the functional capabilities of these hydropower plants [104]. The framework indicates that the strength and health of electricity delivery network is a key factor in the effectiveness of any asset's resilience contribution. The effectiveness of real and reactive power capabilities is tied to the plants' location and the type of transmission or distribution network connected to the plant. Some of the unique attributes of these hydropower are discussed below.

4.4.1 Run-of-River Hydropower

ROR utilizes the natural flow of water from a river through a canal or penstock and the elevation gradient between the diversion and the powerhouse, usually with no or little reservoir [103]. ROR, generally, provides baseload with some variability in operation (typically for hourly or daily water availability fluctuations), but is unable to provide ancillary services to the grid due to inflexibility in generation. Runoff patterns can vary significantly seasonally and are driven by local or upstream hydrologic conditions. Because a plant may not be designed to utlilize less than the seasonal maximum flows for power production, during high inflow seasons, ROR plants may spill a significant portion of the water without generating electricity [29]. ROR hydropower plants are typically designed to optimize financial performance with increasing capacity leading to a more expensive plant but a smaller capacity leading to lower revenues [23]. Although less variable, ROR is similar to solar or wind power, in that it is most often used as a maximum energy production. To achieve flexibility, a trade off between flexibility in power production versus maximum energy conversion must be made.

ROR projects cause less environmental concerns as no major construction of reservoir to raise the head height is needed and minimal amount of storage is involved [53]. However, restrictions on minimum amount and temperature of water discharge, and ramping rates apply for conservation of aquatic species and their habitat [73].

Case Study

We consider a ROR hydropower asset with a nameplate capacity at the current river flow of 10 MW real power and ± 10 MVAR reactive power. No presence of upstream or downstream dams or reservoirs is assumed for this asset. The current operating

output of the turbine generator is 6 MW of real power and 2 MVAR reactive power. As the head height of an ROR asset remains constant, the maximum real power which the asset can produce is dependent only on river flow rate over time. For this reason, the flexibility of power remains constant. It can be ramped up 4 MW to its nameplate capacity of 10 MW or it can be ramped down to 0 MW. At first glance, it would be easy to assume that the asset can also provide ±10 MVAR of reactive power. However, if the real power remains constant at 6 MW the reactive power is limited to ±8 MVAR due to the apparent power constraint. Next, we consider the temporal constraints of the adaptive capacity.

When the generator is providing power, it is synchronized with the grid and the latency to make output adjustments comes from the AGC. Therefore, the latency in this study is set at 1 s, which is a conservative assumption for resolving a frequency measurement that is an input to AGC. The ramp up and down rate for real power is assumed to be linear at 1 MW/min and the rate for reactive power is assumed to be 1.5 MVAR/min. The resulting adaptive capacity from the current operating point is shown by the left plot in Fig. 4.5. The surface represents the maximum change in real and reactive power the asset can have over time. Next, we consider a hydropower asset with reservoir.

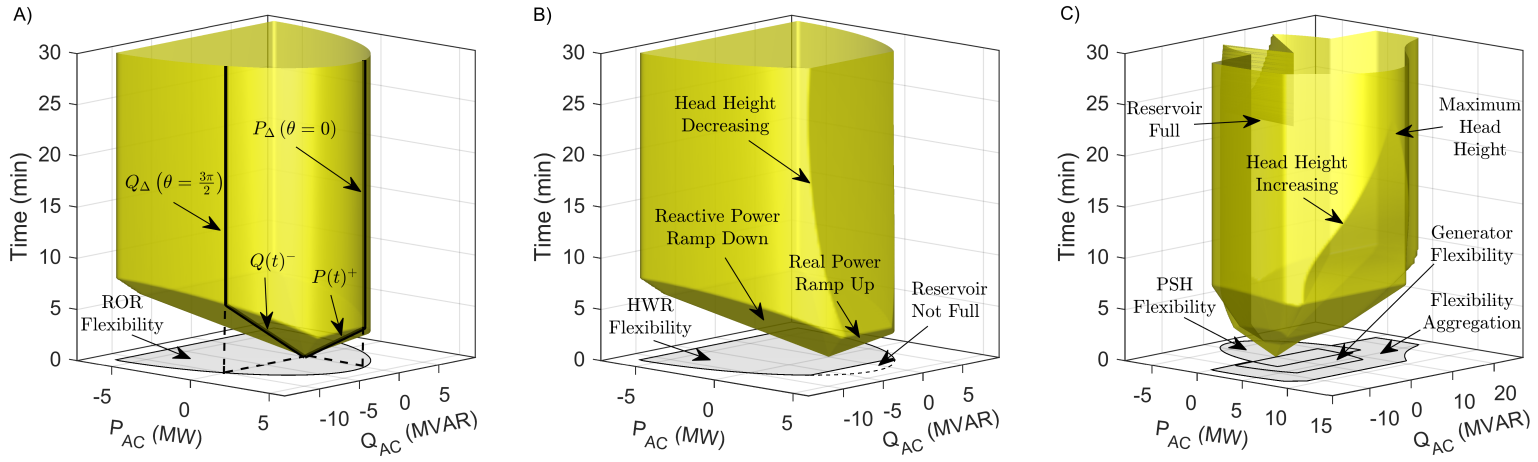

Figure 4.5 **Adaptive capacity in real power, P_{AC}, and reactive power, Q_{AC}, of different hydropower assets. A) 10 MW ROR hydropower asset that is currently operating at 6 MW of real power and 2 MVAR reactive power. B) 10 MW reservoir based hydropower asset that is currently operating at 6 MW and 2 MVAR where head height is decreasing over time. C) Aggregated adaptive capacity of a 10 MW PSH when running in the pumping state at 3 MW and -4 MVAR.**

4.4.2 Hydropower with Reservoir

This type is characterized by the use of dam to store water in a reservoir, which facilitates the alteration of the water flow according to the system demand. It provides base load as well as the ability to shut down and start up quickly during peak load. It also provides the storage capacity to operate independently, without continually adjusting power generated to the flow of the river. The design, type and size of reservoir depends on landscape and nature of the plant site and economics of reservoir construction [23]. HWR have the ability to impound the inflows and then release when necessary for low-cost integration of variable renewables into the grid. However, this flexibility also contributes to increased financial risks, and operations and maintenance costs [56] and potential reduction of generation and reliability of plant components.

These reservoirs are often tied to regulations to serve environmental, recreation and irrigation purposes. Therefore, the release of water from the reservoir is limited to maintain consistent reservoir level for recreation, to prevent flooding, and support the habitat of the aquatic life. The thermal stratification of water and gas dissolution during water spillage also adds to the limitations of reservoir water release. The sediment, accumulated over time, within the reservoir also reduces the available storage capacity, which affects the amount of energy produced by the hydropower asset.

Case Study

In general, HWR has a larger nameplate power capacity than a ROR asset due to increased head height. However, to compare different hydropower assets we consider the same 10 MW, $\pm$10 MVAR generator with the same latency and ramping rates.

Therefore, the difference between the ROR and HWR is the potential for fluctuating reservoir depth, i.e. changing head height. As a result, the real power generation capability of the asset may not stay constant at the nameplate capacity of 10 MW.

To demonstrate how the head height effects the adaptive capacity we use a forecasted head height and apply a linear reduction to the maximum real power. Again, we assume the current operating point of the generator is 6 MW and 2 MVAR. The corresponding adaptive capacity is shown by the center plot in Fig. 4.5. It can be seen that the adaptive capacity in real power is reduced when the head height is decreasing. It should be noted that the reduction in head height here is for demonstration purposes and unlikely that a reservoir would change depth this rapidly. In addition, the head height would be expected to remain constant if the power generating flow and spill were equal to the reservoir inflow and evaporation. When these are not equal changing volume tied to a function of volume versus head height would drive the change in the maximum real power available.

4.4.3 Pumped Storage Hydropower

PSH pumps water to an upper reservoir during low power demand using surplus energy from the system, later releasing it to support peak demand. PSH compliments the intermittent power resources like solar and wind, as it replicates the behavior of a battery to store excess electricity generated and also backs up the sources during low/no production. The amount of electric energy stored depends on the water storage capacity and differential height between the reservoirs [45]. Due to these characteristics, PSH has been an important asset on utility-scale storage, grid reliability, resiliency and many other ancillary services like regulation, operating reserves, etc. Furthermore, adjustable speed PSH can deliver fast ramping and frequency regula-

tion in both the generation and pump modes. This technology also allows turbines to operate in peak efficiency under all head conditions, resulting increased energy generation [55]. Similarly, advanced PSH technology called ternary units, offer additional operational flexibility, increased efficiency and faster transition time between generating and pumping modes [115]. It also operates in hydraulic short circuit (HSC) mode which aids adjustable pump load [72]. Consequently, PSH with advanced design can provide a faster switching from pump to generation utilizing the HSC mode [24].

Conventionally, PSH were integrated on-stream (also known as *open loop*), assisting the ROR for water storage and rarely used in pumped storage mode to meet peak demand. Open loop PSH is subjected to all the reservoir related constraints. The PSH independent of natural water body, referred as *closed loop*, has the advantage of no to minimal impact on existing river systems [55]. The water inflow pattern in closed loop PSH is only affected by evaporation or seepage losses. PSH is confined to reservoir-based constraints similar to HWR, but is more flexible and efficient than the latter.

Case Study

We consider the scenario of excess generation and place a closed loop ternary 10 MW PSH in the pumping state at 3 MW and -4 MVAR. We use the same 10 MW machine as previous case studies and assume the pump has the same latency and ramp rate characteristics as the generator. The adaptive capacity of the ternary PSH is calculated as an aggregation of the adaptive capacity of the pump and generator. However, the pump and generator assets must consider their coupled relationship and transition states. Therefore, the calculated adaptive capacity of the pump and

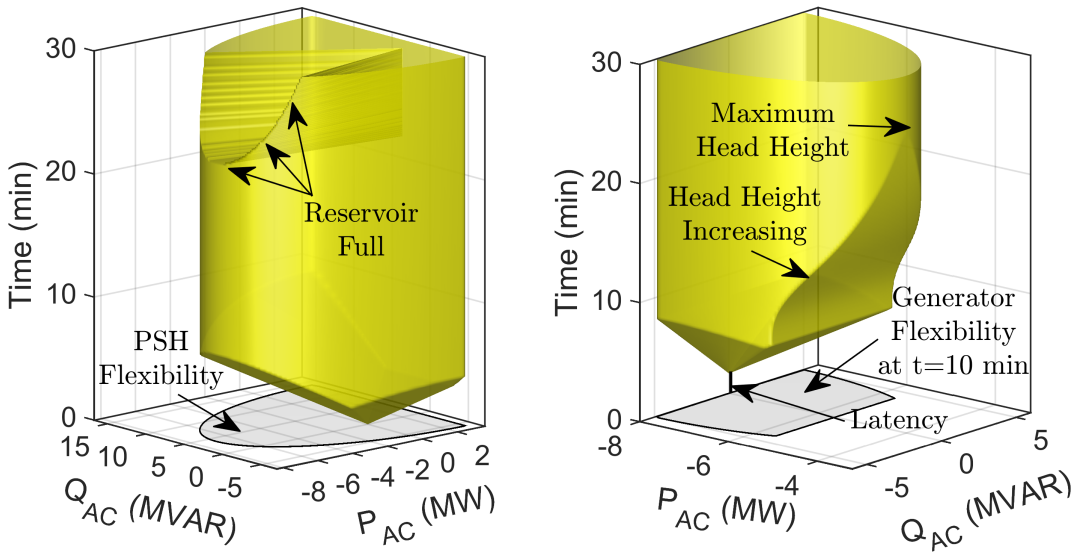

Figure 4.6 The left plot shows the adaptive capacity of the 10 MW pump operating at 3 MW and -4 MVAR. The right plot shows the adaptive capacity of the 10 MW generator at idle with a 90 second latency.

generator are from their current operating point and state of the system. With this consideration, the latency for the pump is 1 second and the latency for the generator is 90 seconds because of the transition state from pumping to generation [24].

Results of the adaptive capacity of the pump and generator are shown in Fig. 4.6, and the aggregation of the assets is shown by the right plot in Fig. 4.5. It can be seen that under current operation and forecasting, the maximum potential of the generator is increasing as the reservoir fills. As a result, the ternary PSH will need to change states to HSC where both the pump and generator are running, or water will need to be passed over the spillway.

4.4.4 Discussion

The following are general observations and comparisons of the three types of hydropower discussed in this paper. The ROR asset operates with constant head with

little to no flexibility in generation and have limited ramping capability. This is reflected through fixed maximum real power capacity in Fig. 4.5(A). Furthermore, bidirectional variation in reactive power capacity exists but is constrained through the ROR asset's apparent power. In general, the reservoir based hydropower offers higher generation and ramping capability with reduced dependence on flow rate of water. However, as shown in Fig. 4.5(B), head uncertainty affects the adaptive capacity with higher variability as compared to ROR hydropower.

PSH with advanced design, for example, the ternary PSH can avoid spillage of excess water in pump mode while reaching the maximum head by operating in HSC mode shown in Fig. 4.5(C). Such spillage is unavoidable for ROR and reservoir based hydropower to maintain water flow rate (ROR) and reservoir capacity (reservoir based).

Overall, PSH offers the highest adaptive capacity through the variable storage and pump-generation switching capability. ROR hydropower offers the least due to the absence of a reservoir while a reservoir based hydropower performs better than ROR. It should be noted that, the current study considers only the effects of generation capacity, ramp rate and storage, while the ageing effects as well as environmental and regulatory constraints will be explored in future works.

Although this paper is focused on the *response* epoch of resilience, hydropower has other attributes that support the other Rs. Table 4.2 provides a qualitative summary of the resilience capabilities of the three types of hydropower assets. *Recon* epoch will determine the bias of the hydropower plants and determine the amount of flexibility the system has. The state of storage and power set points provide the starting point for the response to any disturbance. For example, the current state of

the PSH systems, i.e., pumping or generating, will have a definitive affect on the response latency and ramping ability. *Resist* capabilities reside in the amount of inertia the plants have in their prime movers. Synchronous generators of ROR, HWR, and in instances where PSH is comprised of synchronous machines have these capabilities. Adjustable speed PSH utilizing converter-fed synchronous machines do not have this attribute. All types of hydropower have response capabilities, through governor, AGC, and other real and reactive control. The *recover* epoch is supported through longer term allocation of the *response* phase resources but also include dispatch decisions. While not covered in this paper, the authors anticipate that connecting the response capabilities of resources to production cost modeling would support dispatch decision. This would ensure optimal use of the resources to return the system towards the normal operating state. Finally, *restore* attributes of all hydropower include the use of the plants as the starting point of the black start cranking paths, because they require low initial power to start up, have fast ramping characteristics and large capacities [91, 1], as well as sustained generation for longer time frame after a major event. Restoration must consider the impacts to the hydropower assets during these events that may cause greater maintenance and repair needs of the plants.

Table 4.2 Summary of resilience capabilities of the three types of hy-dropower assets by epochs of resilience.

Epoch	ROR	HWR	PSH
Recon	power/spill bias	storage power bias	storage power bias
Resist	inertia (H)	inertia (H)	depends on type
Respond	real & reactive spinning	real & reactive spinning & non-spinning reserve	real & reactive ramp dependent on direction
Recover	N/A	dispatch/ response	dispatch/ response
Restore	black start & sustained generation	black start & sustained generation	black start & sustained generation

4.5 Conclusion

This chapter has provided a framework for considering the resilience contribution of three classes of hydropower generation plants. The foundations of resilience definitions and measures are considered. The contribution of hydropower systems to resilience is considered in two tiers, system and asset level resilience. System level resilience means the rate at which the operations of the electric grid are brought back to normal after an HILP. The contribution of a class of assets to the return to normal process should be valued in comparison to all supporting assets in the grid. Although the framework for asset level resilience seeks to encompass all the epochs of resilience, the initial focus is on the *response* epoch adaptive capacity for each type of hydropower asset. The comparison discussed is more about making utilities and

stakeholders aware of the resilient capabilities held by these plants than to say one is preferable to another. The value is always in the context of the location of the plants and their role juxtaposed to the capabilities of all of the power system assets.

This work provides a framework for hydropower that could be adapted to the constraints of other energy assets on the grid. The specific capability captured through the adaptive capacity of hydropower assets was needed to allow resiliency analysis of portions of the electric grid and the grid as a whole. The paper focused on the response capacity of the three types of hydropower systems. With this framework and metrics tool, the ability for hydropower-specific assets can be compared or combined with other contributors to resilience: bus level adaptive capacity in transmission[114], distributed energy resources[60] including solar[90] to assess the magnitude and duration of disturbances the system could withstand without further anticipated failures. One of the most striking attributes of hydropower in general is the ability to support all of the time frames considered in the DIRE curve. Of course, there are trade-offs between the use in the response epoch, reserving capabilities for recover and restore, and maximum energy production; however, with an understanding of the capabilities and trade-offs, stakeholders can make informed decisions on prioritization of resource usage.

4.6 Future Work

Several aspects of the framework require additional attention. Firstly, the adaptive capacity needs to incorporate synchronous generators' capability curves [25]. Secondly, there is a need to connect asset level metrics to the predicted outcomes contained in the system level metrics given the scale of HILP. Thirdly, the mechanics to connect the asset contribution to the needed location and the contribution of inertia need

development. Finally, the inputs to the framework require coordination with analysis tools that provide more detailed treatment of the limits from environmental, storage and operational constraints.

The adaptive capacity in real power was demonstrated mathematically. It was shown that the maximum limit in real power is dependant on the head height of the asset. At current state, there is no uncertainty considered with the forecasted head height. In general, the head height estimate of a reservoir will be well known, resulting in a small uncertainty. However, in the case of solar PV the uncertainty in generation can be large and therefore is the topic of the following chapter.

CHAPTER 5:

A FRAMEWORK FOR EVALUATING THE RESILIENCE CONTRIBUTION OF SOLAR PV AND BATTERY STORAGE ON THE GRID[1]

5.1 Introduction

In order to curb climate change, global action has been taken to reduce the amount of carbon emissions. In power generation, this has resulted in an increasing penetration of renewable sources like solar PV and wind power generation. Unlike the traditional generation resources, they provide intermitten and uncertain amounts of generation throughout the day. This has presented utilities and researchers with new challenges. Power system operators have to accommodate for variability in system load and solar PV generation through reserve power that can adjust output levels in dispatchable plants, however, this is not cost effective.

The increasing presence of renewable generation on the power system may have been spurred by climate change concerns. However, the dramatic reduction in investment have made it cost competitive with traditional resources. In early 2011,

[1] © 2020 IEEE. Reprinted, with permission from, T. Phillips, T. McJunkin, C. Rieger, J. Gardner, and H. Mehrpouyan, "A Framework for Evaluating the Resilience Contribution of Solar PV and Battery Storage on the Grid," 2020 Resilience Week (RWS), Salt Lake City, UT, USA, 2020

solar generation comprised less than 0.1% of the U.S. generation supply at just 3 gigawatts, by 2017 this number had grown to over 47 gigawatts. From 2010 to 2017, the adjusted cost for solar PV installed kilowatt-hour dropped from $0.52 to $0.16 for residential, from $0.40 to $0.11 for commercial, and from $0.28 to $0.06 for utility scale generation. The Solar Energy Technologies Office set a 2030 goal for a further 50% reduction to $0.03. Achieving this goal would make solar one of the cheapest sources of electricity generation and push further expansion of solar PV installation [67].

In this work, we present a metric based on the adaptive capacity to evaluate the resilience contribution that solar PV generation and battery storage add to the grid. The novelty of this chapter is capturing the uncertainty of solar PV assets and its effect on the contribution it provides to the adaptive capacity of the grid. The rest of the paper is organized as follows; Section 5.2 introduces solar generation forecast and its uncertainty. Section 5.3 provides the details of our resilience metric framework. We then carry out a case study in Section 5.4 and give concluding remarks and future work in Section 5.5.

5.2 Solar PV Generation

The output of solar PV generation is variable due to the sun changing position throughout the day and seasons. This regularly leads to a 10% change in generation over 15 minutes. However, meteorological phenomena such as moving cloud cover, contribute to uncertainty in the generation and can cause rapid changes in power output. The size of the PV system, cloud speed, cloud height, and other factors influence the rate of change in power generation output. There is a rich body of literature on forecasting solar irradiance and PV generation. They can be broadly classified into four approaches; statistical based on historical measured data [6], artificial in-

telligence or machine learning such as neural networks [100], physics based numerical weather prediction models or satellite images [88, 27], and hybrid models [68].

The practical use of solar forecasting can be characterized at different time horizons. From the perspective of power system operation, very short-term (seconds to minutes) and short-term (up to 48-72 hours) forecasts are particularly useful for activities like real-time unit scheduling, storage control, automatic generation control, and electricity trading [119]. Medium-term forecasts consider week long forecasts and can be used for maintenance scheduling, and long-term forecasts are months or years and useful for solar PV plant planning. In this study, we consider very short-term and short-term time horizons which correlate to the respond and recover of the "R's" of resilience.

There are various evaluation indices to apply to forecasting accuracy. The commonly used indices include mean bias error, mean absolute error, mean square error, and root mean square error. These are all statistical formulas to measure the difference between the predicted forecast and measured data. The purpose of this work is not to cover the accuracy of solar forecast generation, but demonstrate how the uncertainty correlates to resilience of solar PV assets. In the following section, we cover the details of the purposed resilience framework.

5.3 Framework

In this section, we introduce the mathematical background for the resilience metric proposed for solar and battery storage assets. The metric is based on assets adaptive capacity and the following steps are taken for their calculation: determine the potential real and reactive power contribution, the flexibility from the operating point, consider temporal constraints, and then calculate the adaptive capacity.

5.3.1 Adaptive Capacity Calculation with Uncertainty

We begin by defining the potential contribution in real and reactive power an asset has on the grid. The power output of an asset is constrained by the apparent power in the complex S-plane and the limiting power output in the positive and negative plane. The apparent power in the S-plane is given as

$$S(\theta) = \sqrt{P^2 + Q^2} \tag{5.1}$$

where P and Q are the nameplate capacity in real and reactive power, respectively. Here the nameplate capacity is dependent on the real power plane. In the positive plane it is the nameplate capacity when the asset is a source. In the negative plane it is the nameplate capacity as a sink, i.e. a battery at max charging. The real and reactive power components of the apparent power are given as

$$P(\theta) = S\cos(\theta) \tag{5.2}$$

and

$$Q(\theta) = S\sin(\theta) \tag{5.3}$$

respectively. The power contribution of assets are limited by the apparent power and the limit of real power, therefore, the contribution limit of the asset is given as

$$P(\theta) = \begin{cases} \min\left[P(\theta),\ P_{\max}\right], & 0 \leq \theta \leq \frac{\pi}{2} \\ \min\left[P(\theta),\ P_{\max}\right], & \frac{3\pi}{2} \leq \theta < 2\pi \\ -\min\left[|P(\theta)|,\ |P_{\min}|\right], & \frac{\pi}{2} < \theta < \frac{3\pi}{2} \end{cases} \tag{5.4}$$

where $P_{\max}$ and $P_{\min}$ are the maximum output as a source in the positive plane and the maximum output as a sink in the negative plane, respectively.

In the context of solar assets, which only contribute to the grid as a power source, the real power in the negative plane is zero, $P_{\min}= 0$. Additionally, solar assets don't have a constant real power contribution due to changes in solar intensity. This results in an uncertainty, u, in the maximum real power generation. Therefore, the contribution of real power from solar assets is limited by

$$P(\theta)_{\text{Solar}} = \begin{cases} \min\left[P(\theta),\ P_{\max} \pm u\right], & 0 \leq \theta \leq \frac{\pi}{2} \\ \min\left[P(\theta),\ P_{\max} \pm u\right], & \frac{3\pi}{2} \leq \theta < 2\pi \\ 0, & \frac{\pi}{2} < \theta < \frac{3\pi}{2} \end{cases} \tag{5.5}$$

The resulting output bounds of a solar asset is shown notionally by the normalized output in the top plot in Fig. 5.1. Here, the bounding constraints on the output $S(\theta)$, $P_{\min}$, and $P_{\max} \pm u$ can be seen. The green region represents the upper uncertainty, the red is the lower uncertainty, and the line between them is the maximum real power output, which is considered the forecasted output in this work.

On the other hand, battery storage assets may operate in both the positive and negative plane as a source and a sink. However, their nameplate capacity in real power in the positive and negative plane may not be the same. Therefore, the power in the negative plane in Equation 5.4 is not zero. The resulting contribution in real and reactive power of a battery storage asset is shown notionally by the normalized output in the bottom plot in Fig. 5.1. Here, it is shown that the battery asset can only operate at half the real power as a sink as when a source.

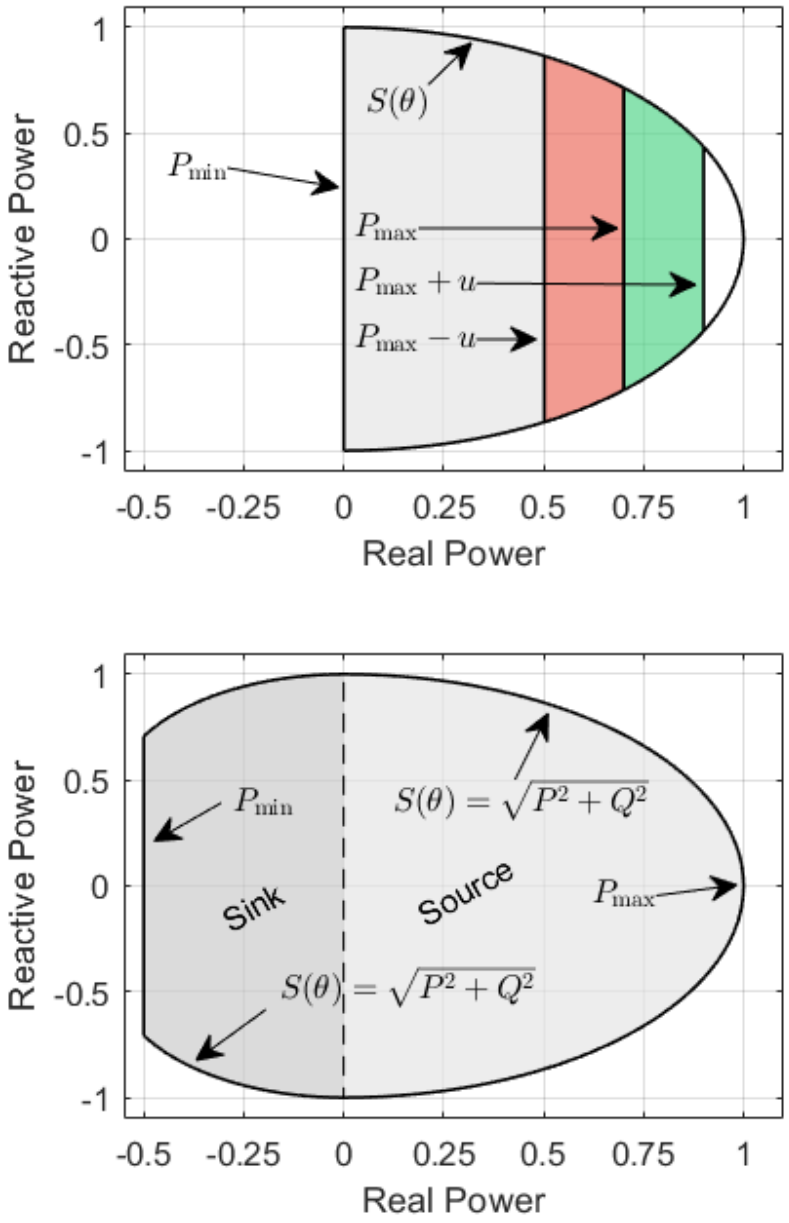

Figure 5.1 Normalized power capability of a solar asset (top) and a battery asset (bottom). The positive uncertainty of the solar asset is shaded green and the negative in red.

Next, we determine the flexibility of the asset which is a measure from the current operating point to the operating capability limits. Thus, the flexibility is a translation from P= 0, Q= 0 to the operating point P_0, Q_0. The limits of the operating power S, $P_{\max}$ and $P_{\min}$ take the form S', $P'_{\max}$, and $P'_{\min}$ after the translation for the flexibility. The flexibility in real power is given mathematically as

$$P_\Delta(\theta) = \begin{cases} \min\left[S'\cos(\theta),\ P'_{\max} \pm u\right], & 0 \le \theta \le \frac{\pi}{2} \\ \min\left[S'\cos(\theta),\ P'_{\max} \pm u\right], & \frac{3\pi}{2} \le \theta \le 2\pi \\ -\min\left[|S'\cos(\theta)|,\ |P'_{\min}|\right], & \frac{\pi}{2} < \theta < \frac{3\pi}{2} \end{cases} \tag{5.6}$$

here, battery assets have an uncertainty of zero. The flexibility in reactive power for both types of assets is given as

$$Q_\Delta(\theta) = S'\sin(\theta) \tag{5.7}$$

The flexibility of a solar asset with uncertainty is shown in Fig. 5.2, the current operation point is P = 0.25 and Q = -0.25.

Next, we consider the temporal limitations of the asset over the flexibility region. Temporal constraints include latency, ramp rates, and energy limitations. The latency, λ, is the time before a control action can make changes to the power output of the system. The ramp rate is how quick the asset can adjust the power output from the current operating point after the latency. The temporal constraint in real power

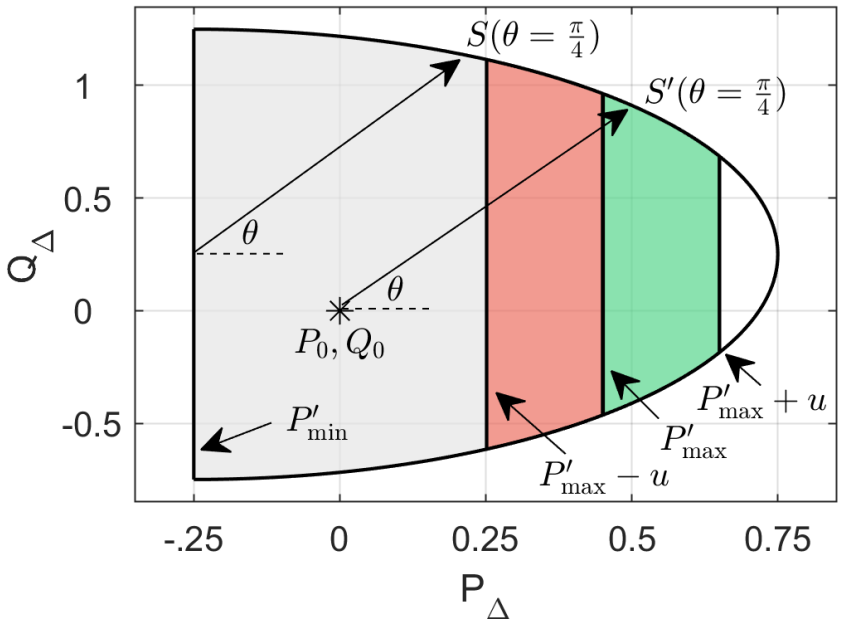

Figure 5.2 Flexibility in real power (P_Δ) and reactive power (Q_Δ) of a normalized solar asset at current operation of P_0= 0.25 and Q_0= -0.25. The flexibility is a translation from $P = 0, Q = 0$ to the operation point.

is given as

$$P(t) = \begin{cases} 0, & t \leq \lambda \\ \frac{dP}{dt}(t-\lambda), & t > \lambda \end{cases} \tag{5.8}$$

and the reactive power is

$$Q(t) = \begin{cases} 0, & t \leq \lambda \\ \frac{dQ}{dt}(t-\lambda), & t > \lambda \end{cases} \tag{5.9}$$

where t is the future time from current operation. Ramp rates may be dependent on direction and non-linear, i.e. the asset may ramp down quicker than it can ramp up. We denote the the temporal real power ramping up as $P(t)^+$ and as $P(t)^-$ when ramping down. The same is done for the reactive power.

With the flexibility and temporal constraints, we can calculate the adaptive capacity at all power factor angles. The adaptive capacity in real power is given as

$$P_{\text{AC}}(\theta, t) = \begin{cases} \min\left[P_\Delta,\ P(t)^+\right], & 0 \leq \theta \leq \frac{\pi}{2} \\ \min\left[P_\Delta,\ P(t)^+\right], & \frac{3\pi}{2} \leq \theta \leq 2\pi \\ -\min\left[|P_\Delta|,\ |P(t)^-|\right], & \frac{\pi}{2} < \theta < \frac{3\pi}{2} \end{cases} \tag{5.10}$$

and the adaptive capacity in reactive power is given as

$$Q_{\text{AC}}(\theta, t) = \begin{cases} \min\left[Q_\Delta,\ Q(t)^+\right], & 0 \leq \theta \leq \pi \\ -\min\left[|Q_\Delta|,\ |Q(t)^-|\right], & \pi < \theta < 2\pi \end{cases} \tag{5.11}$$

The adaptive capacity in real power at a power factor angle of 0 and π is depicted in

Fig. 5.3. In the top plot, it can be seen that the flexibility of the asset is constrained by the maximum and minimum power at these power factor angles. The bottom plot indicates the temporal constraints of the asset. The manifold shows the three dimensional view of these calculations at all power factor angles.

The adaptive capacity of assets can be aggregated together to give the adaptive capacity of a group of asset. The aggregation of real power is given as

$$P_{\mathrm{AC}}(\theta, t) = \sum_{k=1}^{n} P_{\mathrm{AC}_k} \tag{5.12}$$

and the reactive power is given as

$$Q_{\mathrm{AC}}(\theta, t) = \sum_{k=1}^{n} Q_{\mathrm{AC}_k} \tag{5.13}$$

where n is the number of assets. The aggregation of a solar and battery asset is shown in Fig. 5.4. It can be seen that the aggregated adaptive capacity is the sum of the individual assets at any given power factor angle.

5.4 Case Studies

In this section we demonstrate the resilience metric purposed in a case study using very short-term and short-term solar PV forecast data. First, we introduce the data set used in this study.

5.4.1 Solar Generation and Forecast Data Set

National Renewable Energy Laboratory provides synthetic year long data for approximately 6,000 simulated PV plants[2]. The forecast data consist of 60-minute intervals

[2]https://www.nrel.gov/grid/solar-power-data.html

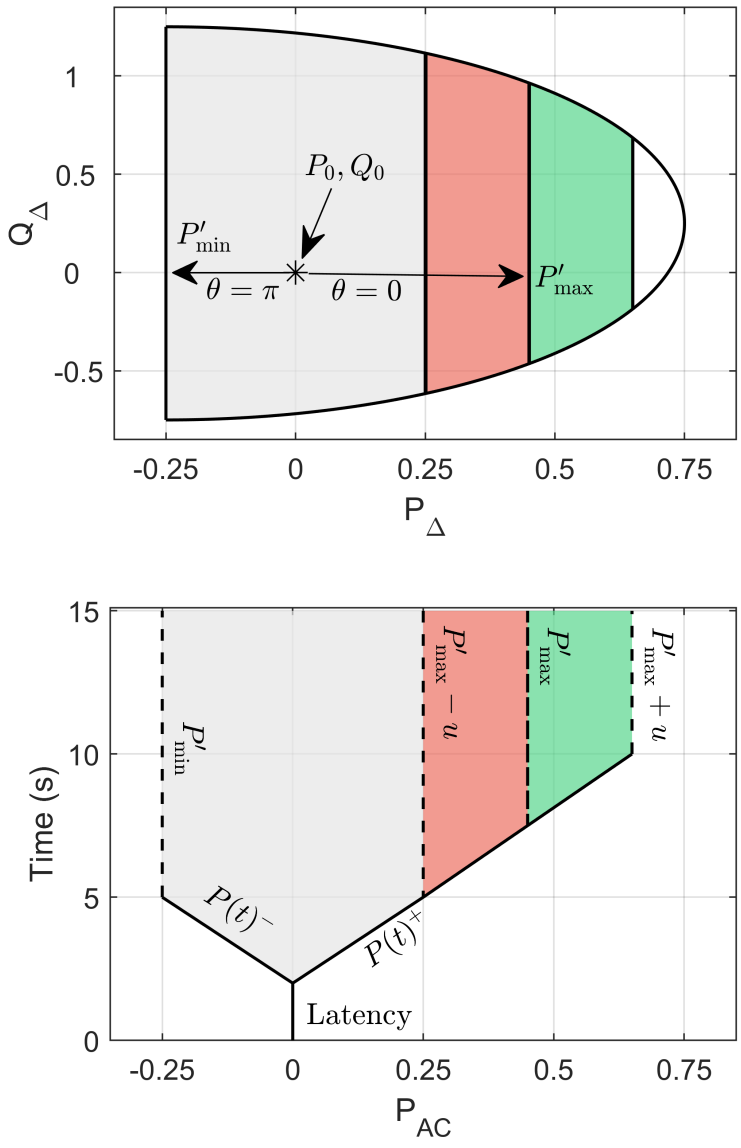

Figure 5.3 Top plot shows the flexibility of a normalized solar asset and indicates the flexibility in real power at power factor angles of 0 and π. Bottom plot shows the real power flexibility from the operation point with latency and ramp rate constraints.

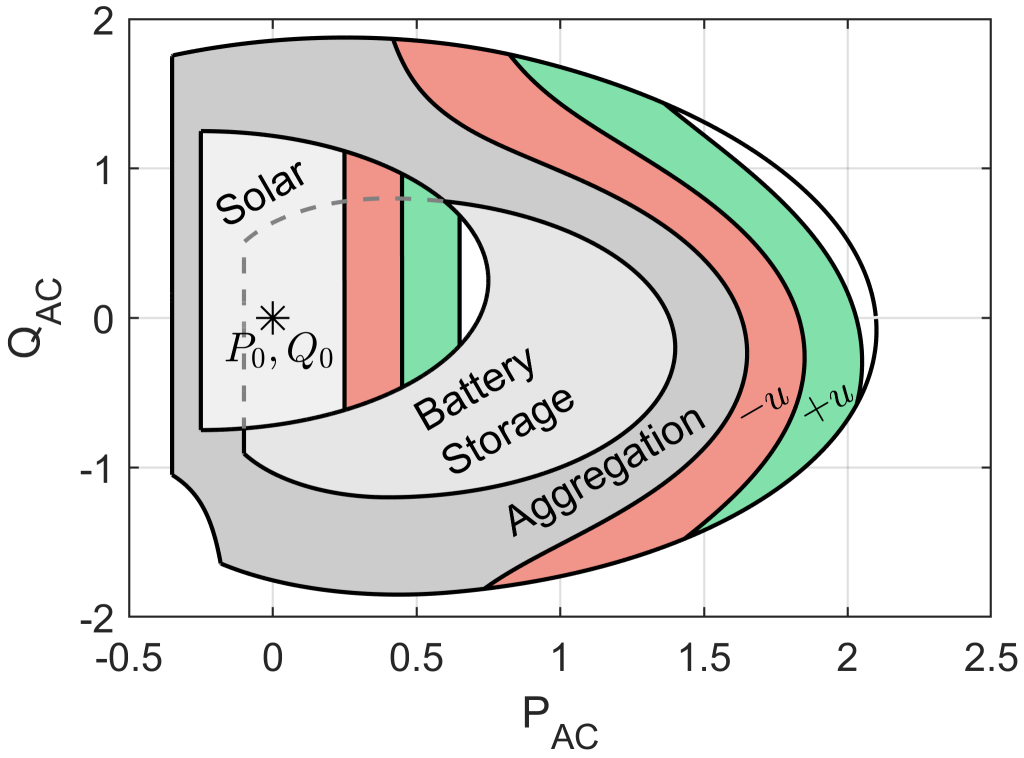

Figure 5.4 Normalized adaptive capacity of solar and battery storage asset with operating point indicated by the data marker. Aggregation is shown and indicates the adaptive capacity of the system assets with uncertainty. Note, that temporal constraints are not considered here.

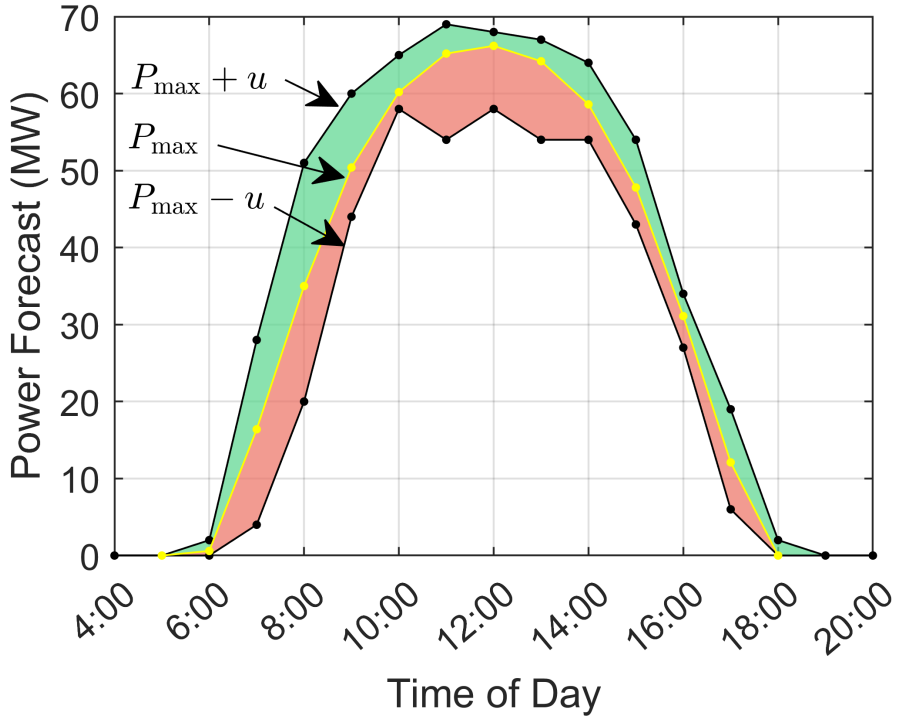

Figure 5.5 Day-ahead solar forecast data. Yellow line represents the forecast ($P_{\max}$) and the green and red regions are the upper and lower uncertainty, respectively.

for both day-ahead and 4 hour-ahead predictions. The data was generated using the 3TIER based on numerical weather predication simulations. In this work, solar data from Saturday, August 19th, 2006, in Arizona at location 33.45, -112.95 (latitude, longitude) was selected. The forecast data does not provide uncertainty, therefore, we generate uncertainty similar to that in [92]. We point out that the accuracy of uncertainty is not the focus of this work, but the effect it has on the adaptive capacity of solar PV generation. The forecast data and uncertainty used in the case studies is shown in Fig. 5.5. We begin with the very short-term forecast.

5.4.2 Very Short-term Power Forecast

Very short-term solar generation forecast are on the order of seconds or minutes. At this time scale the latency and ramp rate constraints are highly important for the assets' adaptive capacity. To demonstrate the very short-term adaptive capacity of a solar PV asset we use the forecast data in Fig. 5.5 at noon. We apply a current power generation output of 50 MW, use a 1 second latency, and assume ramp rates for the real power in the positive and negative direction to be 10 MW/s and the reactive in both directions is 10 MVAR/s. The resulting adaptive capacity of the asset using the forecasted power data is shown by the yellow plot in the top plot of Fig. 5.6. In this figure, the red middle plot represents the negative uncertainty, and the green bottom plot represents the positive uncertainty. The plots have been zoomed in near the operating point to show the difference in the adaptive capacity in the positive real direction (all plots in the negative real direction are identical). It can be seen that when when solar generation is in the negative uncertainty direction the adaptive capacity in real power is very small. On the other hand, when it is in the positive uncertainty direction there is additional adaptive capacity in real power. In the following section, we will look at the short-term forecast using day-long forecast data.

5.4.3 Short-term Power Forecast

In this scenario, we consider the short-term power forecast to be day-ahead forecast power generation over a day, i.e. the full data shown in Fig. 5.5. We assume that the forecasted generation will be the operating point of the asset over the day. The results of the adaptive capacity, again near the origin to highlight the real power adaptive capacity differences, are shown in Fig. 5.7. Here, the top plot represents the asset

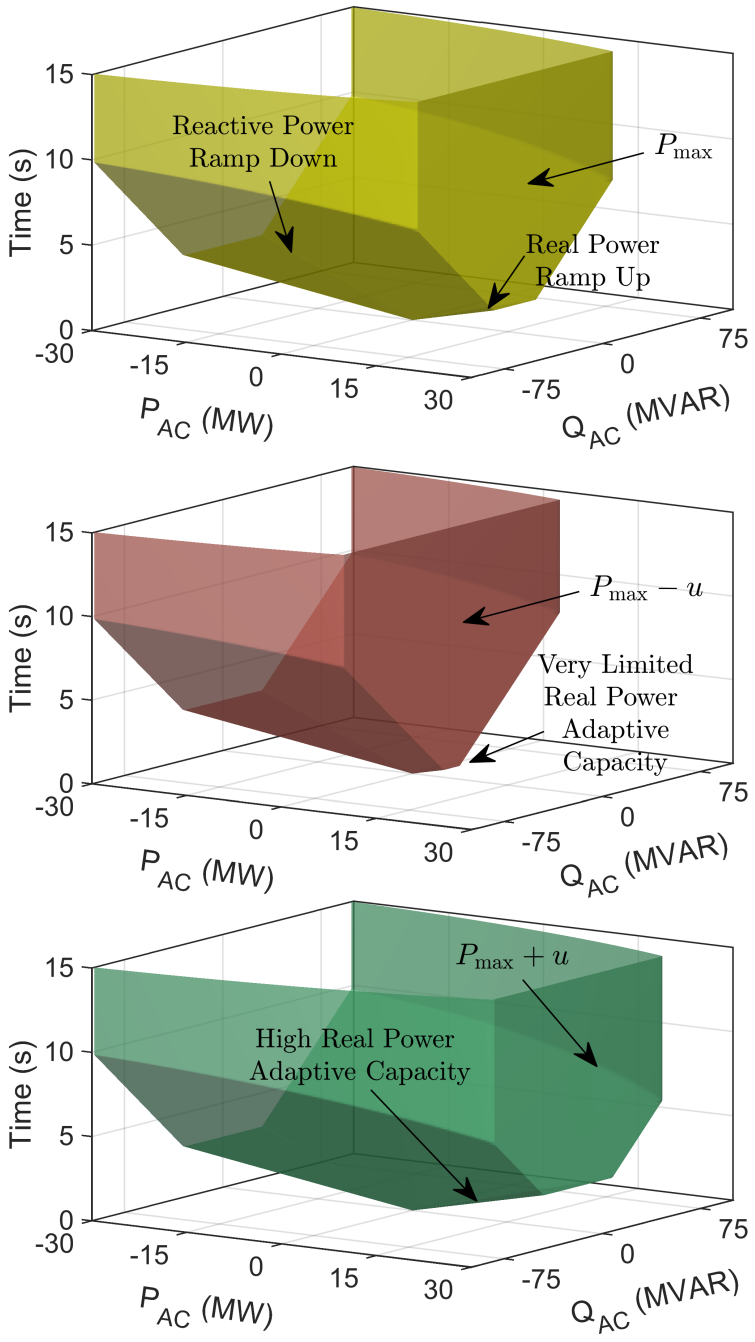

Figure 5.6 Very short-term adaptive capacity at 12:00 noon assuming power output of 50 MW. Top plot represents forecast data, middle represents negative uncertainty, and the bottom is positive uncertainty.

adaptive capacity at the solar forecast, the middle represents the adaptive capacity for the negative uncertainty, and the lower plot represent the adaptive capacity for the positive uncertainty. It can be seen that when the forecast generation is correct the adaptive capacity in the positive real power direction is zero. When the generation is at the positive uncertainty the solar PV asset contributes to additional real power adaptive capacity, therefore adding to the resilience of the overall grid. On the other hand, when the generation is at the negative uncertainty the real power adaptive capacity is negative and the asset may be considered a disturbance on the power system. In this case, reserve power must be used in order to maintain the desired frequency of the grid. For this reason, we next consider the addition of battery storage to this scenario.

The additional battery storage asset is assumed to have a maximum power output of 20 MW as a source and -10 MW as a sink with ±20 MVAR reactive capability. The operating point is assumed to be idle, where $P_0 = 0$ and $Q_0 = 0$. The results of the aggregation of the solar adaptive capacity at negative uncertainty and the battery storage asset is shown in Fig. 5.8. It can be seen that the addition of the battery asset contributes to the adaptive capacity in the positive real power. Therefore, the system has the capability to respond to a disturbances in this direction, i.e. there is reserve power for an operator to maintain frequency stability of the system.

5.5 Conclusion and Future Work

This paper has provided a framework for considering the resilience contribution of solar and battery storage assets to the grid. The novel contribution is addition of uncertainty in adaptive capacity for solar generation assets. We demonstrated the metric in a case study using very short-term (seconds) and short-term (day-long) solar

forecast with uncertainty and provided the resilience that both the solar and battery assets contribute to the grid. It was demonstrated that when solar generation is above the forecast it provides additional adaptive capacity in the positive direction of real power. However, when it is below the forecasted generation, the adaptive capacity in the positive real power direction is negative, and may be considered a disturbance to the system. The addition of battery storage in this case demonstrated the ability to aggregate assets and provide the needed adaptive capacity in real power.

Future work includes implementation of the metric in a simulated environment such as Simulink or OPAL-RT. It is envisioned that the resilience metric will be used to influence the control decisions and result in a lower loss of power served to consumers during physical degradation and cyber attack scenarios.

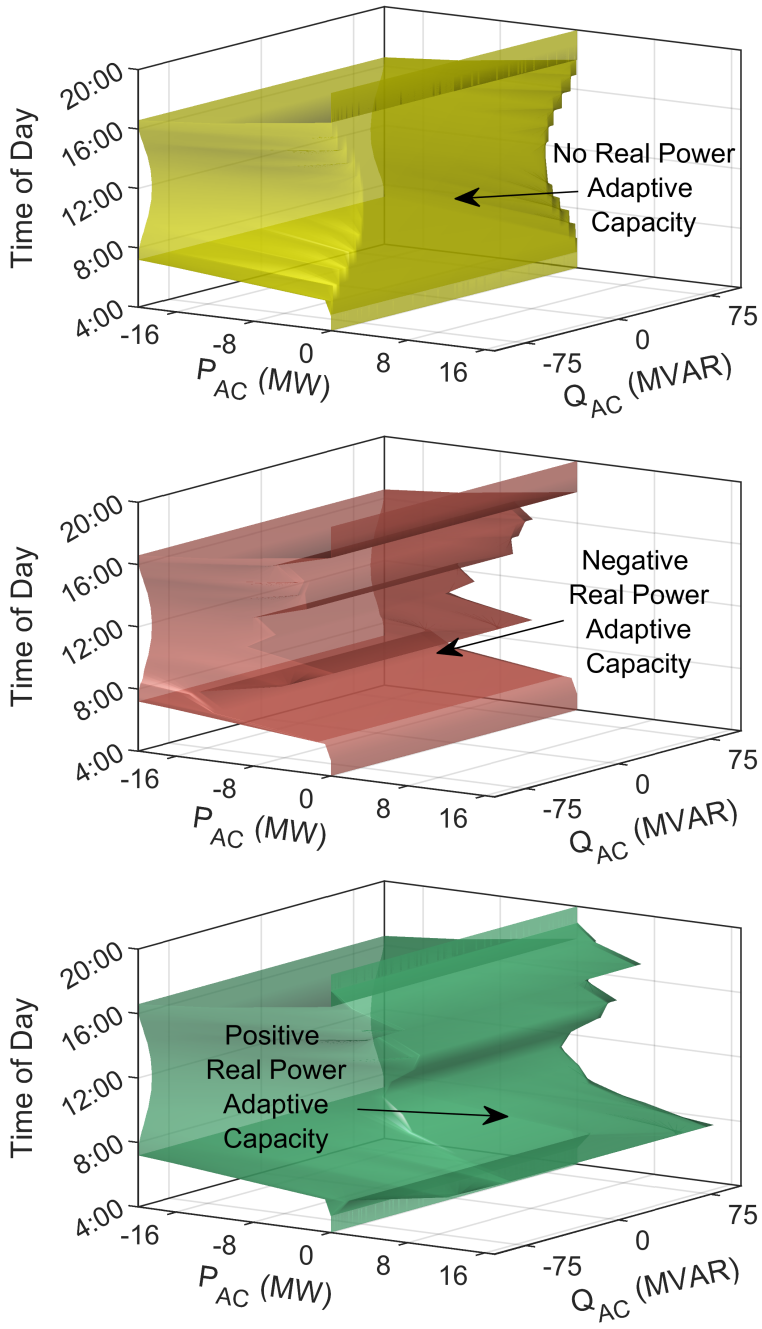

Figure 5.7 Day-long adaptive capacity of the solar asset at forecast gener-ation (top), negative uncertainty (middle), and positive uncertainty (bot-tom). Here the operation point is assumed to be the forecast output in each plot.

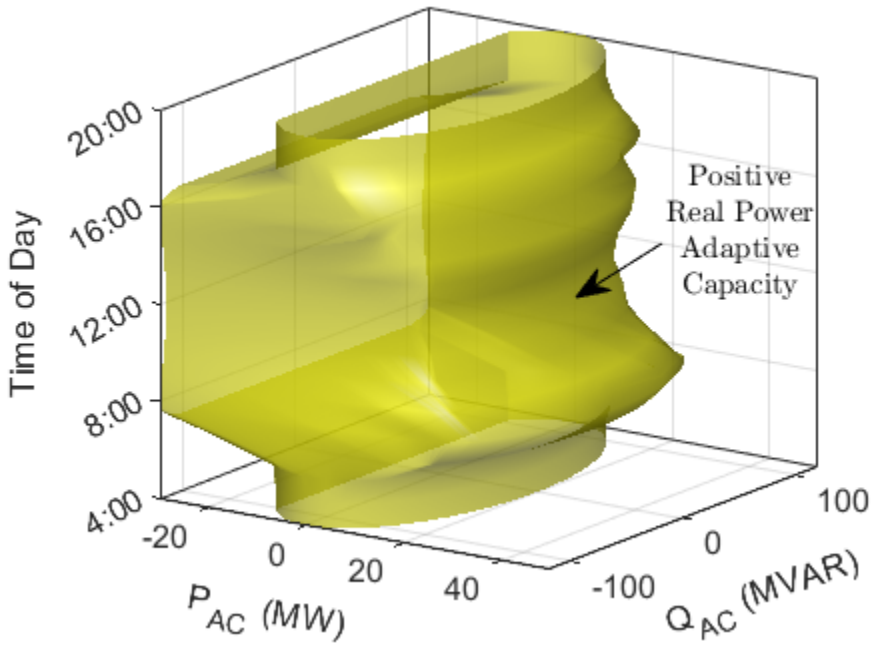

Figure 5.8 Aggregation of day-long adaptive capacity of a solar asset at negative uncertainty (middle plot in Fig. 5.7) and battery storage asset at idle.

CHAPTER 6:

CONCLUSION AND FUTURE WORK

The work in this dissertation covered two main topics; first the identification of a potential cyber threat to control system, and second to lay the foundation for a resilience framework to better ensure a continuous supply of electricity in the grid.

The work in Chapter 2 provided a proof-of-concept which indicates a potential vulnerability to constant setpoint control systems. It was demonstrated that a covert cyberattack which targets a controllers PID algorithm can force excitation in system parameters, giving a more accurate dynamic model of the system through data drive system identification. This attack is shown on a series of simulations and the covertness to physics-based anomaly detection is made. The more accurate dynamic model of the system will allow a cyberattacker to design more sophisticated attacks with a higher likelihood of them being carried out successfully. Therefore, future work includes the development of a machine learning physics-based anomaly detection scheme which can identify the PID attack. Furthermore, it is desired to use a model which better represents critical infrastructure, such as the Tennessee Eastman Process.

The work in Chapter 3 presents an operational resilience metric based on the adaptive capacity in real and reactive power. The mathematical details of the adaptive capacity is covered and considers the real-time operational output of the asset,

its ramp rates, latency, and energy limitations. The metric is applied to different assets and the results are aggregated to indicate the amplitude and duration of a disturbance that a set of assets can withstand. It was demonstrated that the resulting adaptive capacity of a microgrid under different scenarios can be used by operators to make resilience informed decisions. Future work includes improving the metric by the use of higher fidelity models of assets by using more accurate real and reactive power capabilities, non-linear ramp rates, latency, and energy constraints.

The work in Chapter 4 takes a deep dive into the resilience contribution of hydropower assets and provides a framework that could be adapted for other energy assets on the grid. The capability of different types of hydropower assets is captured through the adaptive capacity giving a resilience analysis applied to the grid. At current state the focus is on the response epoch. However, the framework seeks to encompass all the epochs of resilience as hydropower in general has the ability to support all the time frames or "Rs" of resilience. This type of analysis will help operators make informed decisions when considering the trade-offs between the use of hydropower in the response epoch, reserving capabilities for recover and restore, and maximum energy production. Future work includes increasing the fidelity of the modeled assets, including the use of generator capability curves and AGC ramping limitations, and application of the inertia of the generator. Additionally, there is a need to connect the assets contribution to the needed location through the connection of the network through transmission or distribution lines.

The work in Chapter 5 focuses on the resilience contribution of solar PV and battery storage on the grid. The novel contribution is the addition of uncertainty in the adaptive capacity of assets. It was demonstrated using very short-term (seconds)

and short-term (day-long) solar PV generation forecast with uncertainty. It was demonstrated that addition of battery storage to a solar generation asset can be used to maintain adaptive capacity during times where solar generation is at the negative uncertainty scenario. Future work includes the implementation of the metric in a simulated real-time environment such as OPAL-RT and the resulting metric can be used to inform decisions to better serve power to customers and critical loads.

REFERENCES

[1] M. M. Adibi and L. H. Fink. Overcoming restoration challenges associated with major power system disturbances - restoration from cascading failures. *IEEE Power and Energy Magazine*, 4(5):68–77, 2006.

[2] U.S. Energy Information Administration. EIA expects U.S. electricity generation from renewables to soon surpass nuclear and coal, 2020. `https://www.eia.gov/todayinenergy/detail.php?id=42655`.

[3] S. Amin, X. Litrico, S. Sastry, and A. M. Bayen. Cyber security of water SCADA Systems-Part I: Analysis and experimentation of stealthy deception attacks. *IEEE Transactions on Control Systems Technology*, 21(5):1963–1970, Sep. 2013.

[4] M. Amirioun, F. Aminifar, H. Lesani, and M. Shahidehpour. Metrics and quantitative framework for assessing microgrid resilience against windstorms. *International Journal of Electrical Power & Energy Systems*, 104:716–723, 2019.

[5] B. Anderson and M. Bell. Lights out impact of the august 2003 power outage on mortality in New York, NY. *Epidemiology (Cambridge, Mass.)*, 23:189–93, 03 2012.

[6] P. Bacher, H. Madsen, and H. Aalborg Nielsen. Online short-term solar power forecasting. *Solar Energy*, 83(10):1772 – 1783, 2009.

[7] R. E. Brown. Hurricane hardening efforts in Florida. In *2008 IEEE Power and Energy Society General Meeting - Conversion and Delivery of Electrical Energy in the 21st Century*, pages 1–7, 2008.

[8] R.J. Campbell. Weather-related power outages and electric system resiliency. Technical report, CRS Report for Congress, 01 2013.

[9] V. Chalishazar. Evaluating the seismic risk and resilience of an electrical power system. *PhD Dissertation, Oregon State University*, 2019.

[10] V. Chalishazar, T. Brekken, D. Johnson, K. Yu, J. Newell, K. Chin, R. Weik, E. Dierickx, M. Craven, M. Sauter, A. Olennikov, J. Galaway, and A. Radil. Connecting risk and resilience for a power system using the Portland Hills fault case study. *Processes*, 8(10: 1200), 2020.

[11] V. Chalishazar, B. Johnson, E. Cotilla-Sanchez, and T. K. A. Brekken. Augmenting the traditional bus-branch model for seismic resilience analysis. In *2018 IEEE Energy Conversion Congress and Exposition (ECCE)*, pages 1133–1137, 2018.

[12] S. Chanda and A. K. Srivastava. Defining and enabling resiliency of electric distribution systems with multiple microgrids. *IEEE Transactions on Smart Grid*, 7(6):2859–2868, Nov 2016.

[13] L. Che, M. Khodayar, and M. Shahidehpour. Only connect: Microgrids for

distribution system restoration. *IEEE Power and Energy Magazine*, 12(1):70–81, Jan 2014.

[14] C. Chen, J. Wang, F. Qiu, and D. Zhao. Resilient distribution system by microgrids formation after natural disasters. *IEEE Transactions on Smart Grid*, 7(2):958–966, March 2016.

[15] I. Chernyakhovskiy, T. Tian, J. McLaren, M. Miller, and N. Geller. U.S. laws and regulations for renewable energy grid interconnections. Technical report, National Renewable Energy Laboratory, 2016.

[16] K. Choopani, R. Effatnejad, and M. Hedayati. Coordination of energy storage and wind power plant considering energy and reserve market for a resilience smart grid. *Journal of Energy Storage*, 30:101542, 2020.

[17] E. Ciapessoni, D. Cirio, A. Pitto, P. Marcacci, and M. Sforna. Security-constrained redispatching to enhance power system resilience in case of wet snow events. In *2018 Power Systems Computation Conference (PSCC)*, pages 1–7, June 2018.

[18] Congressional Research Service. Electric reliability and power system resilience. Technical report, CRS Insight, 2018. `https://www.everycrsreport.com/reports/IN10895.html`.

[19] A. de Sá, L. Fernando, and R. Machado. Covert attacks in cyber-physical control systems. *IEEE Transactions on Industrial Informatics*, 13:1641–1651, 2017.

[20] A. de Sá, Luiz L. Carmo, and R. Machado. Bio-inspired active system identification: a cyber-physical intelligence attack in networked control systems. *Mobile Networks and Applications*, Oct 2017.

[21] A. Oliveira de Sá, L. F. R. da Costa Carmo, and R. Machado. A controller design for mitigation of passive system identification attacks in networked control systems. *Journal of Internet Services and Applications*, 9:1–19, 2017.

[22] P. Dehghanian, S. Aslan, and P. Dehghanian. Quantifying power system resiliency improvement using network reconfiguration. In *2017 IEEE 60th International Midwest Symposium on Circuits and Systems (MWSCAS)*, pages 1364–1367, Aug 2017.

[23] G Dielen. Renewable energy technologies-cost analysis series: Hydropower. *International Renewable Energy Agency*, 2012.

[24] Z. Dong, J. Tan, E. Muljadi, R. Nelms, and M. Jacobson. Impacts of ternary-pumped storage hydropower on U.S. Western Interconnection with extremely high renewable penetrations. In *2019 IEEE Power Energy Society General Meeting (PESGM)*, pages 1–5, 2019.

[25] D. Esmaeil Moghadam, A. Shiri, S. Sadr, and D. A. Khaburi. A practical method for calculation of over-excited region in the synchronous generator capability curves. In *2014 IEEE 23rd International Symposium on Industrial Electronics (ISIE)*, pages 727–732, 2014.

[26] A. A. Farooqui, S. S. H. Zaidi, A. Y. Memon, and S. Qazi. Cyber security

backdrop: A SCADA testbed. In *2014 IEEE Computers, Communications and IT Applications Conference*, pages 98–103, Oct 2014.

[27] E. Geraldi, F. Romano, and E. Ricciardelli. An advanced model for the estimation of the surface solar irradiance under all atmospheric conditions using MSG/SEVIRI data. *IEEE Transactions on Geoscience and Remote Sensing*, 50(8):2934–2953, 2012.

[28] J. Giraldo, D. Urbina, A. Cardenas, J. Valente, M. Faisal, J. Ruths, N. Tippenhauer, H. Sandberg, and R. Candell. A survey of physics-based attack detection in cyber-physical systems. *ACM Comput. Surv.*, 51(4):76:1–76:36, July 2018.

[29] J. Hanania, K. Stenhouse, E. Cey, L. Goodfellow, B. Afework, and J. Donev. Energy education-run-of-the-river hydroelectricity, 2018.

[30] M. Hellmuth, P. Cookson, and J. Potter. Addressing climate vulnerability for power system resilience and energy security: A focus on hydropower resources. RALI Series: Promoting Solutions for Low Emission Development, May 2017. USAID Report.

[31] D. Henry and J. Ramirez-Marquez. On the impacts of power outages during Hurricane Sandy - a resilience-based analysis. *Systems Engineering*, 19(1):59–75, 2016.

[32] D. Henry and J. Emmanuel Ramirez-Marquez. Generic metrics and quantitative approaches for system resilience as a function of time. *Reliability Engineering & System Safety*, 99:114 – 122, 2012.

[33] C. Holling. Resilience and stability of ecological systems. *Annual Review of Ecology and Systematics*, 4(1):1–23, 1973.

[34] E. Hollnagel, D. Woods, and N. Leveson. *Resilience Engineering: Concepts and precepts*. Ashgate Publishing, 2006.

[35] M. M. Hosseini, A. Umunnakwe, and M. Parvania. Automated switching operation for resilience enhancement of distribution systems. In *2019 IEEE Power Energy Society General Meeting (PESGM)*, pages 1–5, 2019.

[36] G. Huang, J. Wang, C. Chen, J. Qi, and C. Guo. Integration of preventive and emergency responses for power grid resilience enhancement. *IEEE Transactions on Power Systems*, 32(6):4451–4463, Nov 2017.

[37] A. Imteaj, M. Hadi Amini, and J. Mohammadi. Leveraging decentralized artificial intelligence to enhance resilience of energy networks, 2019.

[38] Electric Power Research Institute. Grid resiliency. `https://www.epri.com/#/grid_resiliency`. Accessed: 1/30/2020.

[39] Institute of Electrical and Electronics Engineers. IEEE guide for electric power distribution reliability indices. *IEEE Std 1366-2012 (Revision of IEEE Std 1366-2003)*, pages 1–43, May 2012.

[40] B. Johnson, V. Chalishazar, E. Cotilla-Sanchez, and T. Brekken. A Monte Carlo methodology for earthquake impact analysis on the electrical grid. *Electric Power Systems Research*, 184:106332, 2020.

[41] Shijoe Jose, D. Malathi, Bharath Reddy, and Dorathi Jayaseeli. A survey on anomaly based host intrusion detection system. *Journal of Physics: Conference Series*, 1000:012049, apr 2018.

[42] M. Kazama and T. Noda. Damage statistics: Summary of the 2011 off the Pacific Coast of Tohoku Earthquake damage. *Soils and Foundation*, 2012.

[43] H. Khaloie, A. Abdollahi, M. Rashidinejad, and P. Siano. Risk-based probabilistic-possibilistic self-scheduling considering high-impact low-probability events uncertainty. *International Journal of Electrical Power & Energy Systems*, 110:598 – 612, 2019.

[44] M. Khomami, K. Jalilpoor, M. Kenari, and M. Sepasian. Bi-level network reconfiguration model to improve the resilience of distribution systems against extreme weather events. *IET Generation Transmission & Distribution*, 05 2019.

[45] V. Koritarov, T. Veselka, J. Gasper, B. Bethke, A. Botterud, J. Wang, M. Mahalik, Z. Zhou, C. Milostan, J. Feltes, Y. Kazachkov, T. Guo, G. Liu, B. Trouille, P. Donalek, K. King, E. Ela, B. Kirby, I. Krad, and V. Gevorgian. Modeling and analysis of value of advanced pumped storage hydropower in the united states. Technical report, Argonne National Lab. (ANL), Argonne, IL, 2014.

[46] M. Krotofil and J. Larsen. Rocking the pocket book: Hacking chemical plants for competition and extortion. Report P-41, DEFCON, 2015.

[47] Idaho National Laboratory. Cyber threat and vulnerability analysis of the U.S. electric sector. Technical report, 2016.

[48] R. Langner. Stuxnet: Dissecting a cyberwarfare weapon. *IEEE Security and Privacy*, 9(3):49–51, May 2011.

[49] L. Lerner. *Trustworthy Embedded Computing for Cyber-Physical Control*. PhD thesis, Virginia Tech, 2015.

[50] G. Liang, S. R. Weller, J. Zhao, F. Luo, and Z. Y. Dong. The 2015 Ukraine blackout: Implications for false data injection attacks. *IEEE Transactions on Power Systems*, 32(4):3317–3318, 2017.

[51] L. Ljung. System identification. *Wiley Encyclopedia of Electrical and Electronics Engineering*, 2001.

[52] M. Long, Chwan-Hwa Wu, and J. Y. Hung. Denial of service attacks on network-based control systems: impact and mitigation. *IEEE Transactions on Industrial Informatics*, 1(2):85–96, May 2005.

[53] Y. Luo, M. Mohanpurkar, R. Hovsapian, V. Gevorgian, E. Muljadi, and V. Koritarov. Enhancing the flexibility of generation of run-of-the-river hydro power plants. Technical report, Idaho National Lab.(INL), Idaho Falls, ID, 2018.

[54] A. Magali and M. Montes-Sancho. U.S. state policies for renewable energy: Context and effectiveness. *Energy Policy*, 39(5):2273 – 2288, 2011.

[55] M. Manwaring, D. Mursch, and K. Tilford. Challenges and opportunities for new pumped storage development. *A White Paper Developed by NHAs Pumped Storage Development Council. NHAPumped Storage Development Council, USA*, 2012.

[56] P. March. Flexible operation of hydropower plants. Technical report, Electric Power Research Institute (EPRI), Palo Alto, CA, 2017.

[57] The Mathworks, Inc., Natick, Massachusetts. *MATLAB version 9.5 (R2018b)*, 2018.

[58] The Mathworks, Inc., Natick, Massachusetts. *Simulink version 9.2 (R2018b)*, 2018.

[59] M. McGranaghan, M. Olearczykm, and C. Gellings. Enhancing distribution resiliency: Opportunities for applying innovative technologies. Technical Report 1026889, Electric Power Research Institute, 2013.

[60] T. R. McJunkin and C. G. Rieger. Electricity distribution system resilient control system metrics. In *2017 Resilience Week (RWS)*, pages 103–112, Sep. 2017.

[61] H. Mehrpouyan, D. Giannakopoulou, G. Brat, I. Tumer, and C. Hoyle. Complex engineered systems design verification based on assume-guarantee reasoning. *Systems Engineering*, 19(6):461–476, 2016.

[62] H. Mehrpouyan, D. Giannakopoulou, I. Tumer, C. Hoyle, and G. Brat. Combination of compositional verification and model checking for safety assessment of complex engineered systems. In *ASME 2014 International Design Engineering Technical Conferences and Computers and Information in Engineering Conference*. American Society of Mechanical Engineers Digital Collection, 2015.

[63] H. Mehrpouyan, B. Haley, A. Dong, I. Tumer, and C. Hoyle. Resiliency analysis for complex engineered system design. *AI EDAM*, 29(1):93–108, 2015.

[64] H. Mehrpouyan, I. Tumer, C. Hoyle, D. Giannakopoulou, and G. Brat. Formal verification of complex systems based on sysml functional requirements. Technical report, Columbus State University Columbus United States, 2014.

[65] F. Mengfei, Z. Zhiguo, Z. Enrico, R. Kang, and Y. Chen. A stochastic hybrid systems model of common-cause failures of degrading components. *Reliability Engineering & System Safety*, 172:159 – 170, 2018.

[66] B. Messner and D. Tilbury. Control Tutorials for MATLAB and Simulink (CTMS): Inverted Pendulum System Modeling. `http://ctms.engin.umich.edu/CTMS/index.php?aux=Home`.

[67] C. Murphy, Y. Sun, W. Cole, G. Maclaurin, M. Mehos, and C. Turchi. The potential role of concentrating solar power within the context of DOE's 2030 solar cost targets, 1 2019.

[68] S. Nanou, A. Papakonstantinou, and S. Papathanassiou. A generic model of two-stage grid-connected PV systems with primary frequency response and inertia emulation. *Electric Power Systems Research*, 127:186 – 196, 2015.

[69] National Acedemies of Sciences, Engineering, and Medicine. Enhancing the resilience of the nation's electricity system. `https://doi.org/10.17226/24836`, 2017.

[70] H. Nguyen, J. Muhs, and M. Parvania. Assessing impacts of energy storage on resilience of distribution systems against hurricanes. *Journal of Modern Power Systems and Clean Energy*, 07 2019.

[71] N. Nicolaou, D. G. Eliades, C. Panayiotou, and M. M. Polycarpou. Reducing vulnerability to cyber-physical attacks in water distribution networks. In *2018 International Workshop on Cyber-physical Systems for Smart Water Networks (CySWater)*, pages 16–19, April 2018.

[72] C. Nicolet, A. Beguin, B. Kawkabani, Y. Pannatier, A. Schwery, and F. Avellan. Variable speed and ternary units to mitigate wind and solar intermittent production. *Hydro Vision*, 2014.

[73] S. Niu and M. Insley. On the economics of ramping rate restrictions at hydro power plants: Balancing profitability and environmental costs. *Energy Economics*, 39:39–52, 2013.

[74] M. Oboudi, M. Mohammadi, and M. Rastegar. Resilience-oriented intentional islanding of reconfigurable distribution power systems. *Journal of Modern Power Systems and Clean Energy*, 7(4):741–752, Jul 2019.

[75] M. Hosseini Oboudi and M. Parvania. Quantifying impacts of automation on resilience of distribution systems. *IET Smart Grid*, 02 2020.

[76] L. Obregon. Secure Architecture for Industrial Control Systems. Technical report, SANS Institute, 2015.

[77] Energy Policy Act of 2005. Public Law No. 109-58, 119 Stat. 594, 2005.

[78] U.S. Department of Energy. The smart grid, 2020. `https://www.eia.gov/todayinenergy/detail.php?id=42655https://www.smartgrid.gov/the_smart_grid/smart_grid.html`.

[79] US Department of Homeland Security. Recommended practice: Improving industrial control system cybersecurity with defense-in-depth strategies: Industrial control systems. Technical report, Homeland Security Cyber Emergency Response Team, 2016.

[80] B. Ogunnaike and W. H. Ray. *Process Dynamics, Modeling, and Control*. Oxford University Press, New York, 1994.

[81] M. Ouyang. A three-stage resilience analysis framework for urban infrastructure systems. *Structural Safety*, 36-37:23–31, 03 2012.

[82] M. Ouyang and L. Duenas-Osorio. Time-dependent resilience assessment and improvement of urban infrastructure systems. *Chaos (Woodbury, N.Y.)*, 22:033122, 09 2012.

[83] M. Panteli and P. Mancarella. The grid: Stronger, bigger, smarter?: Presenting a conceptual framework of power system resilience. *IEEE Power and Energy Magazine*, 13(3):58–66, 2015.

[84] M. Panteli, P. Mancarella, D. Trakas, E. Kyriakides, and N. Hatziargyriou. Metrics and quantification of operational and infrastructure resilience in power systems. *IEEE Transactions on Power Systems*, 32(6):4732–4742, Nov 2017.

[85] M. Panteli, D. N. Trakas, P. Mancarella, and N. Hatziargyriou. Power systems resilience assessment: Hardening and smart operational enhancement strategies. *Proceedings of the IEEE*, 105(5):1202–1213, 2017.

[86] M. Panteli, D. N. Trakas, P. Mancarella, and N. D. Hatziargyriou. Power

systems resilience assessment: Hardening and smart operational enhancement strategies. *Proceedings of the IEEE*, 105(7):1202–1213, July 2017.

[87] W. Parker, B. K. Johnson, C. Rieger, and T. McJunkin. Identifying critical resiliency of modern distribution systems with open source modeling. In *2017 Resilience Week (RWS)*, pages 113–118, Sep. 2017.

[88] R. Perez, E. Lorenz, S. Pelland, M. Beauharnois, G. Van Knowe, K. Hemker, D. Heinemann, J. Remund, S. C. Mller, W. Traunmller, G. Steinmauer, D. Pozo, J. A. Ruiz-Arias, V. Lara-Fanego, L. Ramirez-Santigosa, M. Gaston-Romero, and L. M. Pomares. Comparison of numerical weather prediction solar irradiance forecasts in the US, Canada and Europe. *Solar Energy*, 94:305 – 326, 2013.

[89] F. Petit and V. Vargas. Grid modernization: Metrics analysis (GMLC1.1) resilience, 2020.

[90] T. Phillips, T. McJunkin, C. Rieger, John G., and H. Mehrpouyan. An operational resilience metric for modern power distribution systems. In *2020 IEEE International Conference on Software Quality, Reliability and Security Companion (QRS-C), Requirements*, 2020.

[91] F. Qiu and P. Li. An integrated approach for power system restoration planning. *Proceedings of the IEEE*, 105(7):1234–1252, 2017.

[92] S. Rafique, Z. Jian-hua, R. Rafique, J. Guo, and I. Jamil. Renewable generation (wind/solar) and load modeling through modified fuzzy prediction interval. *International Journal of Photoenergy*, 2018:1–14, 2018.

[93] F. Rasapour and H. Mehrpouyan. Misusing sensory channel to attack industrial control systems. In *Proceedings of the Eighth ACM Conference on Data and Application Security and Privacy*, pages 158–160. ACM, 2018.

[94] D. Reed, M. Powell, and J. Westerman. Energy supply system performance for Hurricane Katrina. *Journal of Energy Engineering*, 136(4):95–102, 2010.

[95] M. Rezaeimozafar, M. Amini, and M. Moradi. Innovative appraisement of smart grid operation considering large-scale integration of electric vehicles enabling V2G and G2V systems. *Electric Power Systems Research*, 154:245–256, 01 2018.

[96] C. G. Rieger. Resilient control systems practical metrics basis for defining mission impact. In *2014 7th International Symposium on Resilient Control Systems (ISRCS)*, pages 1–10, Aug 2014.

[97] C. G. Rieger, D. I. Gertman, and M. A. McQueen. Resilient control systems: Next generation design research. In *2009 2nd Conference on Human System Interactions*, pages 632–636, May 2009.

[98] S. M. Rinaldi, J. P. Peerenboom, and T. K. Kelly. Identifying, understanding, and analyzing critical infrastructure interdependencies. *IEEE Control Systems Magazine*, 21(6):11–25, Dec 2001.

[99] Sandia National Lab. Energy: Grid resilience. `https://energy.sandia.gov/programs/electric-grid/resilient-electric-infrastructures/`.

[100] A. Sfetsos and A.H. Coonick. Univariate and multivariate forecasting of hourly

solar radiation with artificial intelligence techniques. *Solar Energy*, 68(2):169 – 178, 2000.

[101] R. Smith. A decoupled feedback structure for covertly appropriating networked control systems. *IFAC Proceedings Volumes*, 44(1):90 – 95, 2011. 18th IFAC World Congress.

[102] R. S. Smith. Covert misappropriation of networked control systems: Presenting a feedback structure. *IEEE Control Systems Magazine*, 35(1):82–92, Feb 2015.

[103] M. Solomon, B. Tew, C. Gerhman, and C. Lehner. Analysis of reservoir-based hydroelectric versus run-of-river hydroelectric energy production. Technical report, LRES Capstone, Montana State University., 2015.

[104] B. Stoll, J. Andrade, S. Cohen, G. Brinkman, and C Martinez-Anido. Hydropower modeling challenges. Technical report, National Renewable Energy Lab.(NREL), Golden, CO (United States), 2017.

[105] L. Sturm, C. Williams, J. Camelio, J. White, and R. Parker. Cyber-physical vulnerabilities in additive manufacturing systems: A case study attack on the .stl file with human subjects. *Journal of Manufacturing Systems*, 44:154 – 164, 2017.

[106] J. Sullivan and D. Kamensky. How cyber-attacks in Ukraine show the vulnerability of the U.S. power grid. *The Electricity Journal*, 30(3):30 – 35, 2017.

[107] B. Sussman. Revealed: Details of 'first of its kind' disruptive power grid attack. Secureworld, 2019.

[108] A. Teixeira, I. Shames, H. Sandberg, and K. Johansson. A secure control framework for resource-limited adversaries. *Automatica*, 51(C):135–148, January 2015.

[109] K. Tierney and M. Bruneau. Conceptualizing and measuring resilience: A key to disaster loss reduction. *TR News*, 250:14–17, 05 2007.

[110] U.S. Department of Energy. 21 steps to improve cyber SCADA security. Technical report, DOE, 2005.

[111] U.S. Department of Energy Office of Electricity Delivery and Energy Reliability. Economic benefits of increasing electric grid resilience to weather outages. Technical report, Executive Office of the President, 2013.

[112] U.S. Department of Homeland Security. Presidential policy directive 21 implementation: An interagency security committee white paper, 2015.

[113] Ö. Usta, M. MUSA, M. Bayrak, and M. Redfern. A new relaying algorithm to detect loss of excitation of synchronous generators. *Turk Journal of Electrical Engineering*, 15, 11 2007.

[114] B. Vaagensmith, T. McJunkin, K. Vedros, J. Reeves, J. Wayment, L. Boire, C. Rieger, and J. Case. An integrated approach to improving power grid reliability: Merging of probabilistic risk assessment with resilience metrics. In *2018 Resilience Week (RWS)*, pages 139–146, Aug 2018.

[115] M. Valavi and A. Nysveen. Variable-speed operation of hydropower plants: Past, present, and future. In *2016 XXII International Conference on Electrical Machines (ICEM)*, pages 640–646. IEEE, 2016.

[116] M. Venmathi, J. Vargese, L. Ramesh, and E. S. Percis. Impact of grid connected distributed generation on voltage sag. In *International Conference on Sustainable Energy and Intelligent Systems (SEISCON 2011)*, pages 91–96, 2011.

[117] T. Veselka, S. Hamilton, and J. McCoy. Optimizing hourly hydro operations at the salt lake city area integrated projects. Technical report, Argonne National Lab. (ANL), Argonne, IL, 1995.

[118] A. Visioli. *Practical PID Control*. Springer. Advances in Industrial Control, London, 2006.

[119] C. Wan, J. Zhao, Y. Song, Z. Xu, J. Lin, and Z. Hu. Photovoltaic and solar power forecasting for smart grid energy management. *CSEE Journal of Power and Energy Systems*, 1(4):38–46, 2015.

[120] H. Wang, S. Wang, L. Yu, and P. Hu. A novel planning-attack-reconfiguration method for enhancing resilience of distribution systems considering the whole process of resiliency. *International Transactions on Electrical Energy Systems*, n/a(n/a):e12199, 2019. e12199 ITEES-19-0457.R1.

[121] Y. Wang, G. Yan, and R. Zheng. Vulnerability assessment of electrical cyber-physical systems against cyber attacks. *Applied Sciences*, 8:768, 05 2018.

[122] H. L. Willis. *Power Distribution Planning Reference Book*. CRC Press, 2004.

[123] H. L. Willis and R. R. Schrieber. *Aging Power Delivery Infrastructures*. CRC Press, Boca Raton, FL, 2 edition, 2013.

[124] B. Wojszczyk and M. Brandao. High penetration of distributed generation and its impact on electric grid performance - utility perspective. In *2011 IEEE PES Innovative Smart Grid Technologies*, pages 1–7, 2011.

[125] D. Woods. *Resilience Engineering: Concepts and Precepts*. CRC Press, 2017.

[126] S. Yao, T. Zhao, P. Wang, and H. Zhang. Resilience-oriented distribution system reconfiguration for service restoration considering distributed generations. In *2017 IEEE Power Energy Society General Meeting*, pages 1–5, July 2017.

[127] M. Zare, A. Abbaspour, M. Fotuhi-Firuzabad, and M. Moeini-Aghtaie. Increasing the resilience of distribution systems against hurricane by optimal switch placement. In *2017 Conference on Electrical Power Distribution Networks Conference (EPDC)*, pages 7–11, April 2017.